18° WATER: THERMAL AND DYNAMICAL BALANCES

by

JOHN LEE LILLIBRIDGE III

B.S., University of Washington
(1976)

SUBMITTED IN PARTIAL FULFILLMENT
OF THE REQUIREMENTS FOR THE
DEGREE OF

SCIENCE MASTER'S

at the

MASSACHUSETTS INSTITUTE OF TECHNOLOGY

SEPTEMBER 1979

Signature of Author.....
Department of Meteorology, September 7, 1979

Certified by.....
Dr. Michael S. McCartney

Accepted by.....
Chairman, Department Committee

18° WATER: THERMAL AND DYNAMICAL BALANCES

by

JOHN LEE LILLIBRIDGE III

Submitted to the Department of Meteorology

on September 7, 1979 in partial fulfillment of the requirements

for the Degree of Science Master's

ABSTRACT

A simple ocean model applicable to the return flow region of the North Atlantic subtropical gyre is formulated to assess the dynamical effects of surface heat fluxes. The model is based on the thermodynamical model developed by Warren (1972). Warren's model satisfies the vertically integrated heat equation of the seasonal layer by means of a vertical temperature prescription which depends only on the surface temperature. The surface heat fluxes in his model also depend on the sea temperature, so that the model can adjust itself to a state in which heat storage changes in the seasonal layer balance the surface heat fluxes. A scale analysis indicates that Warren's model is applicable even for our full ocean depth, extended model.

The thermodynamics force the dynamics in this model by changing the pressure field of the seasonally influenced layers. The model has two free unknowns, the free surface and main thermocline positions, which are governed by two vertically integrated, quasigeostrophic vorticity equations.

The model results indicate that the main response of the free surface is due to thermal expansion. The nonisostatic response gives rise to transports over 1000 km of less than 5 Sverdrups. The main thermocline response is only a few meters when subjected to small scale forcing,

and has a much smaller response to the observed large scale forcing. Larger changes in the circulation resulted during deep convection and eighteen degree water formation, because of larger potential energy changes associated with the buoyancy fluxes in late winter. Even so, only small transport changes across the gyre were indicated. It is concluded that the model response was much weaker than that observed, and that the consideration of wind effects would probably be necessary to better model the observed seasonal and year to year variability within the eighteen degree water formation region.

Thesis Supervisor: Dr. Michael S. McCartney

Title: Associate Scientist, Department of Physical Oceanography, Woods Hole Oceanographic Institution.

Table of Contents

I. Introduction

A. Observations

Many models of the large scale, wind-driven ocean circulation have been formulated, and these have been largely successful in mimicking observed features in the ocean. Thermohaline processes have also received some attention, but models of this type of dynamic forcing have concentrated largely on deep abyssal flows driven by mass sources and sinks.

On the other hand, there is an abundance of surface mixed layer models which focus on the role of buoyancy fluxes and wind stirring in the creation and destruction of the near surface seasonal thermocline. These models often use energetic closure arguments, but generally do not study the dynamics forced by the presence or absence of the seasonal thermocline; they are inherently small scale, local models.

Worthington (1972b) drew attention to the possible importance of thermal forcing to the large scale circulation in the subtropical gyres. He has also proposed (Worthington,(1976))that the seasonal heating cycle may be responsible for fluctuations in the circulation around the subtropical gyres. He suggests that the formation in late winter of deep isothermal mixed layers south of the western boundary currents may increase the transport of the anticyclonic gyre. For example, Worthington attributes the observed variability in Gulf Stream transport to deepening of the main thermocline in late winter associated with the formation of "Eighteen Degree Water." This formation process is due to seasonally large negative heat fluxes from the ocean which cause deep vertical convection and mixing. The data basis for the temporal

transport variability originated as Figure 44 of Worthington (1976). An updated compilation of Gulf Stream transports (0 relative to 2000 db) from the "Bermuda triangle" (Montauk-Bermuda-Hatteras) is presented in Figure 1. It can be seen from this that there is some evidence of seasonal variability, but that year to year variations for any month can be as large as the amplitude of the seasonal signal ∿10-30 Sverdrups. This long-term variability is attributed (Worthington,(1972b)) to "severe" winters in which there are outbreaks of extremely cold, polar continental air and associated anomalously large negative heat fluxes. Worthington believes that there is a deepening of the underlying main thermocline associated with production of excessive amounts of Eighteen Degree Water in these severe winters. As a possible mechanism for the main thermocline deepening, Worthington (1972b), Figure 4 suggests a meridional circulation scheme. In this schematic figure he proposes that during severe winters, and excessive Eighteen Degree Water formation, there is an associated convergence of near surface waters from the south into the "formation" region south of the Gulf Stream. These warm waters are rapidly cooled to the ambient surface temperature and mixed into the homogeneous layer. Some of this excess convergence, or the downward motion of the water itself, is envisioned as causing the main thermocline to be forced downward. The meridional cell is closed by the southward extension of Eighteen Degree Water, flowing above the main thermocline but below the near surface waters which are moving northwards. Worthington suggests that at least part of the mean anticyclonic circulation in the Sargasso Sea is maintained by this process.

These comments are illustrated in Figure 2 by a pair of hydrographic stations taken in the Eighteen Degree Water formation region in a relatively mild and a severe winter. The increased depth of the homogeneous layer in the Researcher station cannot be due solely to convective erosion into the main thermocline, since the temperature is still nearly 18°. Erosion into the roughly 50 m/°C gradient of the main thermocline would be associated with a several degree temperature drop, if mixing alone was the cause of this 100-200 m deepening. Thus the question is whether this main thermocline heaving, and associated baroclinic transport changes, are being driven by the thermodynamic forcing, whether it is associated with changes in the wind-driven circulation in the subtropical gyre as a whole, or possibly if it is driven by the local Ekman pumping. It is the intent of this study to investigate the first possibility.

B. Warren Model

Warren (1972) formulated a seasonal thermocline model applicable to the local heat balance in the formation region of Eighteen Degree Water. In his model a linearized and continuous vertical temperature structure is specified at a point in the formation region. The profile has specified seasonal and main thermocline gradients, with the depth of the main thermocline fixed. With this prescription the structure is only dependent on the surface temperature. However, this dependence changes depending on whether the water column is building a seasonal thermocline, eroding the seasonal thermocline, or is deeply convecting

and eroding into the main thermocline. Thus, the way in which the heat content of the column changes at any point depends upon the phase of the heating cycle to which a column of fluid is being subjected. His vertical temperature profile was modeled after the observed temperature field and an example he used for the North Atlantic is shown in Figure 3.

Since the model is envisaged for the central formation region of Eighteen Degree Water, where both zonal and meridional gradients locally go to zero, Warren can neglect horizontal advection and diffusion immediately. He also assumes the surface heat flux is much greater than vertical diffusion or advection into or out of the seasonal thermocline. These surface heat fluxes depend on sea surface temperature so that the forcing has feedback from the ocean. The effect of the heat flux on the atmosphere is neglected, so that the atmospheric variables are assumed given by observations. He arrives at a purely local model in which heat storage, a function of surface temperature as well as the history of surface temperature, balances the atmospherically forced surface heat fluxes, which also depend on surface temperature.

In his model, Warren integrates the heat equation forward in time from an initial state of excessive heat content, relative to the imposed atmospheric state. This forces a net heat loss for several years and consequently leads to late winter deep convection during those years. He finds that the seasonal limit cycle into which the surface temperatures settle is very close to that observed, if observed atmospheric forcing were used. In this limit cycle, the surface temperature and

therefore the heat fluxes have adjusted to a state where no late winter convection, and no net annual heat loss, occurs. When this limit cycle was subjected to a "severe" winter he found that although erosion into the main thermocline occurred, it was minimized because the seasonal thermocline had to be eroded away first, and then the homogeneous layer below was of such large vertical extent that a very large heat loss was required to change the surface temperature significantly.

Warren's model is a simplified solution to the depth integrated heat equation for the upper waters which are influenced by seasonal heat fluxes. The associated buoyancy fluxes and the dynamical response they excite are not, however, addressed. The model vertical structure in his formulation does not have the freedom to satisfy the depth integrated dynamical equations.

In an attempt to model the dynamical consequences of the seasonal heating cycle and Eighteen Degree Water formation, we decided to build upon the successful thermodynamic framework that Warren's model employed. We extend his model by giving the vertical prescription more degrees of freedom, so that it has dynamical response, and then reconstrain the system with depth integrated dynamic equations.

We first removed the constraint of the "pinned" main thermocline by no longer requiring a fixed temperature at a fixed main thermocline depth. We don't intend that the temperature within the main thermocline should be changed by the surface heating, but rather that the main thermocline is bodily heaving and vertical advection would thereby give rise to a change in temperature at a fixed depth. This

heaving would be associated with concommitant divergences or convergences within the overlying Eighteen Degree Water and seasonal layers and within the underlying deep layers. The vertical temperature prescription is extended to full ocean depth, but to rule out topographic effects we consider a constant depth ocean. In order for the temperature structure to reamin realistic we prescribe a main thermocline of finite thickness with an underlying deep layer. Again for simplicity, the deep waters are considered to be of uniform temperature both vertically and horizontally. This prescription is illustrated in Figure 4.

We also make the kinematical prescription that the bottom of the thermocline is a material, as well as isopycnal, surface, and specify no flow through it. The interface at the bottom of the Eighteen Degree Water layer is not at constant temperature and is eroded during deep convection; thus it is not suitable as a material surface. We have given our model the freedom to respond like a two-layer model with the interior interface lying over a constant density bottom layer, but in our case the density varies continuously, rather than jumping, at that boundary. We make the simplification that when the main thermocline is not being eroded, its temperature gradient as well as thickness remain constant, though it may heave as a whole. This is, in part, based on observations, as can be seen in Figure 2, and is described further in Worthington (1972b)[cf. Figure 5]. With the main thermocline thickness constant, our material surface becomes the only internal, dynamical unknown. We wish to allow for the possibility that the system

will respond in an external manner, and complete the "two-layer" analogy by allowing another variable, material interface at the free surface. We now have two dynamical unknowns in our model which will be constrained by two dynamical, in our case vorticity, equations.

It is necessary to extend the model horizontally as well as vertically to allow for gradients. Our region of interest lies in an area where the Gulf Stream and returning flow are primarily zonal, thus we only extend the model to 2-D and consider a meridional plane running along 55°W with all quantities independent of the zonal direction. We will retain the local nature of Warren's thermodynamic model and will eventually integrate our dynamic equations in such a way as to obtain a quasi-local form in these as well.

We envisage the thermodynamic forcing as entering the dynamics through its effect in changing the density of the seasonally influenced layer and thereby changing our prescribed density and pressure field hydrostatically. It will be shown in the next chapter that although the thermodynamics play a role in the dynamics, to first order it is justified to neglect the effect of the dynamics on the thermodynamics. This arises mainly because horizontal advection is small for this 2-D limit. With this oversimplification, we can take the thermodynamic effects on the pressure field as given, with two free parameters, governed by two vorticity equations, able to respond to this forcing. The form of the equations rendered will thereby be similar to the classical two-layer model of Veronis and Stommel (1956) but with a much different forcing from the buoyancy fluxes rather than the wind stress.

In summary, the model we propose is primarily locally forced, as in Warren (1972), but focuses on the coupled internal/external dynamical response of the system to thermodynamic forcing (via hydrostatics and geostrophy). The forcing is taken as given, and not affected by the dynamic response which ensues. Because we have uncoupled the thermodynamics in this way, it is much simpler to specify the time and space variability of the heat fluxes, based on the observations described by Bunker (1976) and Bunker and Worthington (1976), rather than specifying only the atmospheric fields and allowing the heat fluxes to adjust via the surface temperature. This is again an oversimplification since negative feedback will occur between the ocean and its thermal driving, but since we are trying to establish the nature of the dynamical response to the heat fluxes, we will begin with the fluxes taken as given by Bunker's calculations.

It should be kept in mind that models of this type only satisfy certain integral conservation equations. Thus although the depth integrated equations may be satisfied, one cannot expect that internally, the unintegrated equations will be exactly satisifed. The purpose of the imposed vertical temperature prescription is to mimic the internal response with a simplified, but nonetheless plausible, set of free variables.

We proceed in the next section to the theory necessary to derive our extended model equations.

II. Theory/Scaling

A. Introduction

Rather than developing a complete and systematic set of scaling arguments, in the following, only simple order of magnitude estimates of terms will be utilized to obtain a simplified system of conservation equations from the general equations. In making the magnitude estimates, our temperature prescription will be utilized whenever possible. This is done in part because the vertical prescription is a fair approximation to the observed profile, and also because we will ultimately be utilizing this prescription in our model equations.

We make here a few *a priori* approximations and specifications. First, in computing vertical integrals of the density field we will assume exact hydrostatic balance. Secondly, we will completely neglect effects of horizontal diffusion of momentum and heat. Because of the absence of horizontal boundaries we expect that, in general, vertical diffusion of momentum will dominate horizontal momentum diffusion. Similarly we expect vertical heat diffusion to dominate horizontal diffusion. Since our region of interest remains south of the Gulf Stream, horizontal mixing by eddies can presumably be neglected relative to vertical processes.

We will also neglect vertical diffusion of momentum in order to isolate the thermally-driven effects from the wind-driven field; we won't consider here the ultimate dissipation mechanism of the bottom boundary layer.

Thirdly, we make a rather strong specification on the vertical diffusion of heat or buoyancy. We will assume that below the layer of seasonal influence vertical diffusion of heat is very small, much smaller than the surface heating. We don't expect any internal buoyancy sources, and neglect the vertical diffusion which would tend to smooth regions of rapid change in slope. Since we are specifying a profile with discontinuous slope, these diffusion effects would be large, but only in limited vertical regions. Since we are using the simplest vertical structure to obtain the essence of this system's response, the neglect of vertical diffusion in slightly changing the shape seems justifiable.

Probably the most fundamental assumption we will be making is that there is a large asymmetry between the zonal and meridional length scales. Just how two dimensional the field must be to obtain a consistent set of equations will be discussed in a following section. The simplifications obtained in the 2-D limit will be quite far-reaching. One immediate simplification that results will be the neglect of horizontal advection relative to time rate of change. In the following sections a Cartesian coordinate system is used even though our meridional scale is 1000 km. We neglect the metric terms from the full spherical equations in the following discussion because they are generally the same order as advection and would be neglected ultimately. One exception is a term in the continuity equation which is neglected assuming *a priori* that $L_y \tan\theta/a \ll 1$ where L_y is the meridional scale, θ is latitude and "a" is the earth's radius.

We will combine the equations for heat and salt conservation to obtain a density equation, since density integrals will enter the dynamical equations. This will be done using the simplest linear equation of state. However, we will be focusing only on buoyancy fluxes associated with surface heat fluxes. This is not to say that mass and/or salt fluxes associated with differences between evaporation and precipitation are unimportant. We simply wish to focus on the effect of the seasonal heating forcing.

Lastly, we will be using the Boussinesq approximation throughout to neglect the variations in density relative to a constant mean value, when density appears as a coefficient in the equations.

B. Thermodynamic Equation

Conservation of potential temperature and salt, with neglect of horizontal diffusion, can be written:

$$\rho\, c_p \frac{D\theta}{Dt} = \frac{\partial Q_H}{\partial z} \tag{1}$$

$$\rho \frac{DS}{Dt} = \frac{\partial Q_S}{\partial z} \tag{2}$$

where θ is potential temperature; S is salinity; Q_H and Q_S are vertical fluxes of heat and salt, respectively; ρ is *in situ* density; c_p is specific heat at constant pressure, treated here as a constant for seawater of $c_p = .93$; and D/Dt is the substantial derivative following a fluid parcel.

Our linear equation of state relating potential density to potential temperature and salinity is:

$$\rho_\theta = \rho_o(1 - \alpha_*(\theta-\theta_o) + \beta_*(S-S_o)) \tag{3}$$

where ρ_o is a constant value of average density at temperature θ_o and salinity S_o, and α_*, β_* are the thermal and haline expansion coefficients. We form a density equation from (1) and (2) by multiplying by $-\rho_o\alpha_*$ and $\rho_o\beta_*$, respectively, and adding to yield:

$$\frac{D\rho_\theta}{Dt} = \frac{\rho_o}{\rho}\frac{\partial Q_\rho}{\partial z} \; ; \; Q_\rho \equiv -\frac{\alpha_*}{c_p}Q_H + \beta_* Q_S \quad . \tag{4}$$

By considering potential density we have included the first order effects of compressibility but we have neglected any second order effects between temperature, salinity, and pressure. The subscript θ will now be dropped though we will still be referring to the potential density. In deriving equation (4) we have neglected variations in α_* and β_* relative to those in θ and S in the first term in (4). This is done in anticipation of the neglect of vertical diffusion below the seasonally influenced layer, since α_* and β_* do change by about a factor of two between the surface and deep waters, but we wish to neglect second order effects on ρ below this layer.

We now make scaling arguments to simplify our density equation. As in Warren's model, we shall consider the thermodynamic balance of a

vertical column of unit area. Therefore, in making our approximations we will explicitly use vertical integrals of our prescription to estimate orders of magnitude layer by layer.

Referring again to Figure 4, we see that without diffusion from the main thermocline our thick lower layer cannot change in time since there are no lateral or vertical density gradients specified.* Of course there is a weak vertical gradient in the sub-thermocline waters, and generally non-negligible meridional gradients as well. Were we to include these effects, the arguments for the density equation in the deep water would be similar to those that follow for the main thermocline.

Thus for the lower layer:

$$\int_{-B}^{-H} \frac{\partial \rho}{\partial t} dz = - \int_{-B}^{-H} \vec{u} \cdot \nabla \rho \, dz \equiv 0 \tag{5}$$

or

$$\frac{\partial}{\partial t} \int_{-B}^{-H} \rho dz = -\rho_{-H} \frac{\partial H}{\partial t} . \tag{5a}$$

Within the main thermocline, neglecting vertical diffusive effects at the boundaries, we have:

$$\int_{-H}^{-D} \frac{\partial \rho}{\partial t} dz = - \int_{-H}^{-D} \vec{u} \cdot \nabla \rho \, dz \tag{6}$$

---

*The density prescription is a mirror image of Figure 4, with the same subscript nomenclature on ρ, but with seasonal and main thermocline gradients γ and β.

or

$$\frac{\partial}{\partial t}\int_{-H}^{-D} \rho dz = \rho_{-H}\frac{\partial H}{\partial t} - \rho_{-D}\frac{\partial D}{\partial t} - \int_{-H}^{-D} \vec{u}\cdot\nabla\rho\, dz \ . \qquad (6a)$$

In our prescription we assume the main thermocline gradient, β, is constant in y as well as z so that the advection term can be written as:

$$\int_{-H}^{-D} \vec{u}\cdot\nabla\rho\, dz = \beta\int_{-H}^{-D}[w + v\frac{\partial H}{\partial y} + u\frac{\partial H}{\partial x}]dz$$

or

$$\int_{-H}^{-D} \vec{u}\cdot\nabla\rho\, dz = \beta\{\bar{w} + \bar{v}\frac{\partial H}{\partial y} + \bar{u}\frac{\partial H}{\partial x}\}*(H-D)$$

where overbars indicate vertical averages. Since we will be specifying no cross-isopycnal flow at z = -H, the kinematic boundary condition there will be $w_{-H} = -[v_{-H}\frac{\partial H}{\partial y} + u_{-H}\frac{\partial H}{\partial x} + \frac{\partial H}{\partial t}]$.

Since isopycnals are roughly parallel within the main thermocline, to a good approximation:

$$\bar{w} = -[\bar{v}\frac{\partial H}{\partial y} + \bar{u}\frac{\partial H}{\partial x} + \frac{\partial H}{\partial t}] \ .$$

Thus we find from (6a):

$$\frac{\partial}{\partial t}\int_{-H}^{-D} \rho dz = \rho_{-H}\frac{\partial H}{\partial t} - \rho_{-D}\frac{\partial D}{\partial t} + \beta\frac{\partial H}{\partial t}(H-D) \ .$$

Without deep convection $\partial H/\partial t = \partial D/\partial t$ and we always have, by our profile, that $\rho_{-D} = \rho_{-H} + \beta(H-D)$. Substituting these above gives the expected result:

$$\frac{\partial}{\partial t}\int_{-H}^{-D} \rho dz = 0 \ . \qquad (6b)$$

Thus, the mass of the main thermocline remains constant when not eroded.

If deep convection occurs, the main thermocline thickness (H-D) will be changed proportional to the heat flux. In this case $\frac{\partial}{\partial t}\int_{-H}^{-D} \rho dz = \rho_{-D} \frac{\partial}{\partial t}$ (H-D) $\propto Q$. This will be discussed further when treating the seasonal layer.

In the homogeneous eighteen degree water layer there are no vertical advective or diffusive fluxes. We have specified that without deep convection the late winter density doesn't change, but we really mean it would only be altered slightly by horizontal advection. We show this as follows: In anticipating the 2-D limit of our momentum equations it can be shown that the meridional velocity, v, is of order (ω/f) times the zonal velocity, u (ω,f being the seasonal and inertial frequencies). In the 2-D limit, only meridional advection can be important, thus $\vec{u} \cdot \nabla\rho \, dz \simeq v\frac{\partial \rho_{-D}}{\partial y} \doteq \beta v \frac{\partial}{\partial y}$ (H-D) for this homogeneous layer.

Let us estimate the order of magnitude of the late winter *temperature* change in this case. Following Warren (1972) we estimate the vertical main thermocline temperature gradient as:

$$\beta_T \sim (50 \text{ m/°C})^{-1} \ .$$

Using the seasonal frequency of 2×10^{-7} s^{-1}, an inertial frequency of 10^{-4} s^{-1}, and a zonal velocity scale of 25 cm/s yields:

$$v \sim (\omega/f) \sim .05 \text{ cm/s} .$$

Observed changes in the main thermocline thickness are order 100m/1000 km $\sim 10^{-4}$ so that:

$$\beta_T v \frac{\partial}{\partial y} (H-D) \sim 10^{-9} \ ^{o}C/s .$$

At this rate over a half year ($\sim 10^{7}$ s) changes in late winter temperature of $O(.01^{o}C)$ would be expected. These changes are negligible compared to changes in surface temperature throughout the year and are therefore neglected. So we approximate:

$$\int_{-D}^{-h_D} \frac{\partial \rho}{\partial t} dz = - \int_{-D}^{-h_D} v \frac{\partial \rho}{\partial y} dz \simeq 0 \quad \text{in the 2-D limit} \tag{7}$$

or

$$\frac{\partial}{\partial t} \int_{-D}^{-h_D} \rho dz \simeq -\rho_{-h} \frac{\partial h}{\partial t} + \rho_{-D} \frac{\partial D}{\partial t} .$$

In the seasonally influenced waters, vertical integration of (4) gives

$$\int_{-h_D}^{\eta} \frac{\partial \rho}{\partial t} dz + \int_{-h_D}^{\eta} \vec{u} \cdot \nabla \rho \, dz \simeq Q_\rho \Big|_{\eta} - Q_\rho \Big|_{-h_D} \simeq Q_o \quad \text{to } O(\Delta\rho/\rho_o) \tag{8}$$

where Q_o is the surface density flux. We have again imposed small diffusion out of the seasonal layer, and make the Boussinesq approximation when integrating the right hand side of equation (4).

When building a seasonal thermocline, by our prescription:

$$\int_{-h_s}^{\eta} \frac{\partial \rho}{\partial t}\, dz = (\eta + h_s)\, \frac{\partial \rho_s}{\partial t}$$

so that to $O(\eta/h_s) \sim 10^{-3}$:

$$\int_{-h_s}^{\eta} \frac{\partial \rho}{\partial t}\, dz \simeq h_s\, \frac{\partial \rho_s}{\partial t} = \frac{\partial}{\partial t}\left(\gamma\, \frac{h_s^2}{2}\right) \tag{9}$$

or

$$\frac{\partial}{\partial t} \int_{-h_s}^{\eta} \rho dz \simeq \frac{\partial}{\partial t}\left(\gamma\, \frac{h_s^2}{2}\right) + \rho_s\, \frac{\partial \eta}{\partial t} + \rho_{-h}\, \frac{\partial h_s}{\partial t} \tag{9a}$$

to the same order when the seasonal thermocline is being eroded:

$$\int_{-h_{LS}}^{\eta} \frac{\partial \rho}{\partial t}\, dz \simeq -\frac{\partial}{\partial t}\left(\gamma\, \frac{h_m^2}{2}\right) . \tag{10}$$

During deep convection the appropriate integrals become:

$$\int_{-D}^{\eta} \frac{\partial \rho_{LW}}{\partial t}\, dz = (\eta + D)\beta\, \frac{\partial}{\partial t}\,(H-D)$$

$$\simeq \beta D\, \frac{\partial}{\partial t}\,(H-D) \tag{11}$$

or

$$\frac{\partial}{\partial t}\int_{-D}^{\eta} \rho_{LW}\, dz = + \rho_{LW}\left(\frac{\partial \eta}{\partial t} + \frac{\partial D}{\partial t}\right) + \beta D \frac{\partial}{\partial t}(H-D) \quad . \tag{11a}$$

Gill and Niiler (1973) in their treatise of seasonal variability discuss the relative importance of advection compared with time rate of change of density within the seasonal thermocline. They find that except within the Ekman layer, not present here, advection of the mean density field by seasonal currents, as well as advection of the seasonal density field by mean currents, is much smaller than the surface buoyancy fluxes. Since in our model the zonal/meridional scale ratio is much larger than in theirs, the conclusion reached by them certainly seems justifiable here.

Using our prescription as a check yields:

$$\int_{-h_D}^{\eta} \vec{u} \cdot \nabla\rho \, dz = \int_{-h_D}^{o} \left[v \frac{\partial \rho_s}{\partial y} + \gamma w\right] dz + \int_{o}^{\eta} \left(v \frac{\partial \rho_s}{\partial y}\right) dz \quad \text{(in 2-D limit)}$$

$$= \left[\bar{v} \frac{\partial \rho_s}{\partial y} + \gamma \bar{w}\right] * h_D + \bar{v}_s \frac{\partial \rho_s}{\partial y} * \eta \quad .$$

The relative importance of horizontal advection is therefore

$$\frac{\int_{-h}^{\eta} \vec{u} \cdot \nabla\rho \, dz}{\int_{-h}^{\eta} \frac{\partial \rho}{\partial t} dz} \sim \frac{\bar{v}}{\omega L_y} \quad .$$

Here L_y is the distance across which ρ_s changes by the amount it does seasonally. For a temperature cycle of amplitude 8°, the scale L_y is roughly 1-2000/km [cf. Fuglister (1960)]. Thus:

$$\frac{\bar{v}}{\omega L_y} \sim \frac{.05 \text{ cm/s}}{2\times10^{-7}\text{s}^{-1} \cdot 10^{8} \text{ cm}} \sim 10^{-3}.$$

We see again the importance of our two-dimensionality assumption and the resulting small, ageostrophic, meridional velocity.

The vertical advection, however, may be important in the seasonal layer:

$$\frac{\int_{-h}^{\eta} w \frac{\partial \rho}{\partial z} dz}{\int_{-h}^{\eta} \frac{\partial \rho}{\partial t} dz} \simeq \frac{\gamma \bar{w}}{\omega \Delta \rho_s} = \frac{\gamma \Delta z}{\Delta \rho_s} \sim 10^{-4} \Delta z \text{ (cm)}$$

where Δz is the amplitude of seasonal vertical fluid parcel excursions. For a ten meter excursion (average within the seasonal thermocline) this ratio is O(.1) and may be nonnegligible. It will be seen a posteriori that vertical velocities within the seasonally influenced layers are actually much smaller than this so that vertical advection is also much smaller than local change within the uppermost layer.

We thus find by summing equations (5),(6),(7),& (8), neglecting upper layer advection, and using the form of (9), (10), and (11) that for the *total* field, the thermodynamic equation reduces to:

$$\int_{-B}^{\eta} \frac{D\rho}{Dt} dz \simeq \int_{-h_D}^{\eta} \frac{\partial \rho}{\partial t} dz \equiv \left\{ \begin{array}{l} \gamma h_s \ \partial h_s/\partial t \text{ [heating]} \\ -\gamma h_m \ \partial h_m/\partial_t \text{ [cooling]} \\ \beta D \ \partial/\partial t \text{ (H-D) [convecting]} \end{array} \right\} \simeq Q_o . \quad (12)$$

These are exactly the Warren model equations, in terms of density, but even for the full ocean depth.

We have obtained this simple form because our scale analysis indicates: that advection dominates diffusion and thereby nearly balances the observed time rate of change within the main thermocline; that advection, diffusion, and thereby local change are all small within the deep waters and within the homogeneous eighteen degree water; and that diffusion dominates advection, so that local storage balances the surface fluxes, within the seasonally influenced layer.

It is now possible to use the results of this section to obtain an equation relating the pressure and density fields via hydrostatics. If we know the density field at all depths we can compute currents relative to the bottom, as with oceanographic observations, but we still do not know what the absolute currents are. To obtain all the velocity information it is necessary to know, in addition, the distribution of pressure along the flat bottom. Once this bottom pressure is known, the pressure at all levels is obtained from the hydrostatic equation and our known density field. This barotropic component of velocity due to the bottom pressure gradient therefore fixes the absolute velocity. Thus the bottom pressure is a dynamically important quantity to obtain.

From hydrostatics we define the pressure at the flat bottom as:

$$p_B = \int_{-B}^{\eta} \rho g dz \simeq g[\rho_s \eta + \int_{-B}^{o} \rho dz] \quad .$$

We can obtain an equation for bottom pressure changes by summing equations (5a), (6b), (7a), and (9a), for example:

$$\frac{\partial p_B}{\partial t} = \frac{\partial}{\partial t}\int_{-B}^{\eta} \rho g dz \simeq g[\rho_s \frac{\partial \eta}{\partial t} + (\rho_{-D} - \rho_{-H})\frac{\partial H}{\partial t} + \frac{\partial}{\partial t}(\gamma \frac{h_s^2}{2})]$$

$$\simeq \rho_o g \frac{\partial \eta}{\partial t} + \beta(H-D)g \frac{\partial H}{\partial t} + \frac{\partial}{\partial t}(\gamma g \frac{h_s^2}{2}) \qquad \text{to } O(\Delta\rho/\rho_o) \ . \tag{13}$$

Thus we see that adding the freedom of main thermocline motion and a variable-free surface does not alter the character of the thermodynamics, but the dynamics depend essentially on free surface motion and main thermocline motion as well as thermodynamics. Using (12) we find, for any phase of the heating, that:

$$\frac{\partial p_B}{\partial t} \simeq \rho_o g \frac{\partial \eta}{\partial t} - \rho_o g' \frac{\partial H}{\partial t} + Q_o g \tag{14}$$

where g' is reduced gravity at the main thermocline:

$$g' \equiv (\frac{\rho_{-H} - \rho_{-D}}{\rho_o})g \ .$$

Since the dynamics will thereby depend essentially on the heat fluxes, though the thermodynamics do not depend on the dynamics, it will simplify matters greatly if we specify a given Q_o, rather than integrate the Warren model to obtain Q_o. Since a good observational data base exists for this total Q_o, as tabulated and made available by Bunker, et al., we will utilize this information as our given forcing. This uncoupling will then focus us on the dynamic response, without having to model the feedback mechanism inherent in the thermodynamic response.

C. Mass/Continuity

The general equation for mass conservation can be written:

$$\frac{D\rho}{Dt} + \rho(\nabla \cdot \vec{u}) = 0 \ . \tag{15}$$

In oceanography this is almost always simplified by neglecting density changes relative to velocity divergences, yielding the continuity equation. Because we have neglected wind-induced divergences here, careful consideration of the full equation is necessary.

Below the seasonally influenced layers we have assumed that diffusion is less important than advection. In this case we will obtain continuity since:

$$\nabla \cdot \vec{u} = \frac{-1}{\rho}\frac{D\rho}{Dt} \simeq 0 \qquad -B \leq z < -h_D \ . \tag{16}$$

Within the seasonal layers we expect large buoyancy fluxes and associated large density changes, whereas the velocity divergences we expect are only due to stretching associated with movements of the free surface or by vertical movements imposed from below. Thus a simple scale analysis would be:

$$\frac{\frac{1}{\rho}\frac{D\rho}{Dt}}{\nabla\cdot\vec{u}} \sim \frac{\frac{\Delta\rho}{\rho_o}\omega}{w/h} \sim \frac{\Delta\rho h}{\rho_o \Delta z} \sim \frac{10^{-3} * 10^{4} \text{ cm}}{\Delta z \text{ (cm)}} \qquad -h_D \leq z \leq \eta \ .$$

Thus if the amplitude of vertical parcel motions in the seasonal thermocline, Δz, are, on average, the order of free surface movement, 10 cm say,

this ratio is order one. If vertical velocities are the order of observed main thermocline motions, 10 m say, this ratio would be 10^{-2} indicating continuity is appropriate for the water column as a whole.

To retain the former possibility, we will utilize full mass conservation in the surface layers when deriving our vertically integrated momentum equations in the next section. Nonetheless, we shall eventually join the diffusive layer equations to the nondiffusive lower layers under the Boussinesq approximation to obtain top to bottom momentum integrals. The appropriate approximations to the full mass equation are obtained by combining the thermodynamic equation (4) with the mass equation (15):

$$\rho(\nabla \cdot \vec{u}) = -\frac{\rho_o}{\rho}\frac{\partial \varrho_\rho}{\partial z} \quad .$$

Assuming the density effects are important, and utilizing the Boussinesq approximation, integration over the seasonal layer yields:

$$\int_{-h}^{\eta}(\frac{\partial u}{\partial x} + \frac{\partial v}{\partial y})dz \simeq -(w_\eta - w_{-h} + \frac{\varrho_o}{\rho_o}) \quad \text{to} \quad O(\frac{\Delta\rho}{\rho_o}) \quad . \tag{17}$$

In order to make our "two-layer" dynamical split we have specified $z = -H$ as an isopycnal surface across which there is no flow. With the free surface and main thermocline as our material surfaces the integrals of lower layer continuity, (16), and total mass , (16) combined with (17), thus become:

$$\int_{-B}^{-H} \left(\frac{\partial u}{\partial x} + \frac{\partial v}{\partial y}\right) dz = w_{-B} - w_{-H}$$

$$\int_{-H}^{\eta} \left(\frac{\partial u}{\partial x} + \frac{\partial v}{\partial y}\right) dz = - w_{\eta} + w_{-H} - \frac{\varrho_o}{\rho_o} .$$

Using kinematic boundary conditions at the flat bottom, at η, and H, and going to the 2-D limit, simplifies these to:

$$\frac{\partial}{\partial y} \left[\int_{-B}^{-H} v \, dz \right] = \frac{\partial H}{\partial t} \tag{18}$$

$$\frac{\partial}{\partial y} \left[\int_{-B}^{\eta} v \, dz \right] = - \frac{\partial \eta}{\partial t} - \frac{\varrho_o}{\rho_o} \tag{19}$$

These will be utilized later in our 2-D vorticity equations.

D. Dynamics

1. Total Field Equations

We will now derive the first of our model equations by vertical integration of the full dynamical equations. Simplifications will then be made based on a full scale analysis of the unintegrated, general equations of motion. This scale analysis, starting from the full spherical equations, is presented in Appendix A. The reason that the equations to follow are vertically integrated before simplifying is to avoid the appearance of spurious terms resulting from our variable limits of integration (η and H). The scale analysis in Appendix A is assumed to be valid for comparing integrated terms in this section, since there are not

fundamentally different dynamical balances in the various layers, whereas the thermodynamical balances were quite different. We proceed then, assuming the ratio of vertically averaged terms are essentially the same as the ratio of the terms at any depth.

For the layers not subject to seasonal heat fluxes we combine the Boussinesq horizontal momentum equations with continuity to obtain a flux form of the advection terms:

$$\left.\begin{aligned} &\frac{\partial u}{\partial t} + \nabla \cdot (\vec{uu}) - fv = -\frac{1}{\rho_o}\frac{\partial p}{\partial x} && (20)\\ &\frac{\partial v}{\partial t} + \nabla \cdot (\vec{uv}) + fu = -\frac{1}{\rho_o}\frac{\partial p}{\partial y} && (21)\\ &\nabla \cdot \vec{u} = 0 && (22) \end{aligned}\right\} \quad (-B \leq z < -h_D)$$

Integrating these from the flat bottom to the diffusive interface h_D (which is h_s, h_m, or D depending on the phase of the heating cycle) yields, for example, for x momentum:

$$\begin{aligned} &\frac{\partial}{\partial t}\int_{-B}^{-h_D} u\,dz + \frac{\partial}{\partial x}\int_{-B}^{-h_D} u^2\,dz + \frac{\partial}{\partial y}\int_{-B}^{-h_D} uv\,dz + \\ &u_{-h}\left(\frac{\partial h_D}{\partial t} + u_{-h}\frac{\partial h_D}{\partial x} + v_{-h}\frac{\partial h_D}{\partial y} + w_{-h}\right) - f\int_{-B}^{-h_D} v\,dz \qquad (23)\\ &= -\frac{1}{\rho_o}\int_{-B}^{-h_D}\frac{\partial p}{\partial x}\,dz \end{aligned}$$

where we have used $w_{-B} = \frac{\partial B}{\partial x} = \frac{\partial B}{\partial y} = 0$.

For the region above the diffusive interface we combine the full mass and momentum equations to obtain:

$$\left.\begin{aligned} &\frac{\partial(\rho u)}{\partial t} + \nabla \cdot (\rho \vec{u} u) - \rho f v = -\frac{\partial p}{\partial x} && (24)\\ &\frac{\partial(\rho v)}{\partial t} + \nabla \cdot (\rho \vec{u} v) + \rho f v = -\frac{\partial p}{\partial y} && (25)\\ &\frac{\partial \rho}{\partial t} + \nabla \cdot (\rho \vec{u}) = 0 && (26) \end{aligned}\right\} \quad -h_D \leq z \leq \eta \quad .$$

In this case, integration of the x-momentum equation from the diffusive interface to the surface gives:

$$\begin{aligned} &\frac{\partial}{\partial t}\int_{-h_D}^{\eta} \rho u dz + \frac{\partial}{\partial x}\int_{-h_D}^{\eta} \rho u^2 dz + \frac{\partial}{\partial y}\int_{-h_D}^{\eta} \rho u v dz \\ &\qquad - \rho_{-h} u_{-h}\left(\frac{\partial h_D}{\partial t} + u_{-h}\frac{\partial h_D}{\partial x} + v_{-h}\frac{\partial h_D}{\partial y} + w_{-h}\right) - f\int_{-h_D}^{\eta} \rho v dz \qquad (27)\\ &\qquad = -\int_{-h_D}^{\eta} \frac{\partial p}{\partial x} dz \end{aligned}$$

Integrations of the mass and continuity equations above and below, respectively, h_D yields:

$$\frac{\partial}{\partial x}\int_{-B}^{-h_D} u dz + \frac{\partial}{\partial y}\int_{-B}^{-h_D} v dz + u_{-h}\frac{\partial h_D}{\partial x} + v_{-h}\frac{\partial h_D}{\partial y} + w_{-h} = 0 \qquad (28)$$

$$\int_{-h_D}^{\eta} \frac{\partial \rho}{\partial t}\, dz + \frac{\partial}{\partial x}\int_{-h_D}^{\eta} \rho u dz + \frac{\partial}{\partial y}\int_{-h_D}^{\eta} \rho v dz - \rho_s\left(u_s \frac{\partial \eta}{\partial x} + v_s \frac{\partial \eta}{\partial y} - w_\eta\right)$$

$$- \rho_{-h}\left(u_{-h} \frac{\partial h_D}{\partial x} + v_{-h} \frac{\partial h_D}{\partial y} + w_{-h}\right) = 0 \quad . \tag{29}$$

We now match both the mass and momentum equations, to the order of the Boussinesq approximation, across the diffusive interface. This requires neglecting integrals of $\Delta\rho$ weighted by the velocity relative to ρ_o times the velocity integrals. This should, in general, be to the same order as $\Delta\rho/\rho_o$. This procedure then yields for x momentum:

$$\frac{\partial}{\partial t}\int_{-B}^{\eta} u dz + \frac{\partial}{\partial x}\int_{-B}^{\eta} u^2 dz + \frac{\partial}{\partial y}\int_{-B}^{\eta} uv dz$$

$$- u_s\left(\frac{\partial \eta}{\partial t} + u_s \frac{\partial \eta}{\partial x} + v_s \frac{\partial \eta}{\partial y} - w_\eta\right) - f\int_{-B}^{\eta} v dz \tag{30}$$

$$= -\frac{1}{\rho_o}\int_{-B}^{\eta} \frac{\partial p}{\partial x}\, dz$$

Similarly

$$\frac{\partial}{\partial t}\int_{-B}^{\eta} v dz + \frac{\partial}{\partial x}\int_{-B}^{\eta} uv dz + \frac{\partial}{\partial y}\int_{-B}^{\eta} v^2 dz - v_s\left(\frac{\partial \eta}{\partial t} + u_s \frac{\partial \eta}{\partial x} + v_s \frac{\partial \eta}{\partial y} - w_\eta\right)$$

$$+ f\int_{-B}^{\eta} u dz = -\frac{1}{\rho_o}\int_{-B}^{\eta} \frac{\partial p}{\partial y}\, dz \tag{31}$$

and for mass,

$$\frac{1}{\rho_o}\int_{-h_D}^{\eta} \frac{\partial \rho}{\partial t}\, dz + \frac{\partial}{\partial x}\int_{-B}^{\eta} u dz + \frac{\partial}{\partial y}\int_{-B}^{\eta} v dz + w_\eta - u_s \frac{\partial \eta}{\partial x} - v_s \frac{\partial \eta}{\partial y} = 0 \quad . \tag{32}$$

Finally we apply our kinematic boundary condition at the free surface, and by utilizing the approximate thermodynamic equation (12) obtain:

$$\frac{\partial}{\partial t}\int_{-B}^{\eta} u\,dz + \nabla \cdot \vec{N}_x - f\int_{-B}^{\eta} v\,dz = -\frac{1}{\rho_o}\int_{-B}^{\eta}\frac{\partial p}{\partial x}\,dz \tag{33}$$

$$\frac{\partial}{\partial t}\int_{-B}^{\eta} v\,dz + \nabla \cdot \vec{N}_y + f\int_{-B}^{\eta} u\,dz = -\frac{1}{\rho_o}\int_{-B}^{\eta}\frac{\partial p}{\partial y}\,dz \tag{34}$$

$$\frac{\partial}{\partial x}\int_{-B}^{\eta} u\,dz + \frac{\partial}{\partial y}\int_{-B}^{\eta} v\,dz = -\frac{\partial \eta}{\partial t} - \frac{Q_o}{\rho_o} \tag{35}$$

where $\vec{N}_x$, $\vec{N}_y$ are the nonlinear integrals of advection.

We now form a top-to-bottom vorticity equation using the simplifications indicated by the scale analysis in Appendix A. First we neglect the nonlinear terms in (33) and (34) and then take the curl of these equations. Introducing volume transports (per unit width):

$$U \equiv \int_{-B}^{\eta} u\,dz, \quad V \equiv \int_{-B}^{\eta} v\,dz\ ,$$

we obtain:

$$\frac{\partial}{\partial t}\left(\frac{\partial V}{\partial x} - \frac{\partial U}{\partial y}\right) + f\left(\frac{\partial U}{\partial x} + \frac{\partial V}{\partial y}\right) + \beta V = -\frac{1}{\rho_o}\left(\frac{\partial}{\partial x}\int_{-B}^{\eta}\frac{\partial p}{\partial y}\,dz - \frac{\partial}{\partial y}\int_{-B}^{\eta}\frac{\partial p}{\partial x}\,dz\right)^{*}$$

Since we are considering atmospherically corrected pressure, we say $p_\eta = 0$, so that

---

*Note: β in this section refers to the planetary vorticity gradient.

$$\int_{-B}^{\eta} \frac{\partial p}{\partial x}\, dz = \frac{\partial}{\partial x} \int_{-B}^{\eta} p dz \ .$$

In this case the right-hand pressure terms above cancel. Using integrated mass then yields:

$$\frac{\partial}{\partial t}\left(\frac{\partial v}{\partial x} - \frac{\partial u}{\partial y}\right) = f\left(\frac{\partial \eta}{\partial t} + \frac{Q_o}{\rho_o}\right) - \beta v \tag{36}$$

We now go to the two-dimensional limit. In this limit, as defined by the scale analysis, the mass equation is given by (19) and the momentum equations (33), (34) simplify to:

$$\frac{\partial u}{\partial t} = fv \tag{33a}$$

$$fu = -\frac{1}{\rho_o} \int_{-B}^{\eta} \frac{\partial p}{\partial y}\, dz \ . \tag{34a}$$

Going to the 2-D limit in our vorticity equation, (36), and using (33a), (34a) to express the transports in terms of pressure, gives:

$$-\frac{\partial^2 u}{\partial y \partial t} \simeq \frac{\partial^2}{\partial t \partial y}\left(\frac{1}{\rho_o f} \frac{\partial}{\partial y} \int_{-B}^{\eta} p dz\right) = f\left(\frac{\partial \eta}{\partial t} + \frac{Q_o}{\rho_o}\right) - \beta v$$

$$\simeq f\left(\frac{\partial \eta}{\partial t} + \frac{Q_o}{\rho_o}\right) + \frac{\beta}{f^2 \rho_o} \frac{\partial^2}{\partial y \partial t} \int_{-B}^{\eta} p dz$$

which simplifies to:

$$\frac{1}{\rho_o f}\left\{\frac{\partial^3}{\partial y^2 \partial t} \int_{-B}^{\eta} p dz - \frac{2\beta}{f} \frac{\partial^2}{\partial y \partial t} \int_{-B}^{\eta} p dz\right\} = f\left(\frac{\partial \eta}{\partial t} + \frac{Q_o}{\rho_o}\right)$$

Although the scale analysis in Appendix A shows that the beta term is only marginally negligible for the scales considered, we will proceed now to an f-plane limit to further simplify the analysis. In regions where cyclonic vorticity is being generated (where $\frac{\partial^2 U}{\partial y \partial t} < 0$) the beta effect will tend to augment the circulation if the flow is accelerating to the west (so that $v < 0$) but diminish it if the flow is becoming more eastward. In regions of anticyclonic vorticity generation, eastward flow will be accelerated and westward flow diminished by retaining this beta effect.

So, for an f-plane model our vorticity equation becomes:

$$\frac{\partial^3}{\partial y^2 \partial t} \int_{-B}^{\eta} p dz = \rho_o f_o^2 \left(\frac{\partial \eta}{\partial t} + \frac{Q_o}{\rho_o}\right) . \tag{37}$$

It is now possible to utilize our density prescription to obtain the first of our model equations. We begin by integrating the pressure integral by parts:

$$\int_{-B}^{\eta} p d\hat{z} = \int_{-B}^{\eta} d\hat{z} \int_{\hat{z}}^{\eta} \rho g d\hat{\hat{z}} = \int_{-B}^{\eta} \rho g \hat{z} d\hat{z} + B \int_{-B}^{\eta} g d\hat{z} \equiv \Pi + B p_B .$$

Thus the quasi-geostrophic streamfunction is proportional to the sum of a potential energy term, Π, and a bottom pressure term, Bp_B. Fofonoff (1969) discusses a similar breakdown of the top to bottom transport field. Since the term arising from the bottom pressure is depth independent and is simply the bottom velocity times the total depth, he

refers to this part of the transport field as "barotropic." The depth dependent transport due to relative (to the bottom) velocities, as computed from the potential energy term, is referred to as baroclinic by Fofonoff (1969). It can be shown that to $O(\Delta\rho/\rho_o)$ the potential energy term is equivalent to the oceanographic transport streamfunction, relative to the bottom, as deduced from hydrographic data. The two quantities are not exactly related because of differences in pressure and geometric coordinate derivations, althouth the total transports are equivalent for the two coordinate systems.

Both Π and p_B can be written explicitly in terms of our prescription since $\rho(z)$ is given for all z. These integrals work out to be (refer again to Fig. 4):

$$\Pi = -g \left\{ \rho_B \frac{B^2}{2} + \beta \frac{(H^3-D^3)}{6} + \begin{bmatrix} \gamma h_s^3/6 \\ \gamma(h_{LS}^3 - h_m^3)/6 \\ 0 \end{bmatrix} \begin{Bmatrix} h \\ c \\ cv \end{Bmatrix} \right\} + \rho_s g \frac{\eta^2}{2} \qquad (38)$$

$$p_B = g \left\{ \rho_B B + \beta \frac{(H^2-D^2)}{2} + \begin{bmatrix} \gamma h_s^2/2 \\ \gamma(h_{LS}^2 - h_m^2)/2 \\ 0 \end{bmatrix} \begin{Bmatrix} h \\ c \\ cv \end{Bmatrix} \right\} + \rho_s g\eta \qquad (39)$$

Plugging these results into equation (37); utilizing the fact that B, ρ_B = constant, ρ_{LW} = constant and therefore (H-D) = constant when convection does not occur; and assuming that relative to h_m, h_{LS} is constant during erosion of the seasonal thermocline (all of these with respect to time), yields

$$\frac{\partial}{\partial y^2} \left\{ B(\beta\Delta D \frac{\partial H}{\partial t} + \begin{bmatrix} \gamma h_s \frac{\partial h_s}{t} \\ -\gamma h_m \frac{\partial h_m}{\partial t} \end{bmatrix} + \rho_o \frac{\partial \eta}{\partial t}) - \beta\Delta D \frac{(H+D)}{2} \frac{\partial H}{\partial t} - \begin{bmatrix} \gamma \frac{h_s^2}{2} \frac{\partial h_s}{\partial t} \\ -\gamma \frac{h_m}{2} \frac{\partial h_m}{\partial t} \end{bmatrix} + \rho_o \eta \frac{\partial \eta}{\partial t} \right\}$$

$$= \frac{\rho_o f_o^2}{g} \left(\frac{\partial \eta}{\partial t} + \frac{Q_o}{\rho_o} \right) \quad \text{[no deep convection]}$$

where $\Delta D \equiv H - D$ = constant with respect to time and we have neglected the pieces $\eta \frac{\partial \rho_s}{\partial t}$, $\frac{\eta^2}{2} \frac{\partial \rho_s}{\partial t}$, $\Delta\rho_s \frac{\partial \eta}{\partial t}$ to $O(\frac{\eta}{h}, \frac{\eta^2}{h^2}, \frac{\Delta\rho}{\rho_o})$. When convection occurs, this vorticity equation becomes:

$$\frac{\partial^2}{\partial y^2}\{B(\beta H \frac{\partial H}{\partial t} - \beta D \frac{\partial D}{\partial t} + \rho_o \frac{\partial \eta}{\partial t}) - \frac{\beta H^2}{2}\frac{\partial H}{\partial t} + \frac{\beta D^2}{2}\frac{\partial D}{\partial t} + \rho_o \eta \frac{\partial \eta}{\partial t}\}$$

$$= \frac{\rho_o f_o^2}{g}(\frac{\partial \eta}{\partial t} + \frac{Q_o}{\rho_o}) \qquad \text{[deep convection]}$$

We finally simplify these into one equation in two unknowns by pulling out the pieces which depend directly on the surface heat fluxes and are therefore assumed given by the Warren model thermodynamic equations (12). For the building and erosion of the seasonal thermocline:

$$\frac{\partial^2}{\partial y^2}\{\beta\Delta D(B-H+\frac{\Delta D}{2})\frac{\partial H}{\partial t} + \rho_o B \frac{\partial \eta}{\partial t} + Q_o[B - \{\frac{h_s/2}{h_m/2}\}] = \frac{\rho_o f_o^2}{g}(\frac{\partial \eta}{\partial t} + \frac{Q_o}{\rho_o}) \quad . \quad (40)$$

[no deep convection]

In reaching this equation, we have also neglected the η^2 term to $O(\eta/B)$ and used the constancy of ΔD to write $D = H - \Delta D$. Since h_s and h_m are known at any time from time integration of the thermodynamic equation, this is a nonlinear partial differential equation in η and H if Q_o is known.

The final form for the instance of convection is a bit different. In this case we assume that changes in the main thermocline thickness, ΔD, are due solely to the surface heat losses and that they are consonant with changes in the deep mixed layer density, i.e.,

$$\frac{\partial \Delta D}{\partial t} = \frac{1}{\beta} \frac{\partial \rho_{LW}}{\partial t} = \frac{Q_o}{\beta D} \quad .$$

This implicity assumes "non-penetrative" convection in which no entrainment of main thermocline water into the mixed layer occurs. Rather, the diffusive interface progresses into the main thermocline just at neutral stability by evenly cooling the mixed layer. Anati (1971) compares penetrative and non-penetrative models for deep convection in the Mediterranean and finds that the non-penetrative model predicts the observations much more closely. If wind stirring were included in this model, some penetrative convection might be expected, at least for the shallow convection when the seasonal thermocline is eroded. For the convection associated with cooling, however, we believe, as Warren (1972) did, that non-penetrative mixing is more appropriate.

The form of the vorticity equation during deep convection works out to be:

$$\frac{\partial^2}{\partial y^2} \{\beta \Delta D (B-H + \Delta D/2) \frac{\partial H}{\partial t} + \rho_o B \frac{\partial \eta}{\partial t} + Q_o [1 - D/2]\} = \frac{\rho_o f_o^2}{g} (\frac{\partial \eta}{\partial t} + \frac{Q_o}{\rho_o}) \quad (41)$$

where now ΔD is not constant and D must also be computed using the thermodynamic equation:

$$\frac{\partial D}{\partial t} = \frac{\partial H}{\partial t} - \frac{\partial \Delta D}{\partial t} = \frac{\partial H}{\partial t} - \frac{Q_o}{\beta D} \quad .$$

Although these total vorticity equations (40),(41), look complicated, it is helpful to view the left-hand side of the equations as the streamfunction (differentiated) which is composed of three

contributors: the free surface, the main thermocline, and the seasonal heat storage. Each of these contributions has a "barotropic" piece due to changes in bottom pressure, which are all multiplied by the total depth B. Each of the contributors also has a "baroclinic" piece (with the exception of the η^2 term we neglected) consisting of the nonlinear potential energy terms in H and D and also Q_o. The baroclinic buoyancy flux term is seen to have analogous form throughout the year, i.e., $-(h_D/2)Q_o$, where $h_D = h_s$, h_m, and D in heating, cooling, and deep convection, respectively. It is apparent that during convection larger changes in the baroclinic (Π) term will result for a given heat loss since then $h_D = D$ is about ten times larger than h_s or h_m.

2. Lower Layer Equations

At this point we have a total top-to-bottom vorticity statement in two unknowns, η and H. As a second equation we derive a vorticity statement for the deep, constant density layer. Since this is bounded by a flat bottom and the interface H, which is one unknown, it is suitable for a second equation and is considerably easier to use than the layer above $z = -H$.

The same steps are followed as for the total equation, so only an outline of the procedure is given below.

The two-dimensional, vertically integrated vorticity equation obtained by integrating between -B and -H is:

$$\frac{\partial}{\partial t}\left(-\frac{\partial U_L}{\partial y}\right) = -f_o \frac{\partial H}{\partial t}\ ; \quad U_L \equiv \int_{-B}^{-H} u\,dz\ .$$

Going to the quasi-geostrophic, f-plane limit gives:

$$\frac{\partial^2}{\partial y \partial t}\left(\frac{\partial \Pi_L}{\partial y} + B\frac{\partial p_B}{\partial y} - H\frac{\partial p_H}{\partial y}\right) = -\rho_o f_o^2 \frac{\partial H}{\partial t};\ \Pi_L \equiv \int_{-B}^{-H} \rho g z dz,\ p_H \equiv \int_{-H}^{\eta} \rho g dz\ .$$

However, since $\rho(z) \equiv \rho_B$ in this layer, this simplifies to:

$$\frac{\partial^2}{\partial y \partial t}\left((B-H)\frac{\partial p_B}{\partial y}\right) = -\rho_o f_o^2 \frac{\partial H}{\partial t}$$

showing the barotropic nature of this layer. Here we make a rather crude approximation to linearize this equation somewhat. We write $H = H_o + \delta H$ and neglect terms of $O(\delta H/H_o)$ in the left-hand term. This neglects variations of H in latitude as well as time and thereby also neglects time mean spatial variations. We will comment further on this later. This allows us to write the lower layer vorticity equation as:

$$\frac{\partial^2}{\partial y^2}\left[(B-H_o)\frac{\partial p_B}{\partial t}\right] = -\rho_o f_o^2 \frac{\partial H}{\partial t}\ .$$

Using our prescription for bottom pressure yields:

$$\frac{\partial^2}{\partial y^2}\left\{(B-H_o)\left(\beta \Delta D \frac{\partial H}{\partial t} + \rho_o \frac{\partial \eta}{\partial t} + Q_o\right)\right\} = -\frac{\rho_o f_o^2}{g}\frac{\partial H}{\partial t}$$

which is valid for any time of the year. To be consistent with this order of approximation we must also neglect terms of order $(\delta H/H_o)$ in our total vorticity equation. Our final resulting set of vorticity equations is therefore:

$$\text{Total:}\quad \frac{\partial^2}{\partial y^2}\left\{\frac{\beta\Delta D}{\rho_o}\left(1-\frac{[H_o-\Delta D/2]}{B}\right)\frac{\partial H}{\partial t}+\frac{\partial \eta}{\partial t}+\frac{Q_o}{\rho_o}\left(1-\frac{h_D}{2B}\right)\right\}=\frac{f_o^2}{gB}\left(\frac{\partial \eta}{\partial t}+\frac{Q_o}{\rho_o}\right) \tag{42}$$

$$\text{Lower:}\quad \frac{\partial^2}{\partial y^2}\left\{\left(1-\frac{H_o}{B}\right)\left(\frac{\beta\Delta D}{\rho_o}\frac{\partial H}{\partial t}+\frac{\partial \eta}{\partial t}+\frac{Q_o}{\rho_o}\right)\right\}=-\frac{f_o^2}{gB}\frac{\partial H}{\partial t} \tag{43}$$

where we have divided both equations by $\rho_o B$. It is interesting that the natural scale which multiplies the stretching terms is $f_o^2/gB = 1/\lambda^2$ where λ is the external Rossby Radius of deformation. Since our length scale in y is the same order ($\sim$1000 km) as the external radius of deformation, it is reasonable that the two sides of these equations are comparable. It will be seen later that this scale matching is a very important constraint on the solution.

III. Solution of Equations/Numerical Method

A. Form of Forcing and Boundary Conditions

The magnitude and, to some extent, the shape of the forcing we will use is based on data made available by Bunker. This will specify $Q_o(y)$ in our pair of vorticity equations, (42), (43). Since it is necessary to know the depth of the diffusive interface in computing the buoyancy flux potential energy terms in the total vorticity equation, we will also be integrating Q_o in time and using the time integrals of our density equation, (12), to evaluate h_D. We are, therefore, using the Warren model equations, except that Q_o is not a function of ρ_s (and thereby h_D) as it would normally be. Thus h_D is given directly from the integral of Q_o rather than being given by iteration to an equilibrium value of the two sides of the density equation.*

In Fig. 5 is shown the seasonal cycle of heating, with the annual mean removed, for several latitudes from 10°-40°N averaged between 50°-60°W. These are from monthly averages using all the available data from 1941-1972. It is apparent from this that at the northern latitudes the seasonal signal accounts for almost all the variance about the mean, but that farther south the semiannual oscillations become the same size as the annual signal. The general diminution in amplitude to the south is also apparent. The structure of the heating function in y is more clearly shown in Fig. 6. The destructive interference between the annual and semiannual signals is again apparent to the south.

In order to solve the system (42), (43) we need four boundary conditions. At the southern end of our domain (20-25°N) we say the forcing

* Q_o is given by an average value of α_*/c_p times the heat flux. (see (4))

actually diminishes to zero. This is done to separate the subtropics from the tropics dynamically and also because the annual signal becomes less dominant to the south. We then specify the homogeneous boundary conditions that neither the total nor the lower layer streamfunctions change at the southern end, consistent with zero forcing there. Since we don't know *a priori* how these quantities will respond, we are at a loss to specify more realistic southern boundary conditions.

We envision our northern boundary as the center of the eighteen degree water formation region, the subtropical gyre center, at about 35°N, where meridional gradients disappear. This is consistent with the zonal velocity being identically zero at the gyre center. Because of our simplified meridional momentum equation, the meridional velocity also goes to zero in the gyre center because the zonal acceleration there is zero. Therefore, we specify no slope boundary conditions on the total and lower layer streamfunctions. To be consistent with these homogeneous boundary conditions, we require the forcing to have no slope at the northern boundary also.

Of course it is rather artificial to apply boundary conditions such as these without real boundaries present. The southern condition is especially poor since the observed forcing really does not diminish to zero. Nonetheless, these seem more adequate than periodic domain sorts of conditions, and in the absence of prior knowledge of the system's response, the simplest homogeneous boundary conditions are at least a first step toward obtaining a unique solution to the governing equations.

Thus far, we have considered only the seasonal forcing. Since this has zero annual mean, the model will not be forced to go into deep convection. Rather, a seasonal thermocline will be developed in summer and exactly erased in winter. In Warren (1972) deep convection was forced to occur by beginning in a state with excessive heat content relative to the atmospheric state. Because of the dependence of the heat flux on surface temperature, his model eventually settled into a limit cycle with no net heat loss over a year, and he obtained a deep eighteen degree water layer due to several years of late winter deep convection. In this model, our beginning state is intended to model the observed mean state, which should correspond to the limit cycle reached in Warren (1972). Thus we wouldn't expect a net yearly heat loss to occur even if we had retained the thermodynamic feedback present in Warren's model.

To investigate the response of the model to deep convection and to eighteen degree water formation, we will impose "severe" winters which result in a net heat loss over a year. Warren (1972) defined a "severe" winter as one in which there is a net decrease of about 1°C in air temperature and a net increase of about 5 knots in wind speed averaged over the six months of winter. In terms of his forcing, this resulted in a rate of roughly 30-40 Watts/m^2 additional heat loss during the winter. Observations seem to show anomalies more like 50 W/m^2, possibly as large as 100 W/m^2, for heat flux variations from winter to winter. This is illustrated in Fig. 7 which shows various atmospheric and heat flux parameters for the area 30-40°N, 50-60°W for all years with available data. Although the area represented contains the Gulf Stream, we expect the magnitudes of the heat flux variations to be comparable for

our northern region. It is apparent that the large negative heat fluxes in "severe"* winters are correlated with large latent heat losses. These are not always due to anomalously high winds, though the wind direction is consistently from the northwest. The sensible heat losses, though smaller, are enhanced by anomalously cold air temperatures when the wind comes from this direction, as well as by the increased winds. Often it is the sensible flux which makes the difference between an average or "severe" winter.

An independent method of estimating the expected heat losses is to estimate the change in heat storage after a severe winter. Referring again to Fig. 2, we approximate the change in heat storage as follows: if we say the surface temperature was lowered by approximately 0.2°C in a severe winter, and this occurred over a depth range of 600 meters, the change in heat content would be about 12 kcal. If this was distributed evenly over a six month period, the average heat flux would then be roughly 30 W/m^2, very nearly the figure used by Warren (1972).

In our case studies of severe winters, we will investigate the response to a slowly varying net heat loss over the winter of about 100 $Watts/m^2$ maximum to the north, and to a very event-oriented heat loss of larger amplitude but shorter duration. The latter is intended to model the observed outbreaks of polar continental air in a severe winter. The amplitude of the seasonal forcing will be taken as 200 W/m^2 to the north, with both the seasonal and winter anomalies diminishing to zero at the

*Here heat fluxes larger than -400 W/m^2 (seasonal and mean) are considered "severe" as indicated by the dashed horizontal line in Fig. 7.

southern end. Various shapes in the meridional direction will be used. as will be shown with the results obtained from the model.

B. Method of Solution

Now that boundary conditions have been defined, we can proceed to solve the governing equations (42),(43). Since the Warren model is local in nature, we wish to obtain a quasi-local form of the vorticity equations. This is accomplished by integrating both equations twice with respect to y, with the limits of integration chosen to utilize the boundary condtions explicitly. The form of the equations obtained by these y-integrations ends up being simpler to solve than the finite difference equations obtained without integration. This simplification is only possible because of the integrable form we have arrived at in (42) and (43). If it was necessary to include the nonlinear terms neglected by dropping $\delta H/H_o$ terms, or to include beta effects, it would probably not be to our advantage to utilize this y-integration method.

The simplest trapezoidal rule approximation will be utilized to estimate the two double integrals which result from the integration of the vortex stretching terms. There is a numerical problem with the northern, no-slope boundary condition when this form is used, however, so it is necessary to actually double the domain of interest. The no-slope condition is then obtained by mirror symmetry about the midpoint of the doubled domain. Thus if we have a domain of length L, in the double domain we specify -L as the southern end, 0 as the northern end, and L as the mirror image of the southern end. The following example indicates the derivation:

$\phi_{yy} = \theta;\ \phi(0) = 0,\ \phi_y(L) = 0$ [single domain]

$\phi_{yy} = \theta;\ \phi(-L) = 0,\ \phi(+L) = 0$ [double domain]

integrating once

$$\phi_y(y) - \phi_y(-L) = \int_{-L}^{Y} \theta d\hat{y}$$

integrating again

$$\phi(y) - \phi(-L) = \int_{-L}^{Y} d\hat{y} \int_{-L}^{\hat{Y}} \theta d\hat{\hat{y}} + \int_{-L}^{Y} \phi_y(-L) d\hat{y}$$

by b.c. at -L and since $\phi_y(-L)$ = a constant

$$\phi(y) = \int_{-L}^{Y} d\hat{y} \int_{-L}^{\hat{Y}} \theta d\hat{\hat{y}} + (y+L)\phi_y(-L)$$

by b.c. at +L

$$\phi(L) = \int_{-L}^{L} d\hat{y} \int_{-L}^{\hat{Y}} \theta d\hat{\hat{y}} + 2L\,\phi_y(-L) = 0$$

$$\therefore\ \phi_y(-L) = -\frac{1}{2L} \int_{-L}^{L} d\hat{y} \int_{-L}^{\hat{Y}} \theta d\hat{\hat{y}}$$

final form

$$\phi(y) = \int_{-L}^{Y} d\hat{y} \int_{-L}^{\hat{Y}} \theta d\hat{\hat{y}} - \frac{(y+L)}{2L} \int_{-L}^{L} d\hat{y} \int_{-L}^{\hat{Y}} \theta d\hat{\hat{y}} \quad . \tag{44}$$

The final form obviously satisfies the boundary conditions at $y = \pm L$. It is relatively easy to show that, if θ is an even function about $y = 0$ (as it should be by mirror symmetry), the boundary condition $\phi_y(0) = 0$ is also satisifed.

By direct analogy, the double integration of (42), (43) is equivalent to

$$\phi = \frac{1}{B}\frac{\partial \Pi}{\partial t} + \frac{\partial p_B}{\partial t}, \quad \theta = \frac{f_o^2}{gB}\left(\frac{\partial \eta}{\partial t} + \frac{Q_o}{\rho_o}\right)$$

and

$$\phi = \left(1 - \frac{H_o}{B}\right)\frac{\partial p_B}{\partial t}, \quad \theta = -\frac{f_o^2}{gB}\frac{\partial H}{\partial t}$$

respectively, in (44). The equations obtained from this procedure are then:

$$\frac{\beta \Delta D}{\rho_o}\left(1 - \frac{(H_o - \Delta D/2)}{B}\right)\frac{\partial H}{\partial t} + \frac{\partial \eta}{\partial t} + \left(1 - \frac{h_D}{2B}\right)\frac{Q_o}{\rho_o} = \frac{f_o^2}{gB} I\left\{\frac{\partial \eta}{\partial t} + \frac{Q_o}{\rho_o}\right\} \tag{45}$$

$$\frac{\beta \Delta D}{\rho_o}\frac{\partial H}{\partial t} + \frac{\partial \eta}{\partial t} + \frac{Q_o}{\rho_o} = -\frac{f_o^2}{gB}\frac{I\left\{\frac{\partial H}{\partial t}\right\}}{\left(1 - \frac{H_o}{B}\right)} \tag{46}$$

where

$$I\{\ \} \equiv \int_{-L}^{y} d\hat{y} \int_{-L}^{\hat{y}} \{\ \} d\hat{\hat{y}} - \frac{(y+L)}{2L}\int_{-L}^{L} d\hat{y} \int_{-L}^{\hat{y}} \{\ \}\, d\hat{\hat{y}}$$

is a function of y coupling the left-hand side quantities, defined at that position in y, with all other points in y.

The numerical procedure utilized in the model further simplifies (45), (46) in two ways. First, as mentioned above, a trapezoidal approximation

is used for the double integral "I". The derivation, given in Appendix B, gives a simple set of weights to each point, depending on the position where the equations are to be solved. Thus at a position y_i the double integral is a weighted sum from all points at y_j so that:

$$I_i\{\ \} \simeq (\Delta y)^2 \sum_{j=1}^{2M+1} a_{ij}\{\ \}_j$$

where M is the number of divisions into which the single domain is split, such that $\Delta y = L/M$, and the total number of points is 2M+1.

The second finite element simplification to (45), (46) is a time-stepping integration. Over a small time step we linearize the equations by assuming the coefficients are nearly constant, so that all the terms (except Q_o) are perfect integrals. Since Q_o is given analytically, so is its integral. After each time step, all coefficients are then updated and another time-step is executed.

With these numerical approximations, over any time step δt, we have two algebraic equations to solve at each point:

$$\frac{\beta \Delta D_i}{\rho_o}\left(1 - \frac{(H_o - \Delta D_i/2)}{B}\right)\delta H_i + \delta\eta_i + \left(1 - \frac{h_{Di}}{2B}\right)\frac{\bar{Q}_{oi}}{\rho_o}$$

$$= \frac{(f_o \Delta y)^2}{gB} \sum_{j=1}^{2M+1} a_{ij}\left(\delta\eta_j + \frac{\bar{Q}_{oj}}{\rho_o}\right) \qquad (47)$$

$$\frac{\beta \Delta D_i}{\rho_o}\delta H_i + \delta\eta_i + \frac{\bar{Q}_{oi}}{\rho_o} = \frac{(f_o \Delta y)^2}{-gB} \sum_{j=1}^{2M+1} a_{ij}\delta H_j/(1-H_o/B) \qquad (48)$$

where the subscript "i" refers to the position of interest, the overbar on Q_o is a time integral (which is given), δH and $\delta\eta$ are the changes over δt, and the coefficients of δH and $\overline{Q_o}/\rho_o$ are assumed constant over the time step and equal to their most recent, updated value.

Because of the nature of the Warren model, it is necessary to keep track of the signs of the heat flux as well as the sign of the total heat input for every point in y. We begin the time integrations at a state of rest (except possibly for flows due to the mean field geometry imposed), i.e., $\eta = 0$; $H = H_o$; $h_D = 0$; $Q_o, \overline{Q_o} = 0$ at $t = t_o$. We identify t_o as the time that summer heating begins, roughly the end of March (refer again to Fig. 5). We proceed to step (47) and (48) forward in time, identifying $h_D = h_S$, the depth of the seasonal thermocline. (Refer to Fig. 4.) This continues until the sign of Q_o changes from negative to positive. We then integrate forward with $h_D = h_m$, the depth of the mixed layer that is eroding into the seasonal thermocline. Up to this point ΔD has been held constant. When the sign of $\overline{Q_o}$ changes, i.e., when all the buoyancy gained in summer is lost in winter, or equivalently, when $h_m = h_{LS}$ and the seasonal thermocline is erased, we identify $h_D = D$ and allow ΔD to change as we are now in deep convection. We reiterate that without an imposed winter anomaly, $\overline{Q_o}$ will go to zero at the end of winter but then heating will begin again. Only with a net heat loss over the year will deep convection occur for a finite period of time in late winter.

Since there is no long term adjustment mechanism by feedback between the surface temperature and surface heat fluxes, there is no point in integrating over more than a one-year period. Values of the quantities of interest will thus be presented at two times: the end of heating, when

the fields are perturbed maximally by seasonal heating, and at the end of the year when any net change is due solely to deep convection. The time history between these points is sinusoidal, except for the shape in time of the winter anomalies.

We still have not indicated how the pair of equations (47), (48) is to be solved at each time step for all the points in y. Since all points enter the equations at every other point, we really have a pair of equations for each point in 2*(2M+1) unknowns, with a similar pair of equations for each of the 2M + 1 points.

It would appear that this system of equations could be solved by breaking the integral approximation into individual weighted terms and solving the entire 4M + 2 by 4M + 2 system of algebraic equations. This was in fact done before we realized that the resulting answer was very dependent on the resolution and therefore on M. The reason is that the integral approximation converges to the true integral by summing increasing numbers of terms weighted by increasingly smaller factors ($\Delta y^2 a_{ij}$) as the resolution increases. Thus, the terms from the integral approximation were very small relative to the unintegrated terms. To avoid this problem, we employ an iterative technique whereby only two equations are solved at each point for the two unknowns $\delta\eta_i$, δH_i at that point, holding the two integral approximations (now summed) constant. The integrals are then updated using the new values of $\delta\eta_i$ and δH_i and the next point is solved. After proceeding through all 2M + 1 points, constantly updating the integral, the procedure is repeated beginning again at the first point. This running through all the points is continued until the values of all the $\delta\eta$'s, δH's are not changing by more than a small accuracy criterion.

In this way we iteratively solve for all points in y at each time step, then update all the variables, and solve at the next time step. We proceed to integrate ahead in time for a year in this manner, keeping track of the nature in which the heat fluxes affect the model at each point at any time. This, then, is the actual numerical procedure used to solve the model given by (47) and (48) for the free surface changes $\delta\eta$ and the main thermocline motions δH.

C. Analytic Nature of Equations

Before proceeding to a discussion of the results obtained from the numerical model, let us give a prelude to the ultimate conclusion by analyzing the solutions for a constant coefficient approximation of the governing equations.

We consider the time integrated form of (42), (43) or an unintegrated (in y) form of (47), (48); the constant coefficient (in y) equations are then:

$$\frac{\beta\Delta D}{\rho_o}\left(1 - \frac{(H_o-\Delta D/2)}{B}\right)\delta H_{yy} + \delta\eta_{yy} + (1-h_D/2B)\frac{\overline{Q}_{oyy}}{\rho_o} = \frac{f_o^2}{gB}\left(\delta\eta + \frac{\overline{Q}_o}{\rho_o}\right) \tag{49}$$

$$\frac{\beta\Delta D}{\rho_o}\delta H_{yy} + \delta\eta_{yy} + \frac{\overline{Q}_{oyy}}{\rho_o} = \frac{-f_o^2}{gB}\,\frac{\delta H}{(1-H_o/B)} \tag{49a}$$

It is inconsistent to consider h_D constant in y if Q is not, but for illustrative purposes let us assume constant coefficients and write (49) and (49a) as ordinary differential equations in y:

$$(1-\Delta')\varepsilon\ddot{x}_1 + \ddot{x}_2 + (1-\delta)\ddot{Q} = \lambda^{-2}(x_2 + Q) \tag{50}$$

$$\varepsilon\ddot{x}_1 + \ddot{x}_2 + \ddot{Q} = -\frac{\lambda^{-2}}{(1-\Delta)}\, x_1 \tag{51}$$

where:

$$x_1 \equiv \delta H$$

$$x_2 \equiv \delta\eta$$

$$\Delta \equiv H_o/B$$

$$\Delta' \equiv (H_o - \Delta D/2)/B$$

$$\delta \equiv h_D/2B$$

$$\lambda^{-2} \equiv 1/(\text{Rossby Deformation Radius})^2 \equiv f_o^2/gB$$

$$\varepsilon \equiv \beta\Delta D/\rho_o \sim \Delta\rho/\rho_o \quad (<0)$$

$$(\ddot{}) \equiv (\ )_{yy}$$

$$Q \equiv \overline{Q_o}/\rho_o$$

Since these equations are linear in the unknowns x_1 and x_2, we can go to fourth order to eliminate one unknown between (50), (51). The governing equations work out to be:

$$\Delta'\varepsilon\ddot{\ddot{x}}_1 + \left(\frac{1}{1-\Delta} - \varepsilon\right)\lambda^{-2}\ddot{x}_1 - \frac{\lambda^{-4}}{(1-\Delta)}\, x_1 = \lambda^{-2}\ddot{Q} - \delta\ddot{\ddot{Q}} + [-\lambda^{-2}\ddot{Q}] \tag{52}$$

$$\Delta'\varepsilon\ddot{\ddot{x}}_2 + \left(\frac{1}{1-\Delta} - \varepsilon\right)\lambda^{-2}\ddot{x}_2 - \frac{\lambda^{-4}}{(1-\Delta)}x_2 = -\lambda^{-2}\left(\frac{1-\delta}{1-\Delta}\right)\ddot{Q} + (\delta-\Delta')\varepsilon\ddot{\ddot{Q}} + \left[\varepsilon\lambda^{-2}\ddot{Q} + \frac{\lambda^{-4}}{(1-\Delta)}\, Q\right]$$

(53)

The bracketed terms are separated because they result from retaining the thermal expansion effects within the seasonally influenced layers. It is already apparent that neglecting these effects would be inconsistent since the right hand side terms are comparable.

It is evident from (52), (53) that both unknowns satisfy the same homogeneous equation. It is easy to show that the homogeneous solution is composed of two growing and two decaying exponentials:

$$x_{1\ \text{hom.}} = \sum_{i=1}^{4} c_i\, e^{p_i y}$$

$$x_{2\ \text{hom.}} = \sum_{i=1}^{4} d_i\, e^{p_i y}$$

where the c_i's and d_i's are related by the coupled equations (50), (51).

By plugging in the exponential form to the homogeneous equation and solving the quartic that results, the approximate e-folding scales work out to be:

$$p_{1,2} \simeq \pm\lambda^{-1} \qquad \text{to } O(\varepsilon^{1/2})$$

$$p_{3,4} \simeq \pm \frac{\lambda^{-1}}{\sqrt{\Delta' |\varepsilon| (1-\Delta)}}$$

We recognize λ as the external radius of deformation, and find that

$$\lambda\sqrt{|\varepsilon|} = \sqrt{gB}/f_o * \sqrt{|\beta|\Delta D/\rho_o} = \sqrt{g'B}/f_o$$

is the internal radius of deformation since $g' \equiv \frac{|\beta|\Delta D}{\rho_o} = \frac{\rho_{-H} - \rho_{-D}}{\rho_o} g$.

Thus apart from the $\sqrt{\Delta'(1-\Delta)}$ factor, the e-folding lengths are approximately the internal and external radii of deformation. The "internal" radii solutions give a boundary layer structure to the total solution allowing the two additional boundary conditions, necessitated by the first term in (52), (53), to be met.

For the special case where Q has no fourth derivative (discussed below), it can be seen by inspection that when we retain thermal expansion the main thermocline perturbations (x_1) satisfy the homogeneous equation with no need for a particular solution. It is also evident that the particular solution for the free surface (x_2) in y, will very closely approximate the shape of Q, but will be of opposite sign when we retain the thermal expansion effects.

We actually worked through the complete analytic solution for the coupled pair (52), (53) for the simple case of cubic forcing, retaining thermal expansion.Because we have chosen such a convenient shape for the forcing, which satisfies the same homogeneous boundary conditions that we require the total and lower layer streamfunctions to satisfy, it ends up that if our two unknowns also satisfy the homogeneous boundary conditions, so will the streamfunctions. Thus it was possible to uncouple the boundary conditions and use them explicitly to obtain a closed form solution for the free surface and the main thermocline displacements. The solution indicated a main thermocline displacement of only several centimeters on the 1000 km domain scale. The free surface displacement was within a centimeter of $-Q_o/\rho_o$ everywhere, with the difference between them gradually increasing to a maximum at the gyre center. Since the main thermocline excursions were so tiny, retaining the thermal expansion effects in

the seasonal layer is the only consistent procedure for the total vorticity equation, as indicated by our scale analysis.

The analytic solution indicated that a larger main thermocline response (but still only a few meters displacement) would be excited if the domain scale was on the order of the internal radius of deformation. We also found that a forcing shape which did not satisfy the homogeneous boundary conditions could lead to an internal deformation radius scale boundary layer for the main thermocline, which could have a few meter amplitude. In all cases the free surface was nearly equal and opposite to the integrated density flux divided by ρ_o.

This finding that on large (external radius) scales a very small main thermocline excursion is forced and that on small (internal radius) scales a much larger excursion is forced was the essential conclusion gained from the constant coefficient equations. In the next section we investigate this finding further using the more accurate numerical procedure. The results will nonetheless show that the details of the full model don't greatly alter the result found here.

It should also be mentioned in passing that considering a small domain width doesn't invalidate our scaling arguments for the dynamical equations. As long as we don't consider scales smaller than the internal deformation radius, the scale analysis still holds since we specify a two dimensional limit. Though the main thermocline excursions become order of meters on short scales, retaining thermal expansion in the seasonal layer is still necessary for the mass conservation equation. If main thermocline excursions got to be tens of meters large, this would no longer be necessary and the neglect of vertical advection in the seasonal layer might become inconsistent.

IV. Numerical Model Results/Discussion

A. Introduction

The full numerical model vorticity equations (42), (43) rewritten with our prescribed boundary conditions as (45),(46) were solved with the following values for the parameters entering the formulation:

$$\left.\begin{aligned} \beta &= -\alpha^* \rho_o \beta_T = -(2\times10^{-4\,o}C^{-1})(50\ m/^oC)^{-1}(1g/cc) \simeq -.4\Delta\sigma_T/100\ m \\ \gamma &= -\alpha^* \rho_o \gamma_T = -(2\times10^{-4})(15\ m/^oC^{-1})(1g/cc) \simeq -1.0\Delta\sigma_T/100\ m \end{aligned}\right\} \text{After Warren}$$

$$\begin{aligned} B &= 5000\ m \\ H_o &= 1500\ m \\ \Delta D_o &= 700\ m \\ f_o &= 10^{-4}s^{-1} \\ L &= 1000\ km \\ \Delta y &= 100\ km \\ \delta t &\simeq 2\ wks \\ T_B &= 4^oC \end{aligned} \qquad (54)$$

Increasing the resolution in time or space didn't change the final values of η or H by more than 10^{-2} cm, with a discrimination factor in the iterations of 10^{-3} cm.

Various shapes for the forcing in space were used with two shapes for the winter anomalies in time. The seasonal heating amplitude was 200 W/m^2 and the winter anomalies were 100 W/m^2 amplitude when spread broadly over

six months, and about 400 W/m^2 when occurring over a short (4 week) period.

Variations on the theme ((54) and various mean states for ΔD_o, H_o were run using a single forcing. The basic state was intended to model the horizontal distribution of properties as closely as possible. In the linearization of the vorticity equations, where terms of order $\delta H/H_o$ were neglected, one important effect of the mean state was removed. This linearization not only removes the time varying perturbations about H_o, which is not a bad approximation, but also removes the variations in latitude of the main thermocline depth. Thus the main thermocline slope associated with the mean circulation was also removed. This effect of the mean thermocline tilt would act on the lower layer vorticity analogously to the beta effect already neglected, or similar to a slope in the ocean bottom, also neglected. The order of approximation in neglecting the mean thermocline tilt and the beta effects (both dropping terms of $O(10^{-1})$) was self-consistent albeit marginal. These effects would be the first that need be retained in a less simplified model. It is possible that vortex stretching associated with seasonal meridional movements within a sloping mean state could reduce somewhat the barotropic signal that appears inthe results that follow.

The linearized mean state we used is shown in Figure 8. Note that variations in the main thermocline thickness were retained since it was not necessary to linearize these.

Because it was reasoned that thermal expansion effects within the seasonal layer should be retained (and the results show δH, $\delta\eta$ and $\overline{Q}_o/\rho_o$

are comparable) we won't discuss any incompressible runs in the following.

We will proceed to examine first the system's response to the seasonal, zero-mean, forcing by presenting results at the end of the heating phase when the seasonal perturbations are a maximum. The sensitivity of the model to various oceanic states will be investigated with a given amplitude, and large-scale variations, of the seasonal forcing. We will then examine the model's response to anomalies in winter forcing, and the resulting eighteen degree water formation, by presenting results at the end of a year before heating ensues again. This will be done using a fixed oceanic state, but with various shapes for the winter anomalies in both space and time. We use the large-scale, slowly varying forcing for the seasonal cycle based on the observations shown in Figure 6. The winter anomalies, however, may be quite localized in both time and space, so we investigate the smaller-scale forcing variations in the late winter results.

B. End of Heating Results

We begin this section with a discussion of the terminology used when presenting derived quantities such as transport and velocities, as computed from the perturbation fields $\delta\eta$, δH, and $\overline{Q}_o/\rho_o$. These latter three quantities are the cumulative response of the free surface and main thermocline, and the integrated density flux , respectively, at the end of the heating season.

We partition the total top to bottom transport (per unit width) in the following manner:

$$\text{barotropic transport/width} \equiv \text{TRBTW} = \frac{B}{\rho_o f_o} \{\Delta P_B\}$$

$$\text{baroclinic transport/width} \equiv \text{TRBCW} = \frac{1}{\rho_o f_o} \{\Delta \Pi\}$$

where the difference, Δ, is between two positions in y, as between two hydrostations. The cumulative transports follow from the sums of these quantities over all station pairs. This breakdown into baroclinic and barotropic follows the terminology of Fofonoff (1969) for the transports relative to the bottom as discussed earlier. Since our deep lower layer has no horizontal density gradients and therefore no geostrophic velocity shear, the model baroclinic transport, which is comparable to the oceanographically observed relative transport, is really relative to the deepest depth of the main thermocline. In comparing model baroclinic transports with observations, then, they are really more comparable to transport relative to 2000 m, say, than to the bottom.

The distinction should be kept in mind between barotropic vs. external and baroclinic vs. internal. This is illustrated in Table I. There are three contributions to bottom pressure, and therefore to barotropic transport changes. They are the free surface term, $\rho_o g \delta\eta$, the main thermocline term, $\rho_o g' \delta H$, and the heat flux term $g\overline{Q}_o$. There are similarly three contributions to the potential energy and therefore to baroclinic transport changes, although we neglect the free surface term. If we considered "internal" as synonomous with "oceanographic" these would both then be equivalent to our definition of baroclinic since we've neglected the external potential energy term. If we consider "internal" as being due to everything but the free surface (as in Table I) there

would be barotropic pieces and baroclinic pieces from the heating terms as well as from the main thermocline terms which would be categorized as internal. Only the internal potential energy terms are used in computing oceanographic relative transports.

Rather than breaking down the transport in all these ways, in the following we split it into barotropic, baroclinic (or oceanographic), total, and lower layer (which is a constant fraction, $1 - H_o/B$, of the barotropic transport).

To show the relative importance of the internal, external, heating, main thermocline, etc. contributions, we will present a set of perturbation zonal velocities. The breakdown is as follows:

geostrophic shear across main thermocline $\equiv$ UGM $= \frac{g}{\rho_o f_o} (\Delta(\beta \Delta D \delta H)/\Delta y)$

geostrophic shear across seasonal layer $\equiv$ UGS $= \frac{g}{\rho_o f_o} (\Delta \bar{Q}_o/\Delta y)$

actual surface (external) velocity $\equiv$ US $= - \frac{g}{f_o} (\Delta \eta/\Delta y)$

actual bottom (barotropic) velocity ($\neq 0$ as for rel. vel.) $\equiv$ UB = US - UGM - UGS

In addition we will present the vertically integrated meridional velocities, averaged over the heating cycle, as computed from the momentum equations:

$$VT \equiv - \frac{1}{\rho_o f_o^2} \frac{\Delta(\Pi + B p_B)}{\Delta t \Delta y} \quad \text{where } \Delta t = 6 \text{ months.}$$

If these meridional transports/width were spread over 1000 km in the zonal direction, the cgs units of this quantity would represent 10^{-4} Sv. Now

that semantics are cleared up, let us proceed to the discussion of results.

We begin by testing the model sensitivity to the parameters given in (54). This was done with a forcing which was cubic in y and corresponded to a heat flux maximum of 200 W/m^2 in the gyre center, diminishing to zero to the south.

It was found that even for unrealistically thin main thermocline thickness ($\sim$50 m) and much shallower main thermocline depths (1000 m vs. 1500 m for H_o) the results obtained weren't very different. Similarly, specifying a constant thickness (in y) main thermocline didn't alter the results observably. These results (not presented) indicated that the model is <u>not</u> sensitive to the prescription details as long as they are somewhat realistic. But, as mentioned earlier, retaining the mean tilt of the main thermocline could yield somewhat different results. The main constraint is really that the density difference across the thermoclines be small. Only if we specified a bizarre thermocline with $\Delta\rho/\rho_o \sim 1$ could a vastly different set of results be obtained. Of course, if we weren't prescribing the surface heat fluxes, but rather were using the full Warren model with thermodynamic feedback, it would be very important to have a realistic mean state so that the surface temperature and resulting heat fluxes would also be realistic.

The model did exhibit an interesting response to the total depth, B, however. In the case of an unrealistically deep lower layer ($B \sim 10{,}000$ m) it was found that the main thermocline responded more (but only of order cms) than when the lower layer was very thin ($B \sim H_o$).

In both cases the free surface tracked $-\bar{Q}_o/\rho_o$ closely. These results are shown in Fig. 9.

In light of the constant coefficient equations (50), (51) this result makes sense. In the limit that $B \to H_o$ we see that $\Delta \to 1$. In this case the lower layer equation (51) (when multiplied through by $(1-\Delta)$) must have both sides go to zero. This requires the main thermocline response (as x_1) to vanish. We are then left, in this limit, with only the first equation to be satisfied by the free surface response (as x_2) alone. The total boundary conditions can be satisfied for $x_1 \equiv 0$ if x_2 satisfies the same homogeneous boundary conditions, given the forcing we have imposed. If the forcing itself did not satisfy the homogeneous boundary conditions it would still be possible to obtain a solution, in this limit, with no main thermocline motion. Physically this would say that when the lower layer becomes very thin the stretching associated with main thermocline motions causes large changes in this layer's total vorticity. But since the only way to balance this is through changes in quasigeostrophic relative vorticity, and since these changes are small because $\delta\eta + \bar{Q}_o/\rho_o$ is small and because main thermocline contributions are diminished by reduced gravity, the only balance that can be obtained is for the stretching to be very small. When the layer is very deep this constraint is relaxed and the main thermocline can move more, but still only on the order of centimeters.

It is interesting that in the limit of infinite lower layer depth, there is a particular solution to the constant coefficient equations which also has no main thermocline response. Returning to (50), (51) it can

be seen that when $B \to \infty$ the small terms Δ, Δ', δ all approach zero. It can be seen by inspection that the particular solution to this limiting system is $x_2 = -Q$, $x_1 \equiv 0$. The homogeneous solution collapses to: $x_{1h} \simeq C_{\pm}\exp(\pm y/\lambda)$; $x_{2h} = -x_{1h}$, which can only satisfy two boundary conditions. This results because the potential energy term, Π, is negligible compared to Bp_B when $B \to \infty$, so that only two boundary conditions, on p_B, can be satisfied. With our homogeneous boundary conditions, and our forcing which also satisfies those conditions, the two homogeneous solutions are identically zero so that the total main thermocline response is zero. For a more general forcing shape, a nonzero response of the main thermocline, equal and opposite to the homogeneous free surface response, would be obtained.

In the process of going to the limit of infinite lower layer depth, it can be seen from the uncoupled constant coefficient equations (52), (53) that the boundary layers on the internal deformation radius scale get narrower as the fourth order terms are diminished when $\Delta' \to 0$. Going to $\Delta' \equiv 0$ is then like a singular perturbation limit where we lose the boundary layer solutions.

For our region of interest, however, a flat bottom model would have a deep lower layer as prescribed in (54). The only parameters left to vary, then, are the domain length and the shape of the forcing itself. In Fig. 10 we compare the values of $\delta\eta$ and δH at the end of heating for various domain lengths but with the same relative shape of the forcing. The horizontal scale is nondimensionalized by the total domain length, but the resolution in each case is ten. For the large domain, which has a forcing shape more close to that observed, the main thermocline response

is diminished relative to the smaller domains. Coincident with this, the free surface is actually further from balancing $-\bar{Q}_o/\rho_o$. For the small domain there is closer balance between $\delta\eta$ and $-\bar{Q}_o/\rho_o$ and a larger main thermocline response.

The transports for these three runs are compared in Table II. It can be seen that for the large domain the larger imbalance of $\delta\eta$ and $-\bar{Q}_o/\rho_o$ results in a barotropic transport of about 3 SV to the east after summer heating, compared with only about .5 SV for the 500 km domain.

Although the main thermocline response is greater for the 500 km domain, the resulting effect on baroclinic transport is still small, so that for both the large and small domains the baroclinic transport is nearly the same, and due primarily to potential energy changes associated with the surface buoyancy fluxes. The total transports are very small for the small domain since the small barotropic transports are nearly equal and opposite to the baroclinic ones. The large domain has a significant total transport which is primarily barotropic.

The main thermocline response is similarly amplified if the forcing varies over shorter scales, for the same domain length. This is illustrated in Fig. 11 where a Gaussian forcing with a decay scale of 500 km is used for comparison with the smoother cubic forcing used previously. Besides the change in the shape of the main thermocline response, the amplitude is larger when the forcing has larger curvature. The differences in shape are not so large in this case as to yield great differences in response, but the tendency is the same as that due to reducing the whole domain length. This example also shows that a forcing with non-zero fourth derivatives doesn't excite a particularly different response than the simple cubic forcing investigated analytically.

The reason that the main thermocline responds more when the scale of the forcing variations is diminished can be seen by evaluating one limiting case of the simplified analytic equations (50), (51). Because the homogeneous roots of these equations have two distinct decay scales, the internal and external deformation radii, it would be expected that two rather distinct solutions would be obtained, depending on the ratio of L/λ. If we nondimensionalize the differentiation on the left hand side of (50), (51) by the domain length L, over which order one variations in forcing occur, the ratio L/λ then multiplies the right hand stretching terms. Rewriting the main thermocline terms, in anticipation of a much larger response, transforms these equations to:

$$(1-\Delta')\hat{x}_1'' + x_2'' + (1-\delta)Q'' = (L/\lambda)^2(x_2+Q) \tag{55}$$

$$\hat{x}_1'' + x_2'' + \quad Q'' \quad = -(L/\lambda)^2 \frac{\hat{x}_1}{\varepsilon(1-\Delta)} \tag{56}$$

where primes denote the nondimensionalized differentiation and $\hat{x}_1 \equiv \varepsilon x_1$.

If we go to a small-scale limit where L is the order of the internal deformation radius, i.e., $L \sim \sqrt{|\varepsilon|}\lambda$, these equations become:

$$\left.\begin{aligned} (1-\Delta')\hat{x}_1'' + x_2'' + (1-\delta)Q'' &= |\varepsilon|(x_2+Q) \qquad (57)\\ \hat{x}_1'' + x_2 \quad + \quad Q'' \quad &= + \frac{\hat{x}_1}{(1-\Delta)} \qquad (58) \end{aligned}\right\} L \sim \sqrt{|\varepsilon|}\lambda$$

In this limit we can make a kind of rigid lid approximation and neglect the stretching term from the free surface/buoyancy flux difference,

$x_2 + Q$, and the main thermocline stretching term on the right hand side of (58) is $O(1)$ rather than $O(1/\varepsilon)$, as it would be in this formulation for the large scales heretofore considered. Physically this would say that on scales of the internal deformation radius, the total top to bottom relative vorticity is very nearly conserved. The lower layer relative vorticity is still changed by stretching associated with main thermocline heaving. Even so, the relative vorticity changes for the lower layer are much larger because of the short scales, so that even for the stretching caused by tens of meters of main thermocline motion, the relative vorticity can easily adjust to balance this. Because of the reduced gravity factor on the main thermocline contribution to relative vorticity (incorporated in $\hat{x}_1$ above), if large heaving results, the main thermocline part of vorticity changes becomes as important as the free surface and buoyancy flux parts, rather than much larger.

It is apparent from (57), (58) that $\hat{x}_1$ and x_2 will be the same order as Q, in general, so that the main thermocline response could be on the order of $Q/|\varepsilon|$, which is tens of meters. It works out that the actual solution to (57), (58) satisfying the homogeneous boundary conditions on the unknowns x_1 and x_2 (and thereby for the total and lower layer streamfunctions since Q also satisfies these conditions) gives as the order of magnitude:

$$x_1 \sim \frac{\delta}{|\varepsilon|} Q, \quad x_2 \simeq -Q \ .$$

For the heating phase just considered, the ratio $\delta/|\varepsilon|$ would be about three so that main thermocline excursions greater than a meter wouldn't be

expected even for small-scale variations in forcing. However, during deep convection $\delta(=D/2B)$ is nearly an order of magnitude larger, so that sizable main thermocline motion might occur. Examining this possibility will be part of the aim of the next section where we investigate the model response to winter anomalies of various shapes in time, as well as space, and see the response forced by the deep convection that ensues.

C. End of Convection Results

We have thus far considered only the zero mean, seasonal heating cycle and the dynamic response to it. In a time average sense, the latitudinal variations of the heating function occur over 1000 km scales and the time history for any year is very nearly sinusoidal away from the tropics.

On the other hand, winter anomalies are often observed to have very event-like characteristics. This could be manifested in a localization in time, space, or both. The thermodynamic response to winter anomalies is also fundamentally different from the seasonal cycle. When deep convection occurs, there are associated density changes at a much greater depth and consequently larger potential energy changes. In the framework of this model there is now erosion into the main thermocline which reduces this layer's thickness, which will also alter the overall response.

We first compared the model's response to an anomaly with two different shapes in time, but which both resulted in the same net heat loss over the winter. The two forcing shapes and cumulative heat input are

shown in Fig. 12. It was found that the response followed the time history of the forcing so closely that there was no difference in the cumulative response at the end of winter, even though the time of onset of convection was different. It was concluded from this that the total change in heat content, rather than the distribution in time, was the important factor. The smoother time history was then used in the following.

From all the previous results it seems that, other than lower layer depth changes, the ratio L/λ is the critical parameter governing the system's respose, especially that of the main thermocline. To investigate this notion further, two runs were done to vary this ratio, but in two independent ways. In one run the domain was shrunk from 1000 km to 100 km, with the same relative forcing shape. In the second run λ was artificially increased 10 times by letting gravity be 100 times larger (or the earth's rotation to be 10 times smaller), leaving L at 1000 km. These both reduce L/λ by a tenth, and sure enough the system's response was identical in both cases. The free surface and main thermocline response for these runs is compared with a run using the original λ and L values in Fig. 13. Note the change in scale for δH. We see that, as indicated earlier, the small scale response has an order of meters main thermocline excursion. During deep convection, however, the free surface doesn't balance $-\overline{Q}_o/\rho_o$ as well in the small domain as it does in the large domain. This is the exact opposite tendency shown in the heating cycle. It can be shown from the analytic results that this is another indication of the much larger potential energy changes induced by buoyancy fluxes during deep convection which, through the coupled nature of the problem, effect different responses in the free surface.

In Table III are presented the transports for the two runs shown in Fig. 13. In addition in this table we present the cumulative change in the depth of the eighteen degree water layer, D. For a ten meter erosion into the main thermocline (with a 50 m/^{o}C temperature gradient) there is a drop of .2^{o}C in the late winter surface temperature. It should be recalled, however, that the depth D changes as much as the depth H does even without main thermocline erosion, so that the change in thickness of the main thermocline is $\delta H - \delta D$. In the small domain run, even though the free surface doesn't balance the buoyancy change term as well as in the large domain run, the resulting barotropic transport is actually smaller. This is because the main thermocline contribution to bottom pressure becomes important on small scales and is in the opposite sense to the buoyancy flux contribution. Similarly, the baroclinic transport for the small domain run is reduced because the larger main thermocline contribution to potential energy opposes the change due to buoyancy fluxes. On the other hand, the main thermocline is more effective in reducing the barotropic transport in the small domain than in reducing the baroclinic transport, such that there is a larger total transport (primarily baroclinic and due to the heat flux) in the small domain as opposed to the large domain. The reason that the potential energy changes due to the main thermocline are relatively less important than the bottom pressure changes, is because the changes in main thermocline thickness due to erosion act counter to the main thermocline motion itself, as far as potential energy changes are concerned. Thus for a given main thermocline excursion, the potential energy change will be larger if the main thermocline thickness is preserved, and smaller if erosion is also occurring.

Nonetheless in both cases shown in Table III the resulting transports are still quite small.

To examine the effect of changing domain length while retaining the same absolute scale of forcing, two runs were done with small-scale forcing but with a large and small domain length. The resulting free surface and main thermocline distributions are shown in Fig. 14, where both runs have the same resolution in terms of Δy. It is evident from this that it is the forcing structure and not the domain length per se that determine the system's response. This result is also reassuring that the southern boundary condition does not cause any artificial response. Increasing the number of points for the small domain did not change the picture very much.

To estimate the maximum possible main thermocline excursion due to the thermodynamic forcing, we go to the small scale limit analyzed in the last section. We run the model for a domain length of only 50 km which is roughly the internal deformation radius scale. The results for this run are shown in Fig. 15 and the transports are presented in Table IV. We find that the main thermocline response is still much smaller than the 100 meter excursions that are observed. The baroclinic transports in the model are still of the wrong sign and of smaller amplitude than those expected in the subtropical gyre return flow given the baroclinic transport changes observed in the Gulf Stream after a severe winter.

The conclusion we are faced with is that the thermodynamic effects on the dynamics of the subtropical gyre recirculation cannot account for the observed seasonal variability. In regions where the thermodynamic

forcing varies on scales of the order of the internal radius of deformation, only a few meters of main thermocline motion are expected. For larger scale variations in forcing the response is even less. In all the cases analyzed the associated transports were less than a few Sverdrups.

It might seem inconsistent to compare the model transports for the broad subtropical gyre return flow with the variability in observed Gulf Stream transports. In the model, a transport line is fixed to the south so that the total transport change across our domain is directly related to potential energy changes at the northernmost gyre-center station. On examining the hydrographic data from the station pairs giving the most and least transport shown in Fig. 1, it was found that, as in the model, the gyre-center stations exhibited the largest variability in potential energy, though for the observations there was some seasonal and year to year change in the slope water station used on the opposite side of the Gulf Stream. Thus the model transports should be comparable to the seasonal variability of the Gulf Stream, but are found here to be much less. In the concluding section to follow we summarize the findings of the model and offer some extensions to the work presented here which may bring about closer agreement between the observed variability and the predictions of the simple model we have used.

V. Conclusions

We have attempted here to estimate the response of the free surface and the main thermocline to forcing from surface buoyancy fluxes. The theoretical formulation was similar to that of a two-layer ocean model with a slightly more realistic vertical density prescription within the upper layer, but still retaining only one external and one internal free variable. The governing equations for the model were a pair of vorticity equations in which the prescribed density field and the hydrostatic equation were used to obtain equations in which the two unknowns and the buoyancy flux forcing appeared. A scale analysis for a zonally independent model indicated that the buoyancy changes in the model could be taken as given by the surface buoyancy flux, and that the vorticity equations for each layer of the model specified a balance between relative vorticity changes and vortex stretching.

Further simplifications were made to the depth integrated vorticity equations in which beta effects, bottom topography variations, and interaction with slopes of the mean main thermocline were neglected. All three of these effects were only marginally negligible and warrant further examination within the framework presented here. The vorticity input from wind stress curl was not included here, as the intent was to study the possible dynamical effects of surface heat and buoyancy fluxes alone.

The simplified form for the dynamical equations that was rendered was then solved numerically for a given, observationally based, forcing. The results presented in the last section indicate, however, that the essential information about the system's response can be gleaned from a further simplified set of time-integrated, constant (in latitude) coefficient vorticity equations, coupling the unknown free surface and main thermo-

cline perturbations.

The constant coefficient form for the time integrated, total depth and lower layer vorticity equations was cast as a coupled pair of ordinary differential equations. Inspection of these equations and verification from the numerical model runs indicated the following important results. Independent of our rather artificial boundary conditions, the forced solution for the main thermocline was zero unless there were regions where the fourth derivative of the forcing (in space) became large. If we had not specified the space and time variability of the total heat and density fluxes, but rather had retained thermodynamic feedback and only specified the meteorological variables, the heat fluxes might have adjusted in such a way as to have short scale spatial variability, giving rise to a significant forced main thermocline response. The forced solution of the free surface was found to be very nearly that of an "inverted dynamic height barometer", i.e., there was almost a perfect isostatic response of the free surface to the surface buoyancy fluxes, so that only small net bottom pressure changes resulted. If we had not considered the role of potential energy changes induced by changes in heat storage, we would find that the forced main thermocline response would be identically zero, and that perfect isostatic response of the free surface by thermal expansion would be obtained. (To see this, examine equations (52), (53) with $\delta \equiv 0$, thus neglecting the heat storage, potential energy terms.) Since this potential energy forcing is greatest during deep convection, larger barotropic flows are driven by the imbalance of the free surface and buoyancy flux effects during eighteen degree water formation, and larger baroclinic flows are effected by the associated deep density changes themselves.

The unforced, homogeneous solutions to our governing equations were found to be composed of two pairs of exponentials. One pair was scaled by the external deformation radius, the other pair by a sort of internal deformation radius. The internal radii solutions give a boundary layer appearance to the homogeneous solution and result from retaining the dynamical effects due to main thermocline motion, the small parameter being $\Delta\rho/\rho_o$.

Since we had no prior indication of how this model would respond, we chose rather artificial boundary conditions consistent with an artificial forcing shape across our region of interest. The simplest homogeneous boundary conditions which seemed appropriate for the return flow half of the subtropical gyre were utilized. A next step to this model would be the formulation of more realistic boundary conditions, consistent with a spatial distribution of forcing closer to that observed. Even better would be to specify only the atmospheric variables, and have a forcing which could adjust by feedback.

When we applied our simple boundary conditions, it was found that an important parameter governing the total solution was the ratio L/λ, λ being the *external* deformation radius. The internal, baroclinic response was larger when the scale of variation of the forcing was on the internal deformation radius. When the forcing varied on the external radius scale, the main thermocline response was no greater than that of the free surface, thus giving rise to negligible changes in the current and transport fields.

Variations of the lower layer depth were found to cause different responses, pointing to the importance of retaining mean thermocline slopes and topography effects. The main thermocline response diminished when the lower layer depth approached zero. For realistic ocean depths a non-zero main thermocline response was obtained, though this response could be diminished in the limit of unrealistically great ocean depth.

The most obvious result of the model which simulates observation is the rather dynamically uninteresting, isostatic free surface response. Studies by Patullo (1960) and others have long documented this sort of response of the free surface to changes in heat content of the seasonal layer. It is interesting that this result is nearly obtained even when we impose our governing vorticity equations. As mentioned earlier, the primary nonisostatic part of the free surface response results from potential energy (rather than pressure) changes associated with changes in heat storage.

The aim of this study, however, has led us to a rather negative result. Even with small-scale variations of forcing during deep convection, the largest main thermocline response we obtained was less than 5 meters. Thus we are led to believe that, at least for the 2-D model we've investigated, the dynamical consequences of the surface heat fluxes cannot be responsible for the observed variations in main thermocline depth. In Table V we compile a summary of the baroclinic, barotropic, total, and lower layer transports across the entire domain for the runs discussed in the last section. These results indicate that the observed variations, both seasonally and year-to-year, in Gulf Stream transport, cannot be accounted for in terms of this model. As discussed earlier, this table only predicts potential energy changes at the gyre center, but the majority of the variations in baroclinic transport from observations are due to potential energy changes in the region of maximum dynamic height (representing about 10 - 20 Sv if $f_o = 10^{-4}$ as in the model). Thus Table V reiterates that the model's response is not nearly as strong as the observed variability.

Our finding that the internal response was much larger when forced

on internal radius scales is intriguing in light of recent studies on "chimney" formation during bottom water production (e.g., Killworth (1979)).

It has been proposed that there is a preconditioning phase to bottom water production, in which regions of cyclonic circulation, with associated upward doming of isopycnals, are favorably selected for chimney formation. Nonetheless the chimneys that are formed are smaller in scale than the mean cyclonic circulation in which they are embedded. In the case of eighteen degree water formation the mean circulation is anticyclonic. Even so, the presence of the Gulf Stream to the north makes the eighteen degree water formation region an area where there is a local minimum in surface temperature. This state of affairs leads to outcroppings of temperature surfaces in late winter, similar to the preconditioning phase discussed in Killworth (1979) and by the Medoc Group (1970). Thus it may be the structure of the near surface temperature field, rather than the sense of the mean circulation, which makes an area more prone to deep convection. The deeper convection that occurs during bottom water formation, however, may be due to the mean cyclonic circulation, since isopycnals are domed upward at greater depth than in the subtropical gyre. The presence of a strong main thermocline gradient is also probably responsible for the shallower depth of convection found in eighteen degree water formation, as opposed to deep bottom water formation.

The indication of our model is that a large main thermocline depression, similar to that observed, could be obtained during eighteen degree water formation if a stronger forcing than that investigated here were to act on a small, internal radius scale, region. The resulting response would look very similar to chimney formation on small spatial scales,

though the vertical extent would be less.

The results presented here really lead one to believe that wind effects must somehow be responsible for the observed main thermocline heaving. The structure of the seasonally varying wind stress south of the Gulf Stream (c.f., Leetmaa and Bunker (1978), Fig. 6) is consistent with downward Ekman pumping in winter, which could conceivably advect the main thermocline by the amount observed. It would be a relatively easy extension of this model to add the surface wind stress, and possibly a simple bottom stress parameterization, to investigate the effects of friction.

Gill and Niiler (1973) estimated the oceanic response to the seasonally variable wind and found that the resulting motions were primarily barotropic, but had a significant baroclinic component between 15° - 30°N. It would be interesting to see how our more asymmetric 2-D model would respond to the observed seasonally varying wind in the eighteen degree water formation region. In particular, it is expected that the internal response would be particularly strong when forced by an outbreak of polar continental air with associated short scale variations in the wind in the vicinity of cold fronts. If we were to include wind effects in this model, it would be advisable to retain feedback between the surface temperature and the surface heat flux, and also to account for Ekman fluxes of heat which would change the local heat flux through the surface. In this way the dynamic and thermodynamic response to the specified meteorology would be internally consistent, whereas it would not be if we retained a specified total heat flux.

There are other effects that we have omitted which would be desirable to investigate in terms of this model. In order to simplify the analysis,

we neglected terms arising from slopes of the main thermocline in the mean state. This needs to be retained as a further step in this model since this assumption was not completely justifiable in terms of our scale analysis, though these effects were presumably negligible to the same order as other effects that were dropped, based on the scale analysis. Retaining beta effects would be fairly simple in the 2-D limit as the model is now formulated. Accounting for fluxes of *mass* across the surface associated with the deficit of precipitation and evaporation could force a significant response since this is a more direct, external forcing which can't be compensated simply by steric expansion, contraction effects.

In a more general scheme it would be necessary to account for around-gyre advection of fluid parcels, possibly considering a Lagrangian frame and subjecting a tagged column to the forcing it would see in transiting the subtropical gyre. It might be possible to remain in our 2-D framework and consider the entire subtropical gyre with boundary conditions of a fixed streamline at both the North and South boundaries. In this case it would surely be necessary to retain the effects of the steeply sloping main thermocline in the Gulf Stream. Since this slope occurs over roughly internal deformation radius scales, the effects from the mean state could alter the seasonal response more than the broad slope of the main thermocline in the return flow.

Our conclusion that the observed variability in main thermocline depth and the observed variability in transport around the subtropical gyre couldn't be accounted for by the effects of surface heat fluxes may be an artifact of our simple 2-D system. However, if we were to find that wind effects in our 2-D model could produce changes similar to those observed, the dynamic role of the heat fluxes would then be positively

shown to be small. If the model with wind still could not simulate observations, this would indicate a need to consider a more general 3-D framework.

The methodology presented in this thesis could be used to investigate other dynamical effects neglected in the present model, as discussed above, as well as to investigate the effects of deep convection applicable to the formation of other water masses. Although the numerical schemes might need alteration, we believe the basic approach we've formulated could be used to study the dynamical consequences of eighteen degree water formation within a more generalized framework. Since we are at a loss to envision another mechanism by which surface heat fluxes can effect a dynamic response, the first extension to this work that seems in order, is to evaluate the response of the present model to wind stress effects. It is believed that inclusion of the observed wind may well yield results much closer to those observed.

References

Anati (1971) On the mechanism of the deep mixed layer formation during Medoc '69. Cahiers Océanographiques, XXIII: 4, 427-443.

Bunker (1976) Computations of Surface Energy Flux and Annual Air-Sea Interaction Cycles of the North Atlantic Ocean. Monthly Weather Review, 104: 9, 1122-1140.

Bunker and Worthington (1976) Energy Exchange Charts of the North Atlantic Ocean. Bulletin of the American Meteorological Society, 57: 6, 670-678.

Fofonoff (1969) Dynamics of Ocean Currents. In: The Sea Vol. I, M. N. Hill, ed., John Wiley and Sons, N. Y., 323-395.

Fuglister (1960) Atlantic Ocean atlas of temperature and salinity profiles and data from the International Geophysical Year of 1957-1958. Woods Hole Oceanographic Institution Atlas Series, 1, 209 p.

Gill and Niiler (1973) The theory of the seasonal variability in the ocean. Deep-Sea Research, 20, 141-177.

Killworth (1979) On "Chimney" formations in the Ocean. Journal of Physical Oceanography, 9, 531-554.

Leetmaa and Bunker (1978) Updated charts of the mean annual wind stress, convergences in the Ekman layers, and Sverdrup transports in the North Atlantic. Journal of Marine Research, 36: 2, 311-322.

Medoc Group (1970) Observations of formation of deep water in the Mediterranean Sea. Nature, 227, 1037-1040.

Patullo (1960) Seasonal changes in sea-level. In: The Sea, Vol. II, M. N. Hill, ed., John Wiley and Sons, N. Y., 485-496.

Veronis and Stommel (1956) The action of variable wind stresses on a stratified ocean. Journal of Marine Research, 15: 1, 43-75.

Warren (1972) Insensitivity of subtropical mode water characteristics to meteorological fluctuations. Deep-Sea Research, 19: 1, 1-19.

Worthington (1972b) Anticyclogenesis in the oceans as a result of outbreaks of continental polar air. In: Studies in Physical Oceanography — A tribute to George Wüst on his 80th birthday, A. L. Gordon, ed., Gordon and Breach, N. Y., 1, 169-178.

Worthington (1976) On the North Atlantic Circulation, The Johns Hopkins Oceanographic Studies #6, Johns Hopkins University Press, Baltimore, 110 p.

Acknowledgements

I would like to sincerely thank the people who helped me put this thesis together. Thanks to Mary Raymer for the drafting of so many figures so quickly and effectively. Thanks to Doris Haight for all the hours she spent typing this manuscript with so many equations. Thanks to Roger Goldsmith for helping me obtain the meteorological and heat flux data. Thanks to Audrey Williams for lending me her typewriter during a hurricane and for helping with the text. Thanks to Val Worthington, Henry Stommel, Nick Fofonoff and others for helpful discussions. Most of all, I'd like to thank Mike McCartney for his patient advice and constant support, and for the critical review of this thesis. And I would especially like to thank Patrisha, whose help, devotion, and encouragement made the timely completion of this work possible.

Figure Captions

Figure 1. Updated version of Worthington (1976), Figure 44 showing all available baroclinic transport measurements (relative to 2000 m) of the "deep" Gulf Stream within the Montauk-Hatteras-Bermuda Triangle, plotted by the month that the section was occupied.

Figure 2. Late winter temperature profiles in the eighteen degree water formation region in a relatively mild (KNORR 48) and a severe winter.

Figure 3a. Schematic of heat storage prescription and vertical temperature prescription as a function of surface temperature, during the heating phase of the Warren Model. Starting with the previous winter's deep mixed layer of depth D, a seasonal thermocline of constant gradient is built of depth h_S, as a function of T_S. The maximum depth reached in late summer is h_{LS}, when the maximum temperature T_{LS} is reached.

Figure 3b. Same as 3a for the cooling phase. In this phase a mixed layer of depth h_m erodes into the existing seasonal thermocline of constant depth h_{LS}. As the temperature drops to the old late winter temperature, the seasonal thermocline is erased.

Figure 3c. Same as 3a for the deep convection stage. When the seasonal thermocline is completely erased in late winter and there is still a negative heat flux as in a "severe" winter, erosion into the main thermocline occurs. This convection deepens the late winter mixed layer proportional to the cooling of the late winter surface temperature.

Figure 4a. Changes to the Warren Model during the heating phase. The temperature prescription now has a deep lower layer of temperature T_B, a main thermocline of thickness (H-D) which is constant in this phase, and a variable main thermocline and free surface position. The building of the seasonal thermocline occurs as in the Warren Model with the surface temperature assumed constant over the height η.

Figure 4b. Same as 4a for the cooling phase. The main thermocline thickness is still constant though the main thermocline may heave as a whole.

Figure Captions (cont.)

Figure 4c. Same as 4a for the onset of deep convection. Changes in the depth D are now due both to motion of the main thermocline as a whole and due to erosion, as in the Warren Model. Thus the main thermocline thickness is not preserved in this phase as the late winter temperature decreases.

Figure 5. March of the seasonal surface heat flux as computed by Bunker, with the annual mean removed. The data are presented at various latitudes centered on 2° latitudinal averages. The data is also averaged over 50°-60°W and by month for all years for which data existed.

Figure 6. Same data described in Fig. 5 but plotted as a function of latitude. The quantities plotted occur at different times at various positions, so the month of occurrence is plotted beside each curve. Points between labels for the same month have the same phenomena occur during the month labeled by the bracketing points. Note how the month of June goes from a summer maximum to a summer minimum between 20° and 15° N.

Figure 7. Monthly averages of meteorological and heat flux data ,as computed by Bunker, for Marsden Square 114 (50°-60° W., 30°-40° N.) for all years observed.

Figure 8. Temperature prescription in numerical model as a function of depth and latitude. Note that the depth of the mixed layer crosses isotherms since the late winter temperature varies with latitude.

Figure 9. Cumulative density flux, free surface response, and main thermocline response at the end of summer heating for the parameters given by (54), cubic forcing as described in text, and two values for the ocean depth.

Figure 10. Same as Fig. 9 with B = 5000 m and three different domain lengths. In each case the shape of the forcing is cubic and has the same relative shape across the domain.

Figure 11. Same as Fig. 10 for L = 1000 km, but with two forcing shapes. The cubic forcing is the same as shown in Fig. 9. The Gaussian shape has an e-folding scale of 500 km.

Figure 12. Shape of winter anomaly of heat flux forcing in time for the case of a very event-oriented outbreak, and for a smoother time history of heat flux. The upper panel shows the heat flux itself, whereas the lower panel is the time-integrated change in heat content, normalized by the seasonal frequency. The broad time scale anomaly was used in the late winter runs discussed in the text.

Figure Captions (cont.)

Figure 13. Cumulative density flux, free surface response, and main thermocline response after a "severe" winter for the parameters given by equation (54), but for two domain lengths. The relative forcing shape is the same for both domains and is a Gaussian that has an e-folding scale of L/2. Note the changes in sign for the free surface and density flux terms and the change in scale of the main thermocline response.

Figure 14. Same as Fig. 13 except the absolute shape of the forcing is the same for two different domain lengths. The decay scale of the Gaussian forcing is 100 km in both cases.

Figure 15. Same as Fig. 13 for an internal deformation radius scale domain.

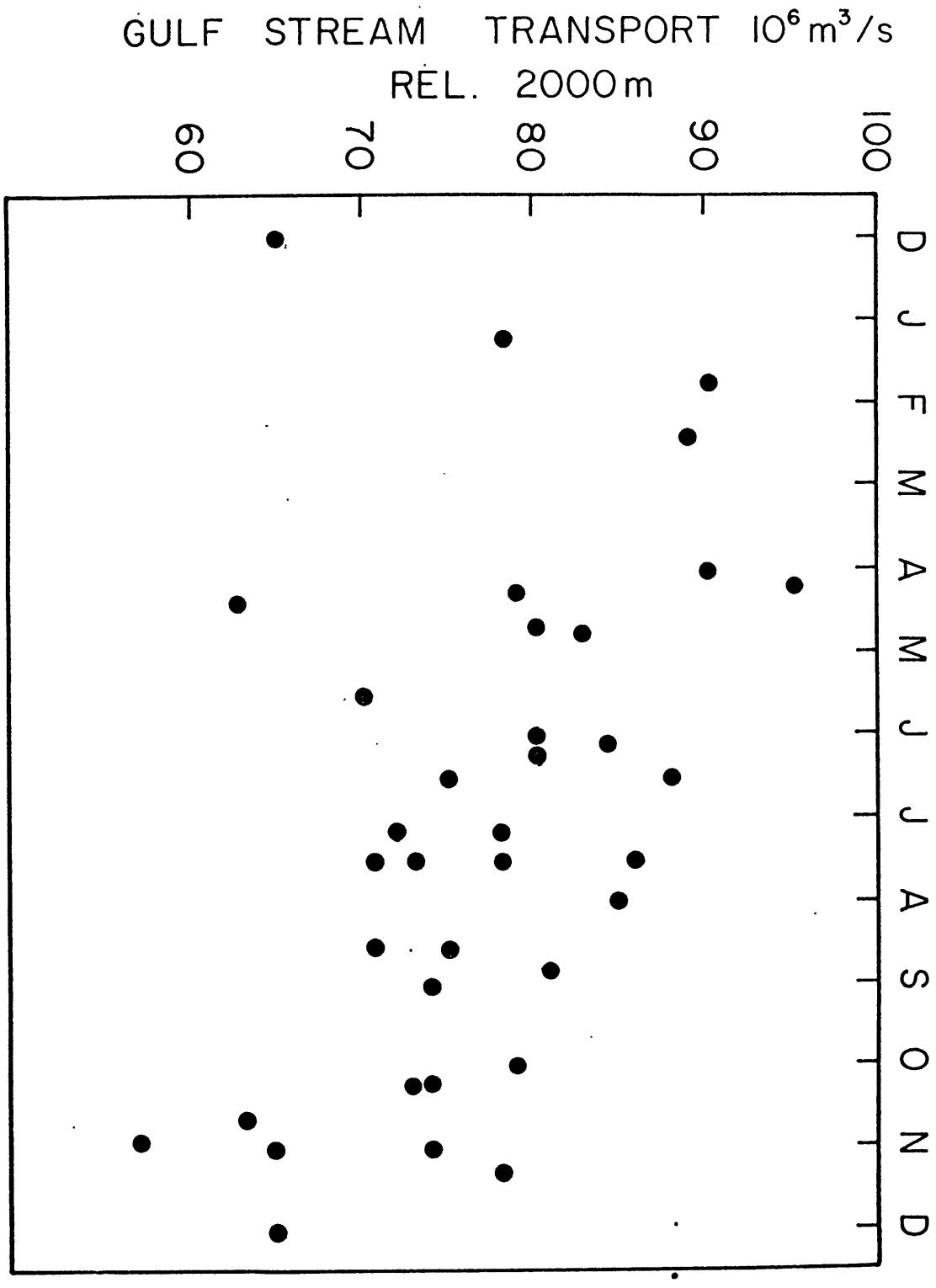
GULF STREAM TRANSPORT $10^6 m^3/s$
REL. 2000m
60
70
80
90
100
D
J
F
M
A
M
J
J
A
S
O
N
D

FIGURE 1

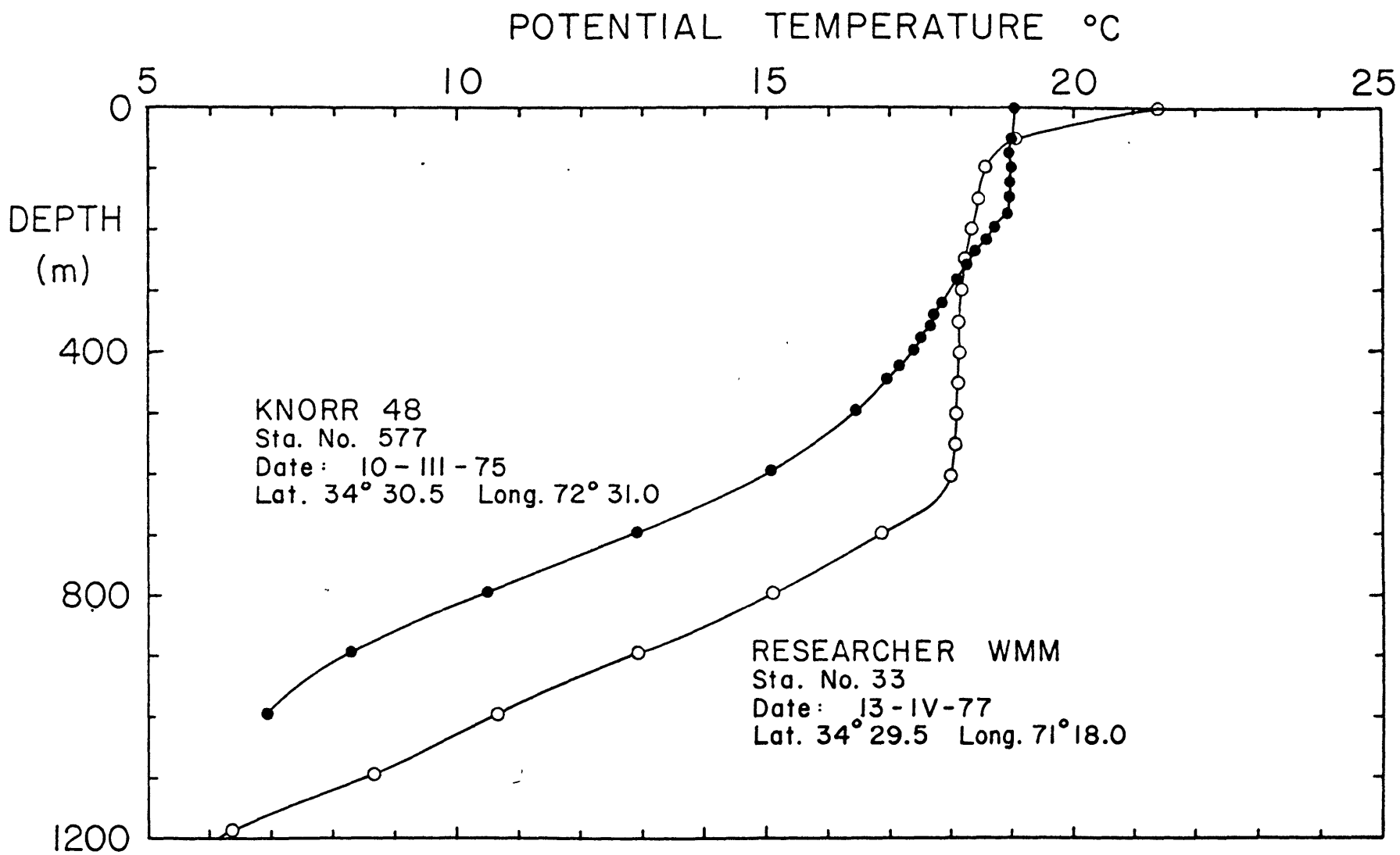
POTENTIAL TEMPERATURE °C
5
10
15
20
25
0
400
800
1200
DEPTH
(m)
KNORR 48
Sta. No. 577
Date: 10-111-75
Lat. 34° 30.5 Long. 72° 31.0
RESEARCHER WMM
Sta. No. 33
Date: 13-IV-77
Lat. 34° 29.5 Long. 71° 18.0

FIGURE 2

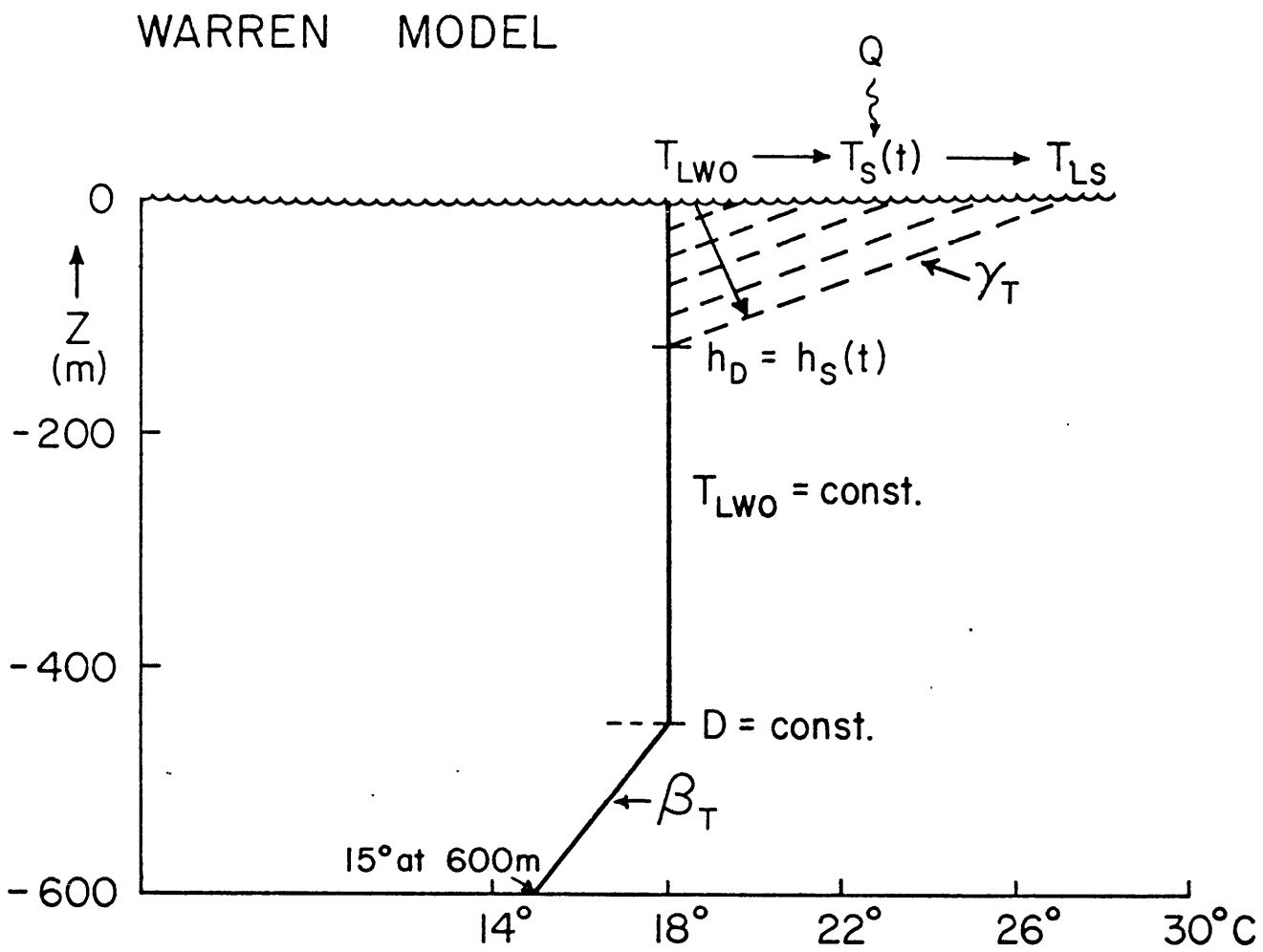

Heating Phase : Seasonal Thermocline Growth

$\frac{\delta T_s}{\delta t} > 0 \quad T_{LW} \leq T_s \leq T_{LS}$

FIGURE 3A

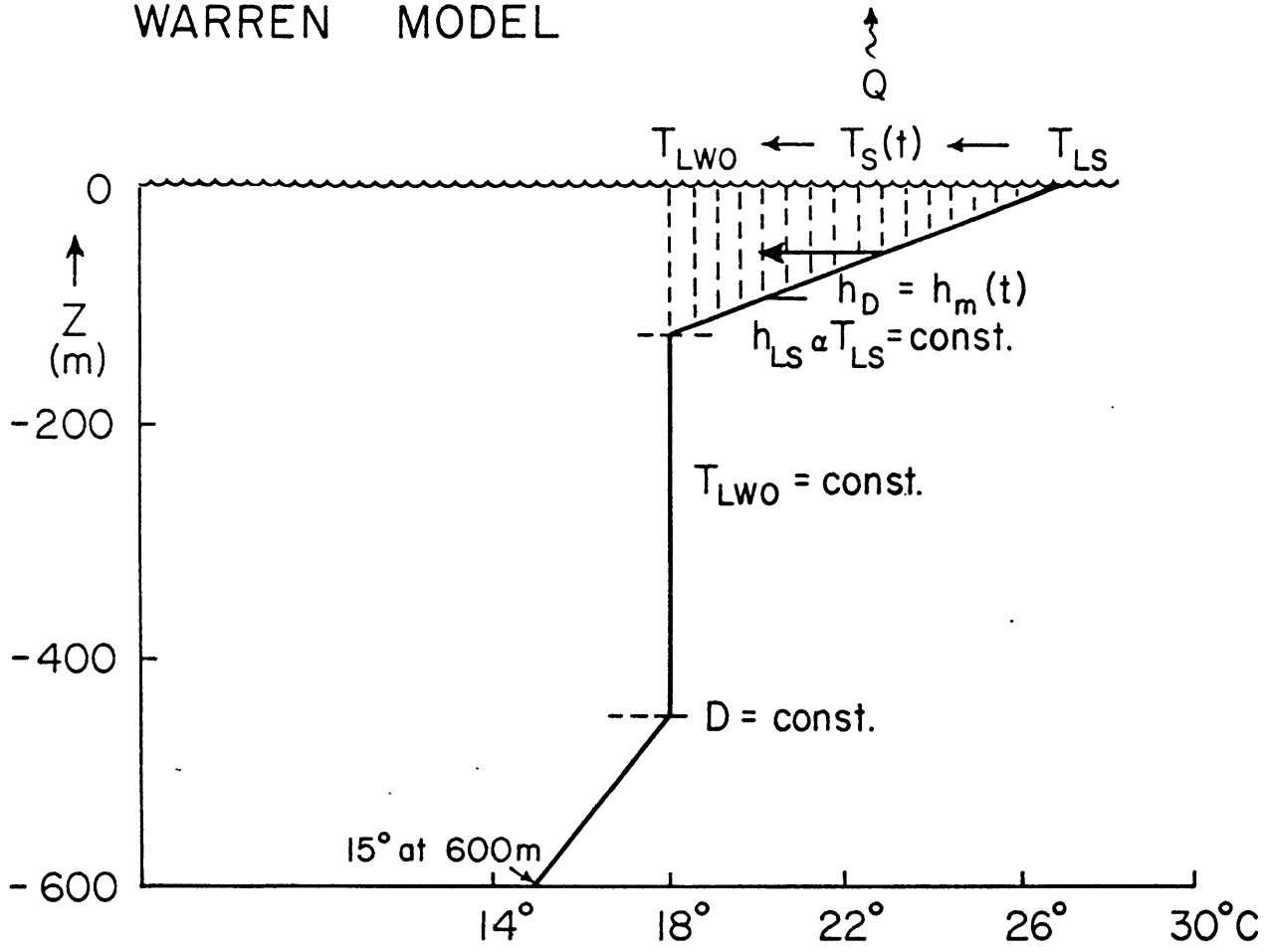

Cooling Phase : Seasonal Thermocline Erosion

$\frac{\delta T_s}{\delta t} < 0 \quad T_{LW} \leq T_s \leq T_{LS}$

FIGURE 3B

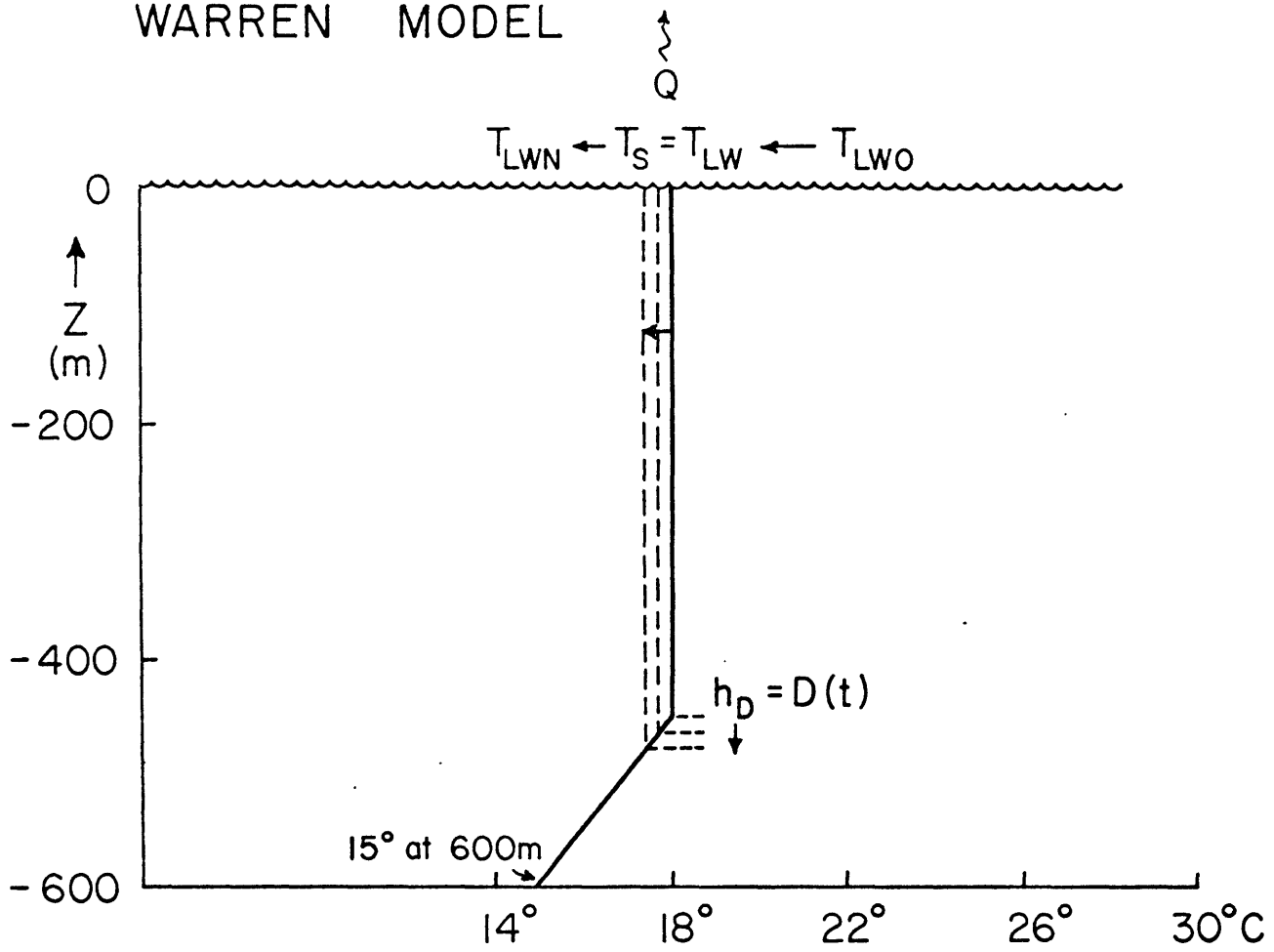

Deep Convecting Phase : Main Thermocline Erosion

$$\frac{\delta T_s}{\delta t} < 0 \quad T_s = T_{LW} \leq T_{LWO}$$

FIGURE 3c

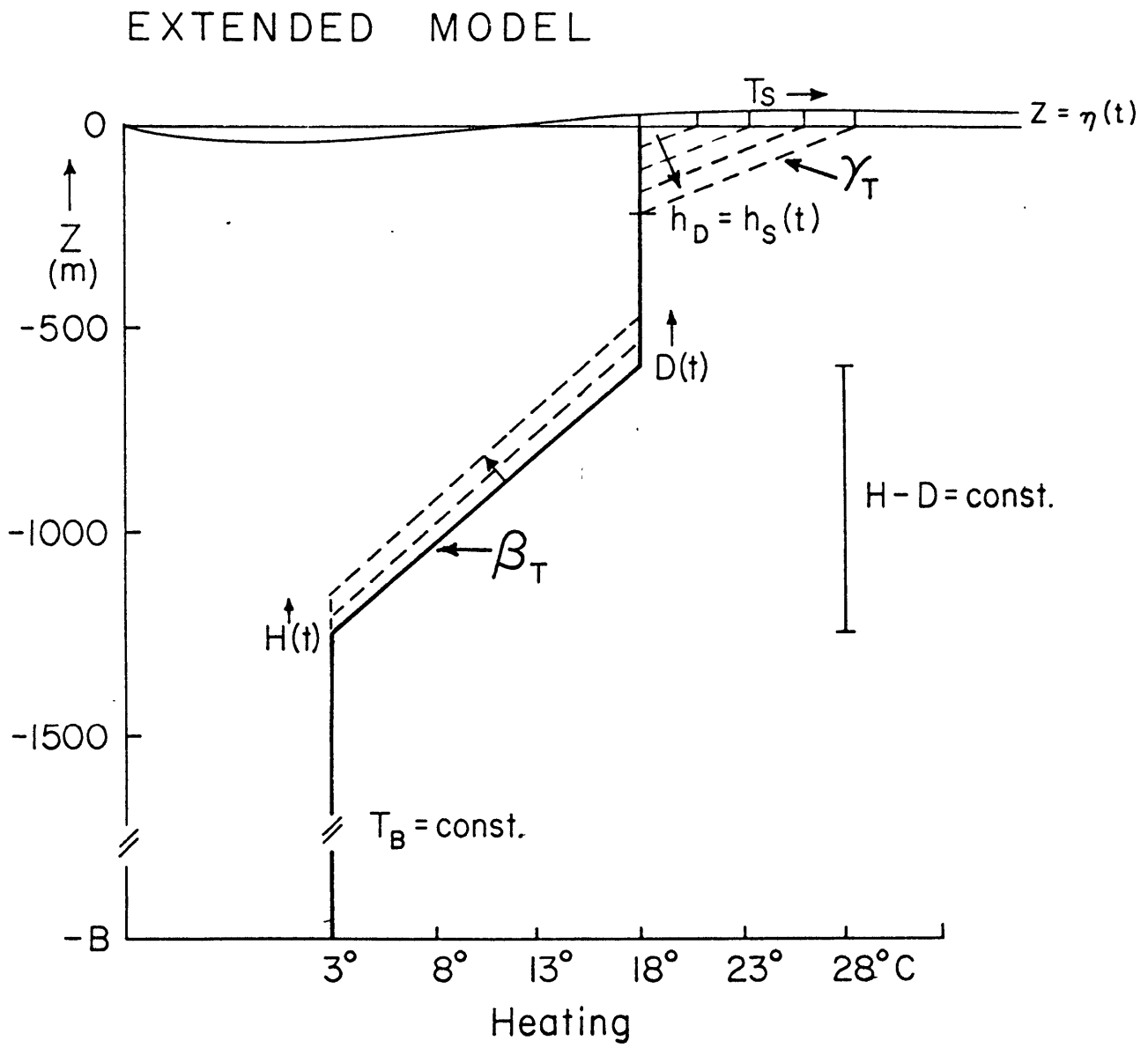
EXTENDED MODEL
Ts
Z = η(t)
0
Z
(m)
γT
hD = hS(t)
-500
D(t)
H - D = const.
-1000
βT
H(t)
-1500
TB = const.
-B
3°
8°
13°
18°
23°
28°C
Heating

FIGURE 4A

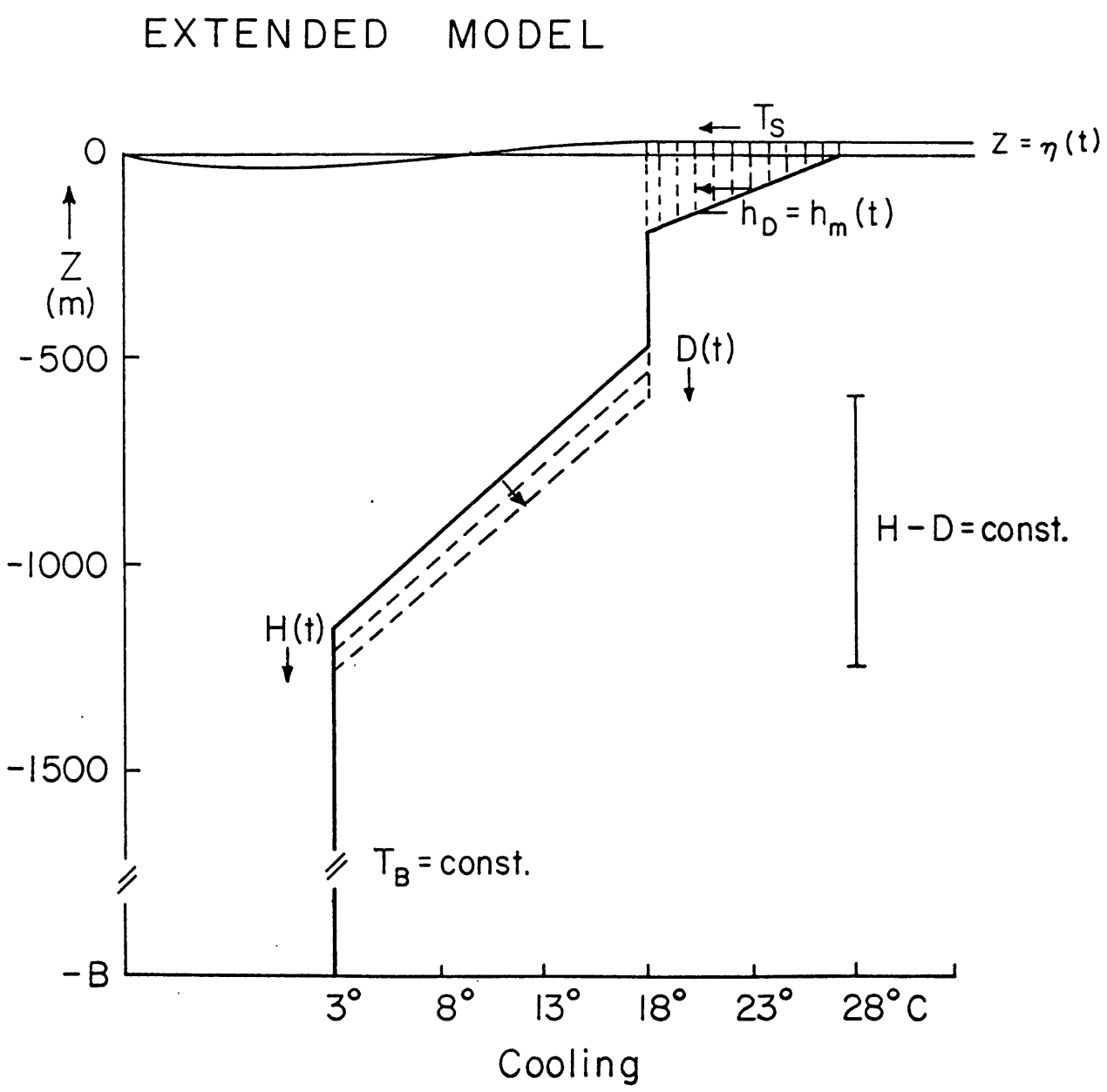
EXTENDED MODEL
T_S
$Z = \eta(t)$
0
Z
(m)
$h_D = h_m(t)$
D(t)
-500
-1000
-1500
H(t)
H - D = const.
T_B = const.
-B
3°
8°
13°
18°
23°
28°C
Cooling

FIGURE 4B

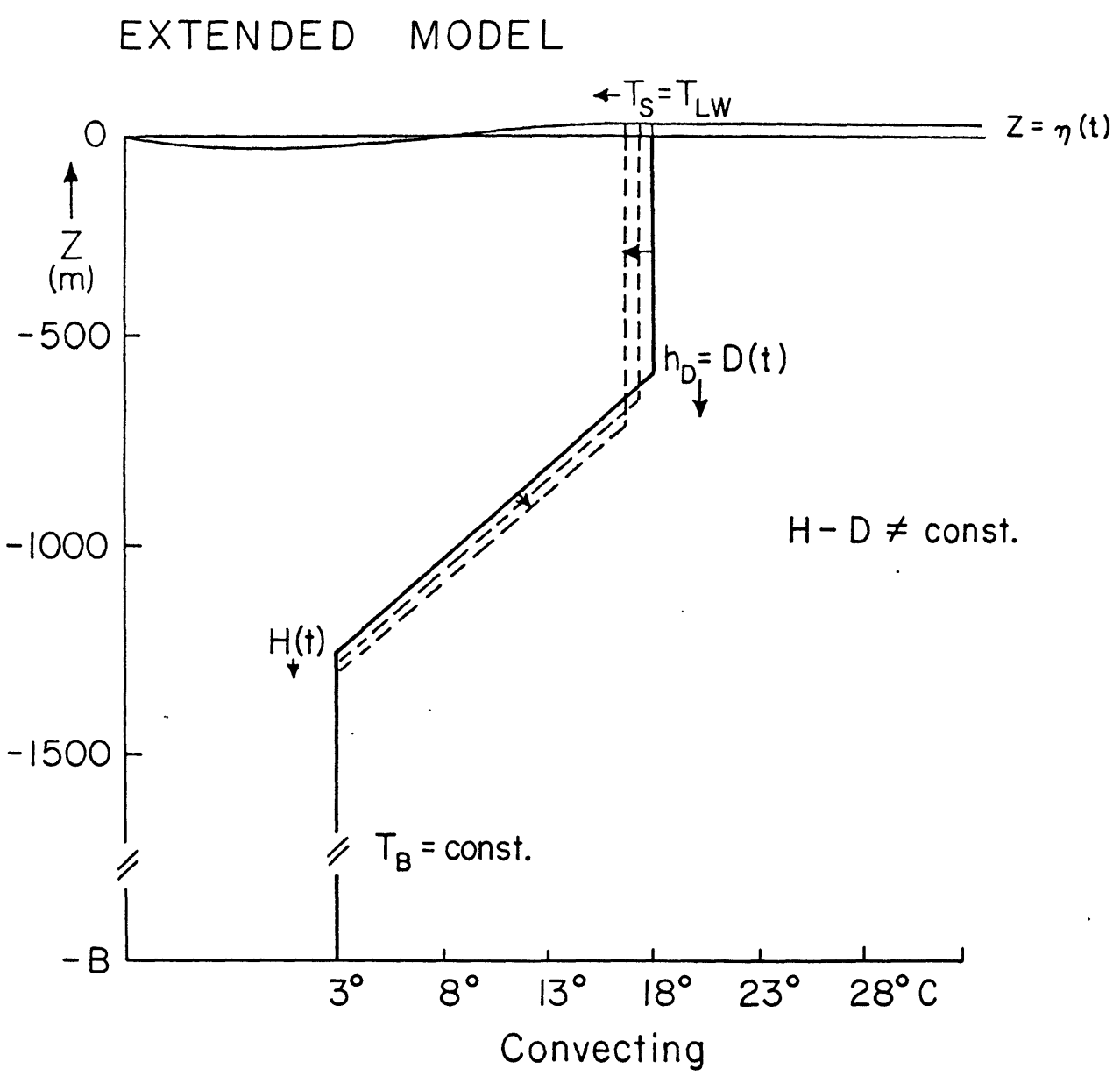
EXTENDED MODEL
$T_S = T_{LW}$
$Z = \eta(t)$
0
Z (m)
-500
-1000
-1500
-B
$h_D = D(t)$
H(t)
T_B = const.
H - D ≠ const.
3°
8°
13°
18°
23°
28° C
Convecting

FIGURE 4c

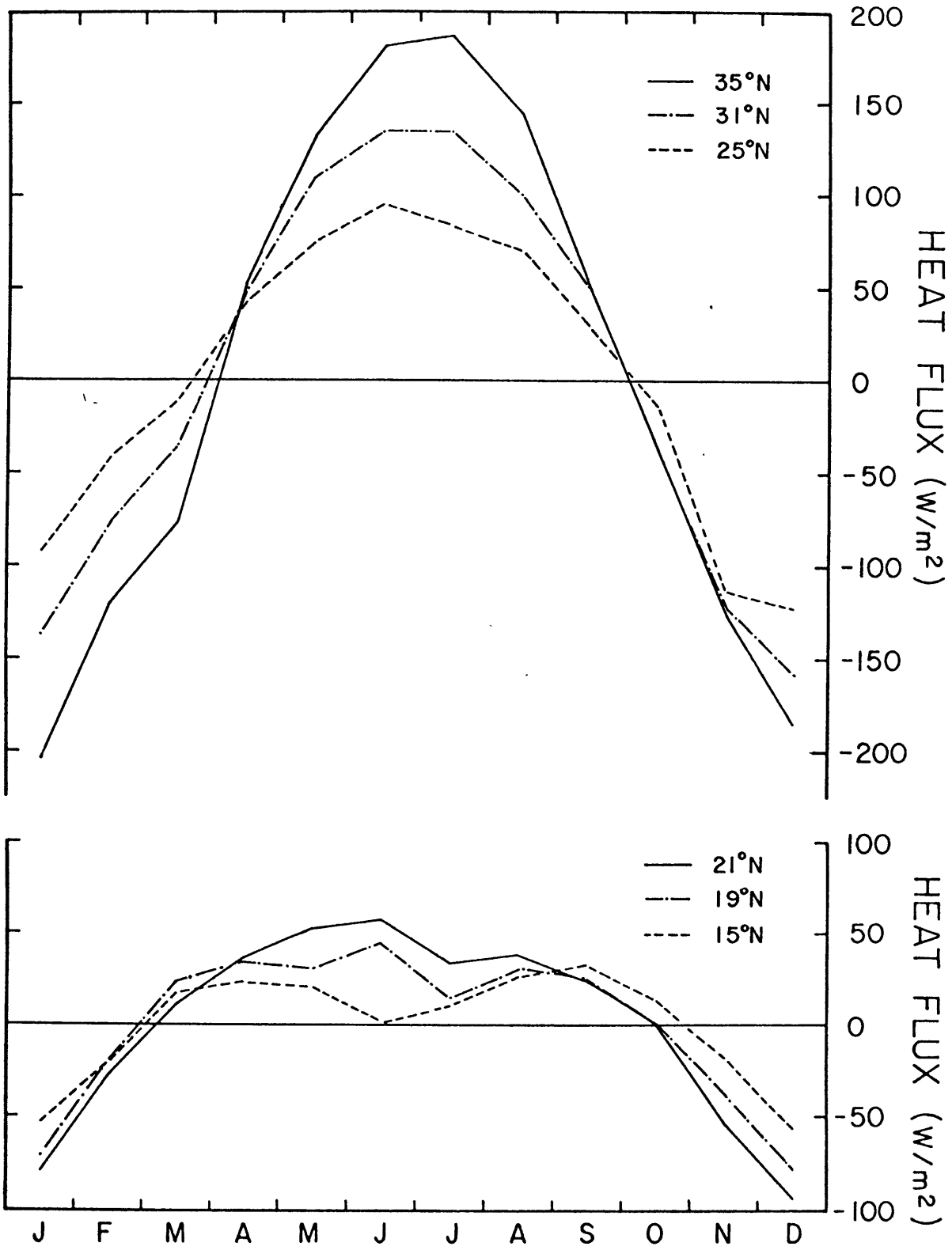
35°N
31°N
25°N
200
150
100
50
0
-50
-100
-150
-200
HEAT FLUX (W/m²)
21°N
19°N
15°N
100
50
0
-50
-100
HEAT FLUX (W/m²)
J F M A M J J A S O N D

FIGURE 5

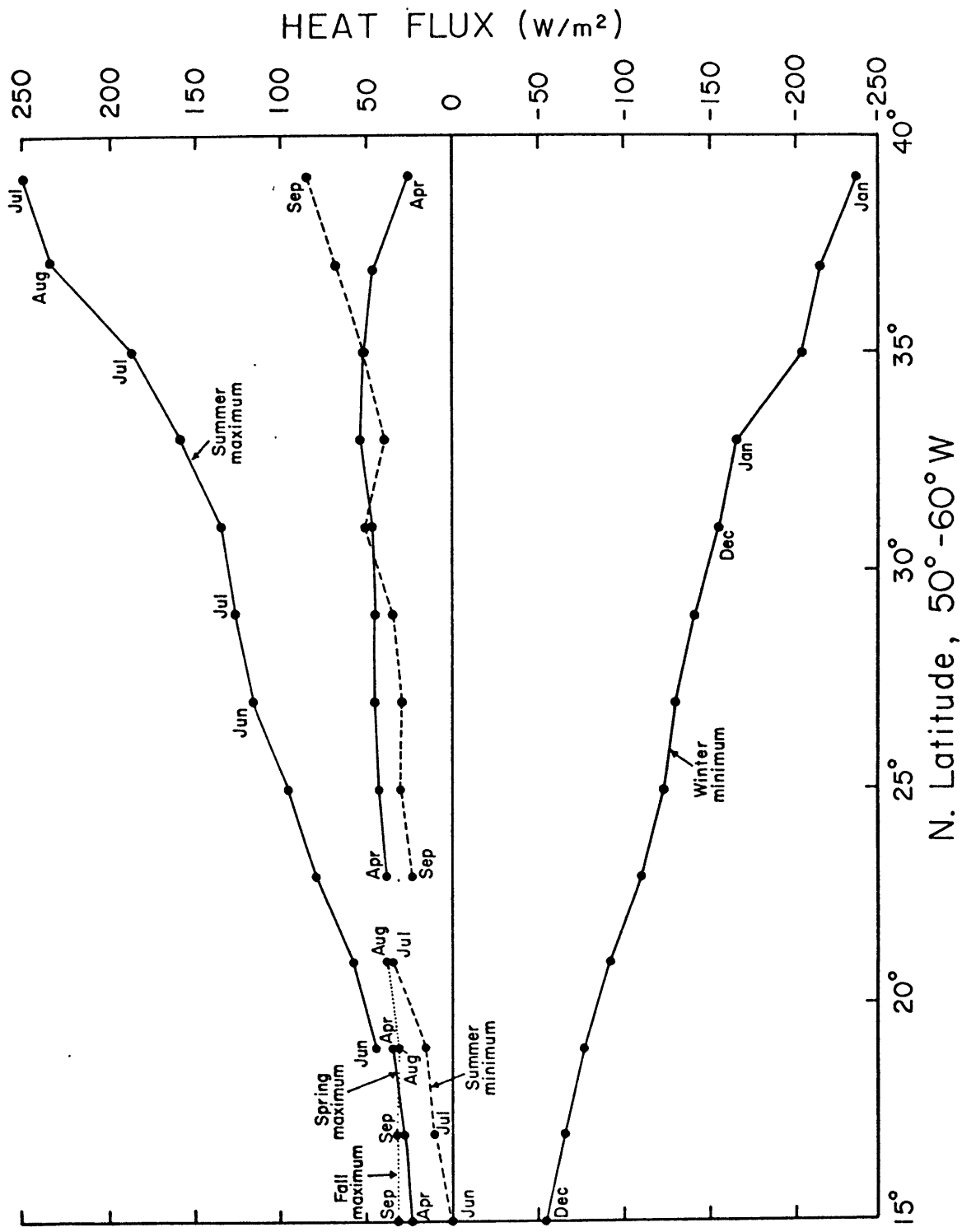
HEAT FLUX (W/m²)
250
200
150
100
50
0
-50
-100
-150
-200
-250
40°
35°
30°
25°
20°
15°
N. Latitude, 50°-60° W
Jul
Aug
Jul
Summer maximum
Jul
Jun
Sep
Apr
Apr
Sep
Aug
Jul
Jun
Spring maximum
Apr
Aug
Sep
Fall maximum
Sep
Apr
Jul
Summer minimum
Jun
Jun
Dec
Winter minimum
Dec
Jan
Jan

FIGURE 6

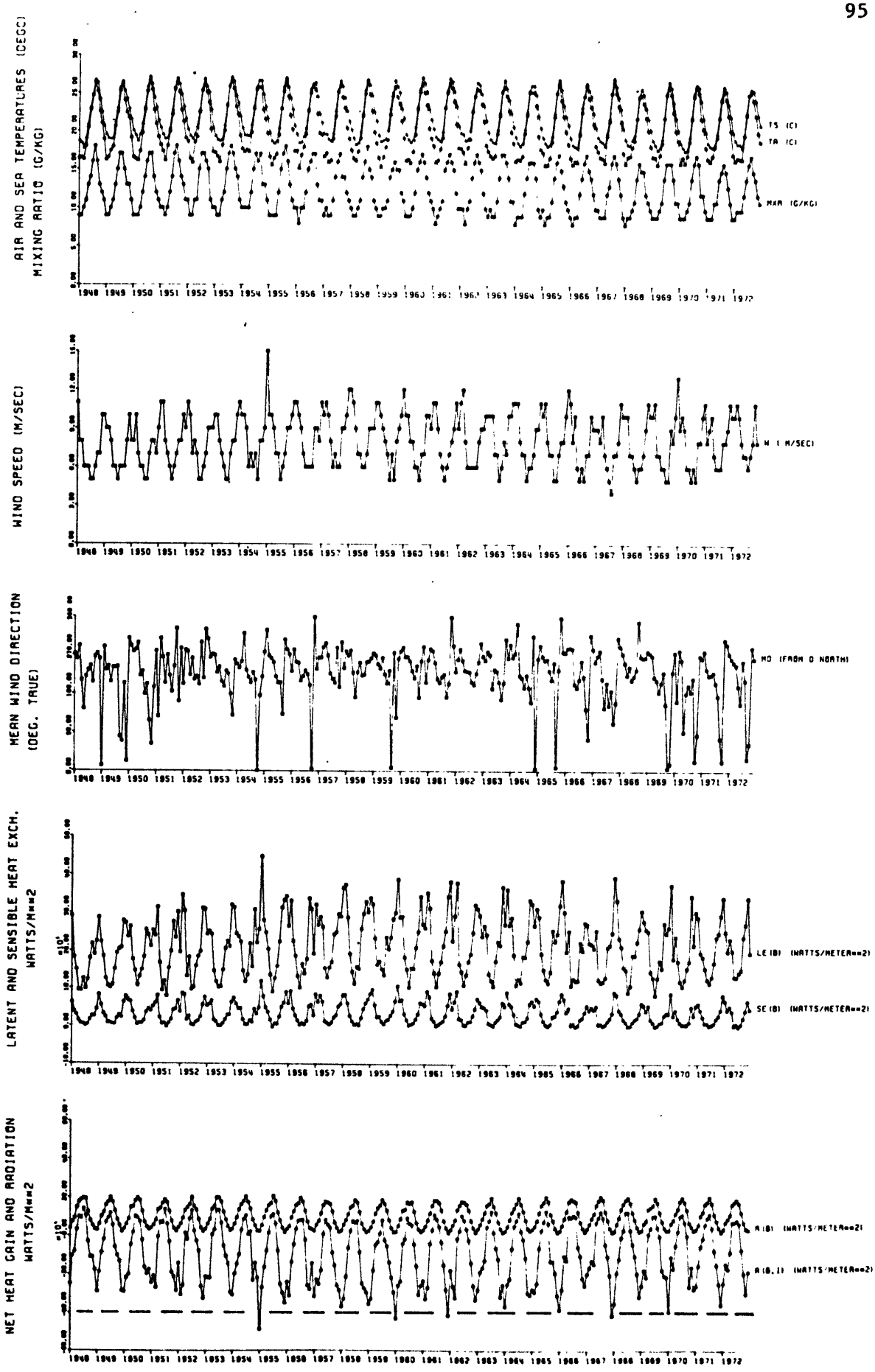

M.S. :14

FIGURE 7

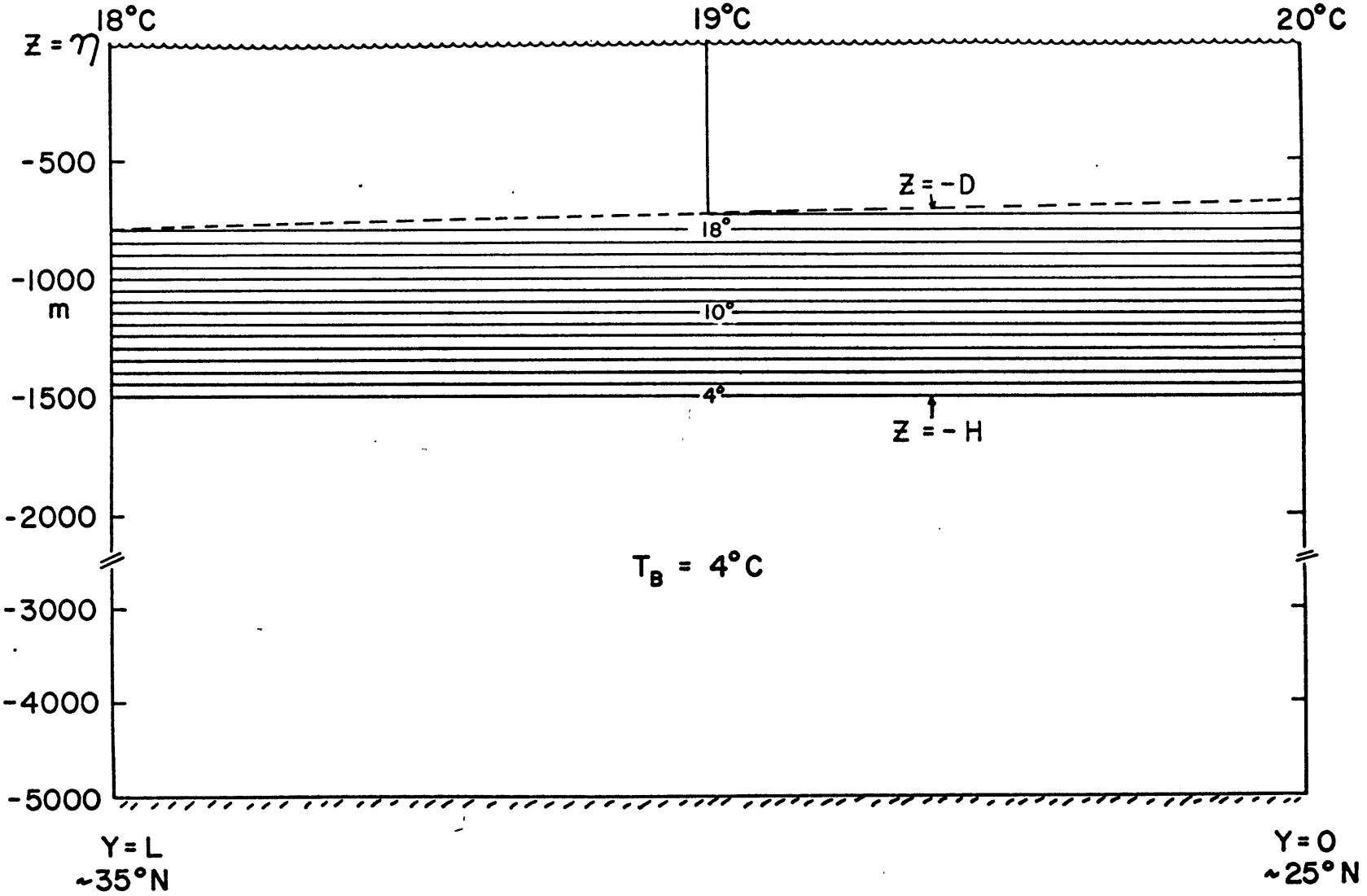
18°C
19°C
20°C
Z = η
-500
Z = -D
18°
-1000
m
10°
-1500
4°
Z = - H
-2000
T_B = 4°C
-3000
-4000
-5000
Y = L
~35°N
Y = 0
~25°N

FIGURE 8

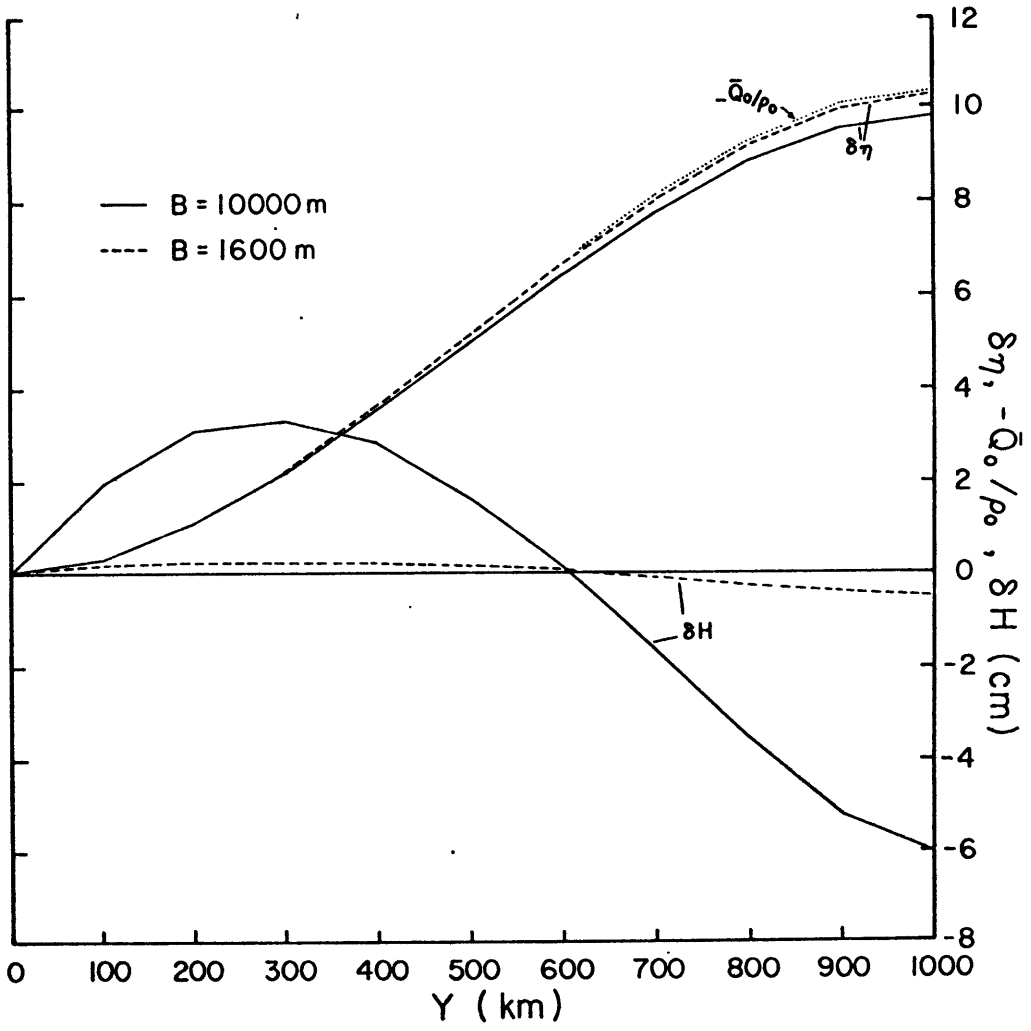
B = 10000 m
B = 1600 m
$-\bar{Q}_0/\rho_0$
$\delta\eta$
δH
12
10
8
6
4
2
0
-2
-4
-6
-8
0
100
200
300
400
500
600
700
800
900
1000
Y (km)
$\delta\eta$, $-\bar{Q}_0/\rho_0$, δH (cm)

FIGURE 9

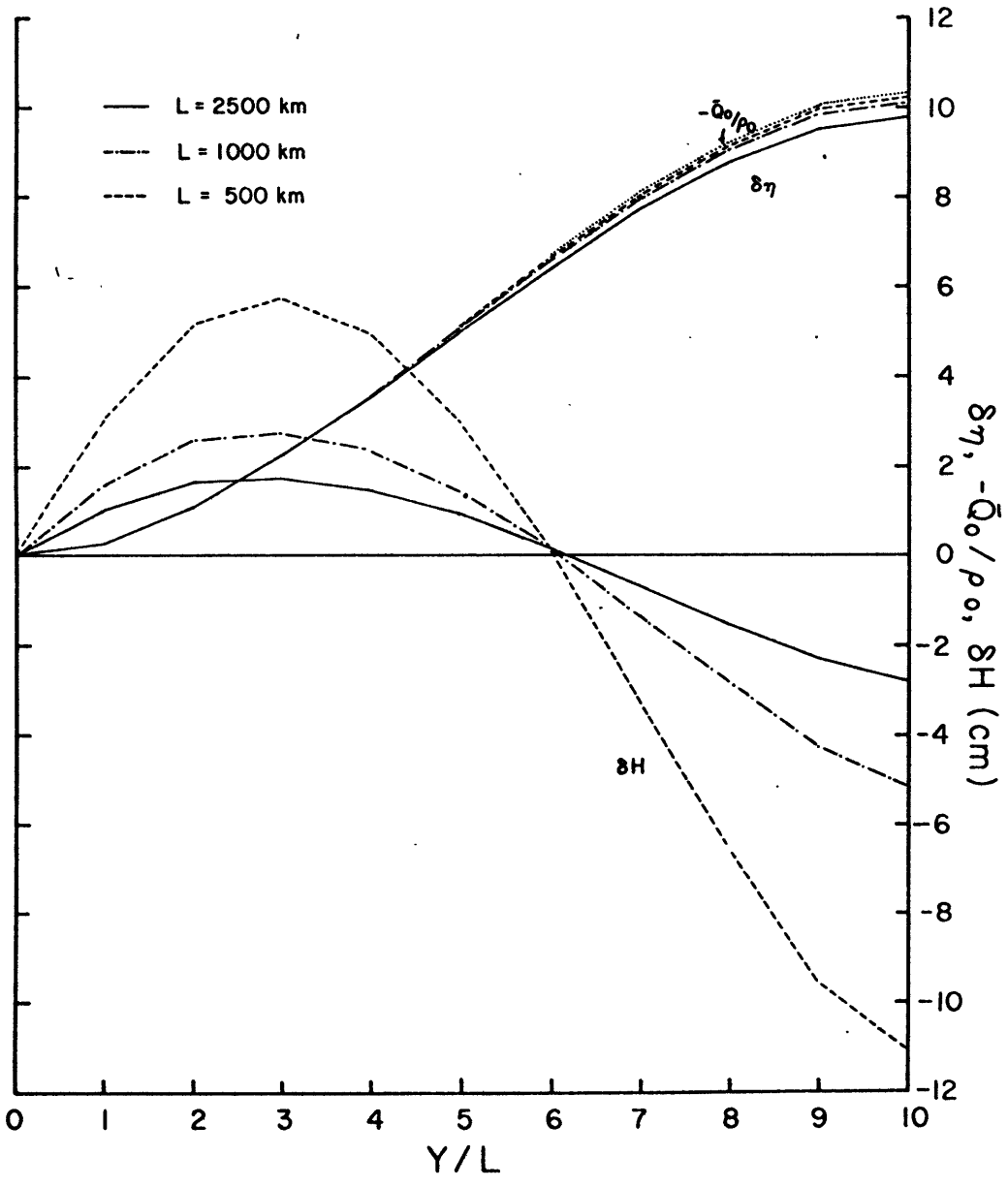
L = 2500 km
L = 1000 km
L = 500 km
$-\bar{Q}_o/\rho_o$
$\delta\eta$
δH
$\delta\eta, -\bar{Q}_o/\rho_o, \delta H$ (cm)
Y/L
12
10
8
6
4
2
0
-2
-4
-6
-8
-10
-12
0
1
2
3
4
5
6
7
8
9
10

FIGURE 10

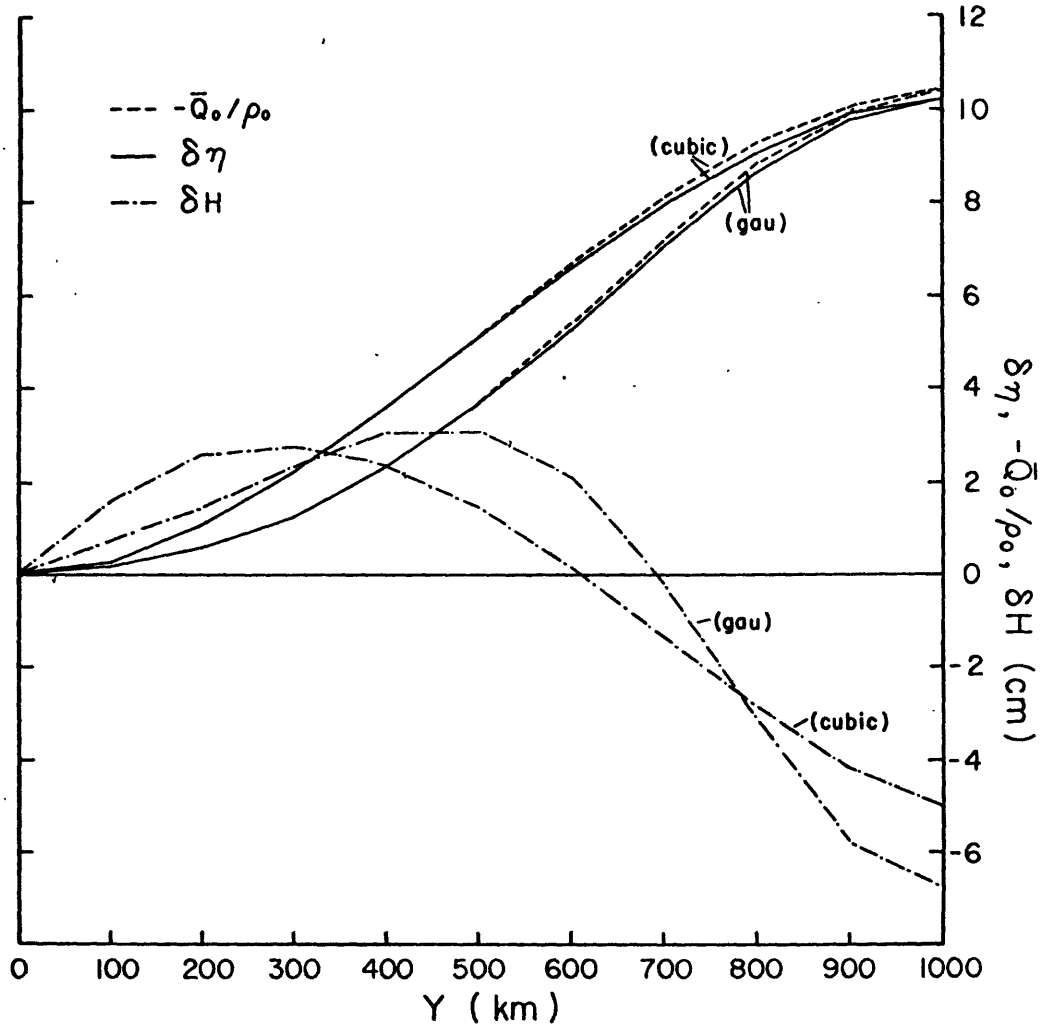
--- $-\bar{Q}_0/\rho_0$
— $\delta\eta$
-·- δH
(cubic)
(gau)
(gau)
(cubic)
12
10
8
6
4
2
0
-2
-4
-6
0
100
200
300
400
500
600
700
800
900
1000
Y (km)
$\delta\eta$, $-\bar{Q}_0/\rho_0$, δH (cm)

FIGURE 11

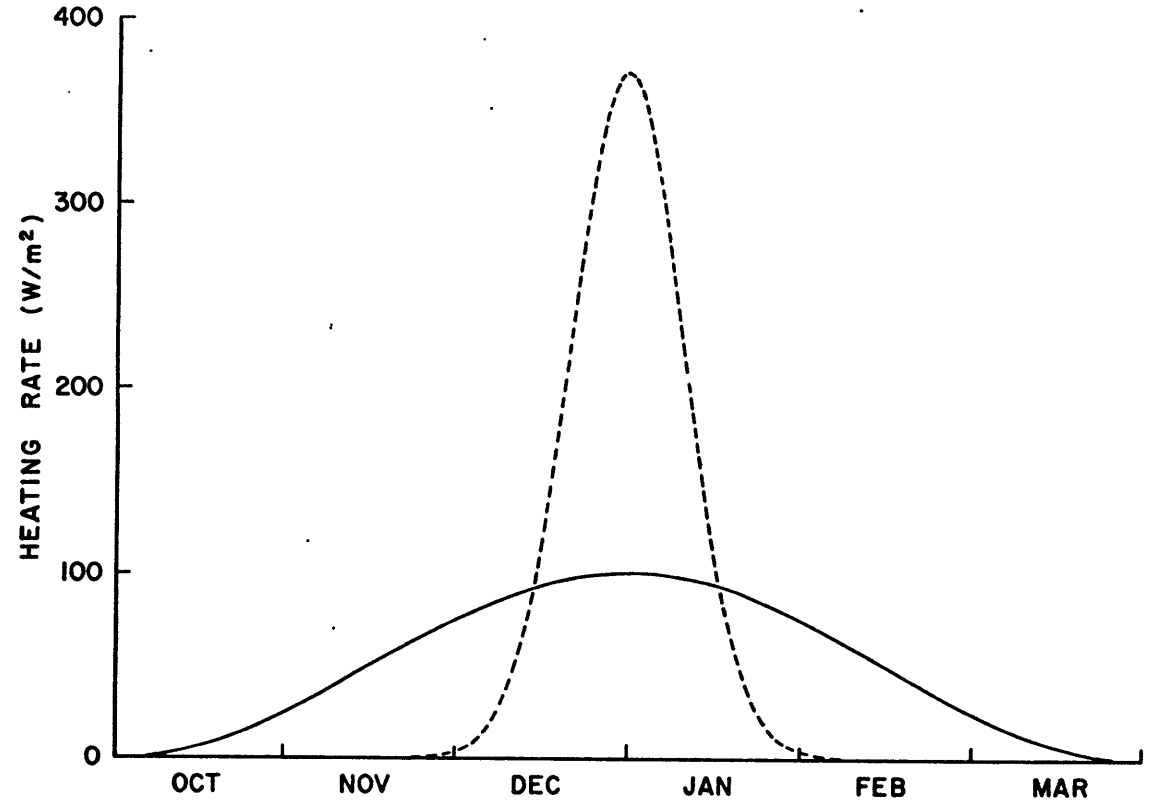
400
300
200
100
0
HEATING RATE (W/m²)
OCT
NOV
DEC
JAN
FEB
MAR

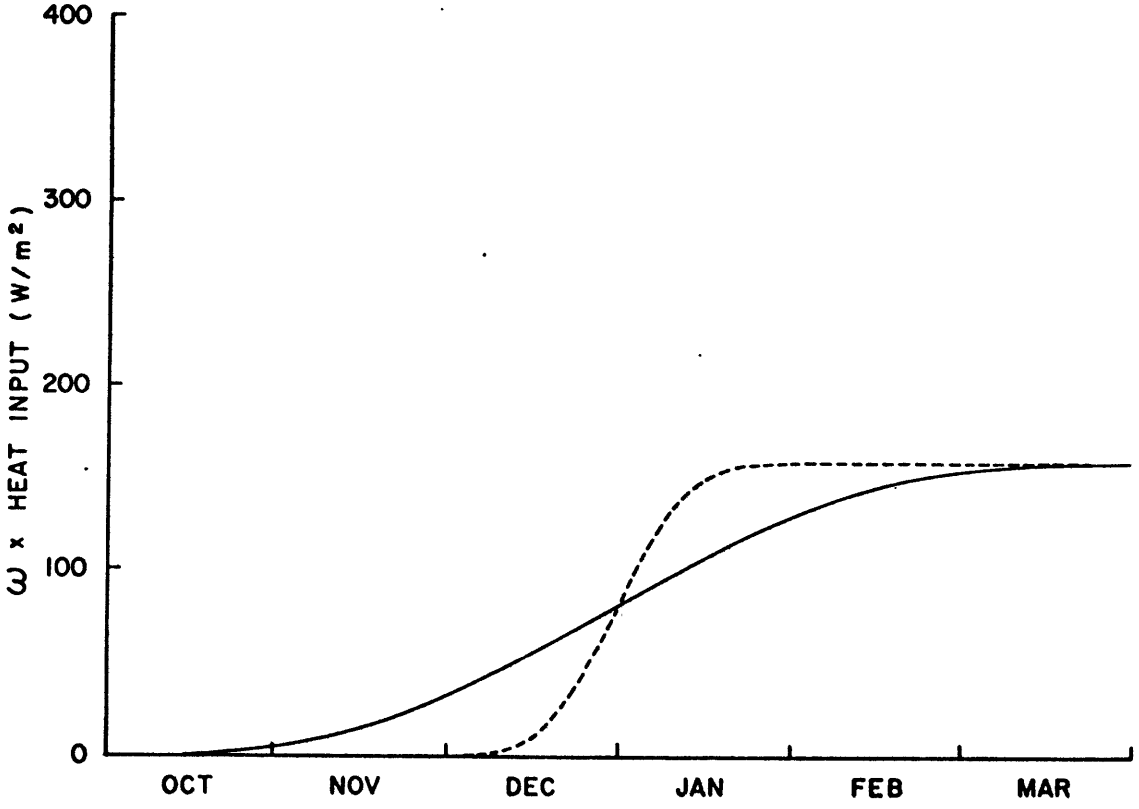
400
300
200
100
0
ω x HEAT INPUT (W/m²)
OCT
NOV
DEC
JAN
FEB
MAR

FIGURE 12

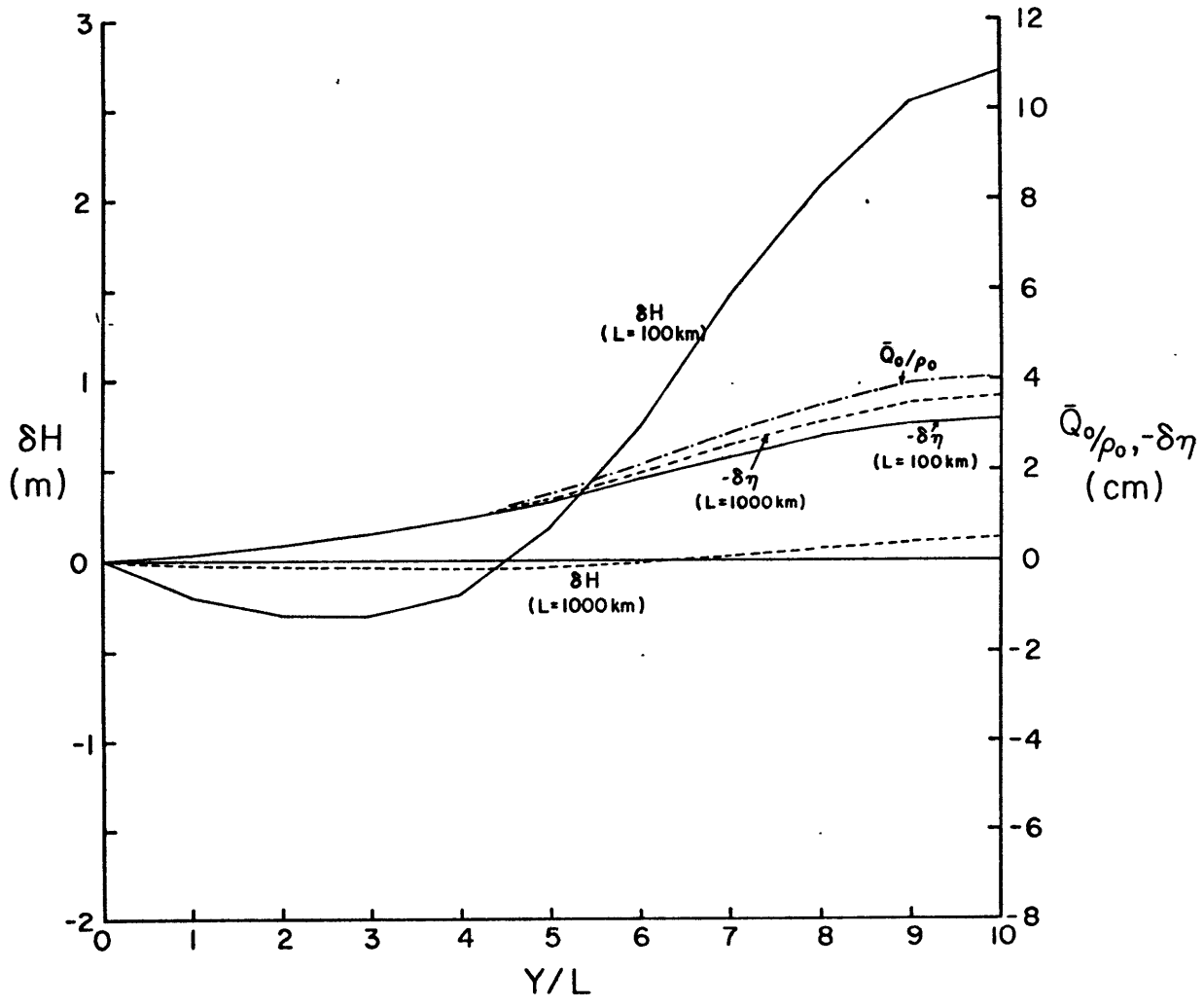
δH
(m)
Q̄o/ρo, -δη
(cm)
Y/L
δH
(L=100km)
Q̄o/ρo
-δη'
(L=100km)
-δη
(L=1000km)
δH
(L=1000km)

FIGURE 13

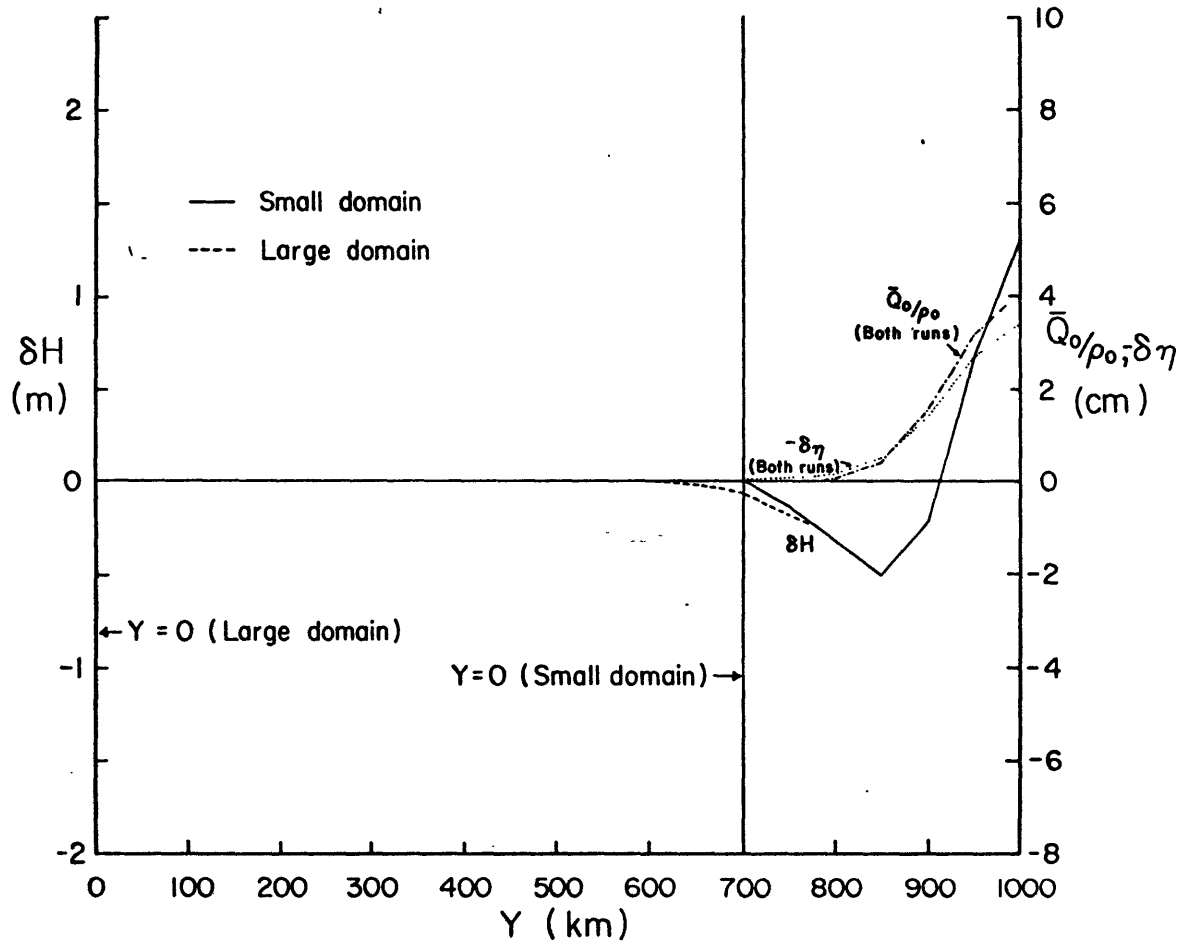
Small domain
Large domain
δH
(m)
$\bar{Q}_o/\rho_o$
(Both runs)
$-\delta\eta$
(Both runs)
δH
$\bar{Q}_o/\rho_o$, $\delta\eta$
(cm)
Y = 0 (Large domain)
Y=0 (Small domain)
Y (km)
2
1
0
-1
-2
10
8
6
4
2
0
-2
-4
-6
-8
0
100
200
300
400
500
600
700
800
900
1000

FIGURE 14

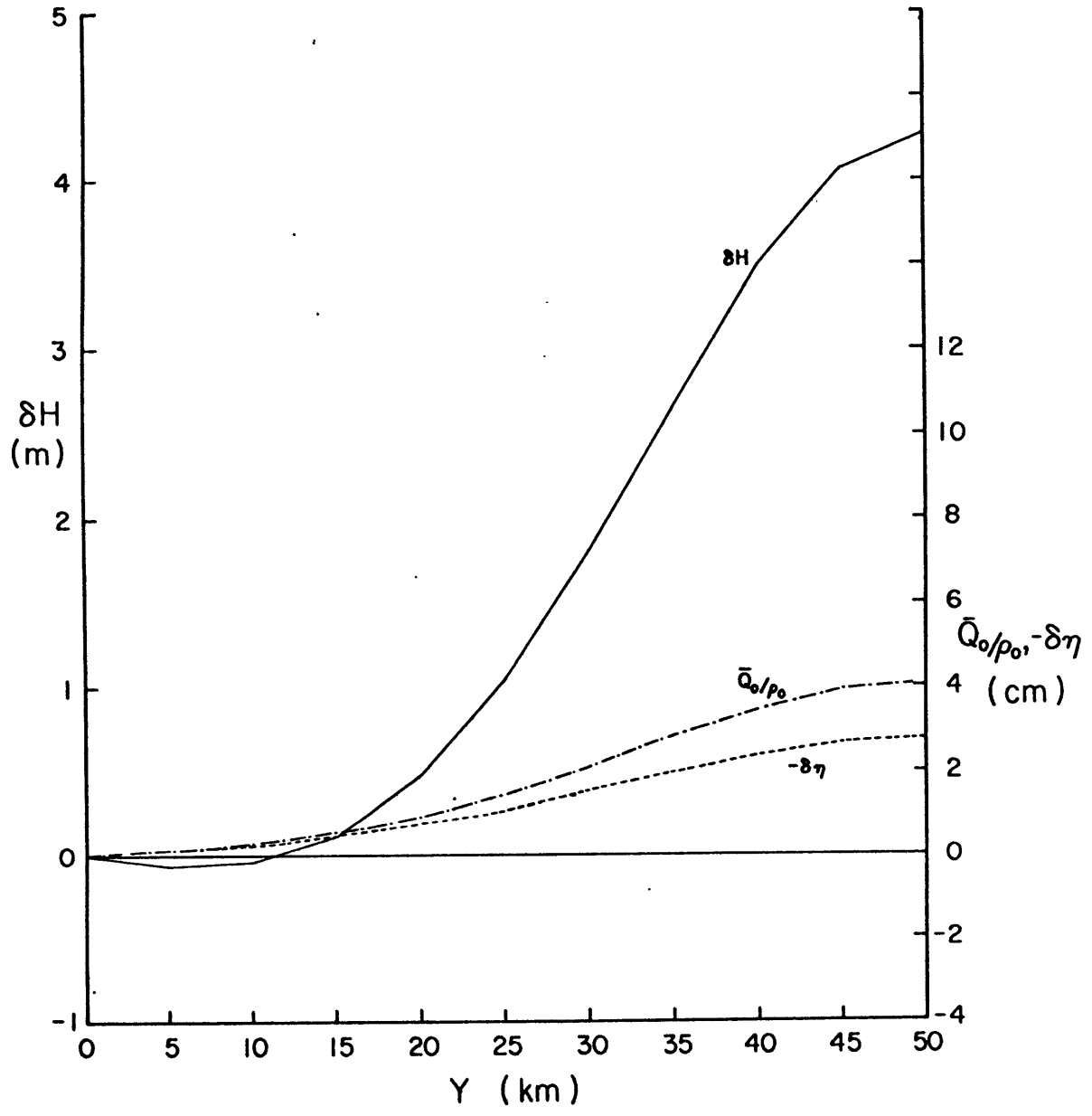

FIGURE 15

Table Captions

Table I: Semantics breakdown for transport fields, in terms of contributions from pieces of model vertical density prescription.

Table II: Transports and velocities for the three runs presented in figure 10. Definitions of the terms are given in the text.

Table III: Same as Table II for the runs presented in Fig. 13. The column marked δD gives the cumulative change in the depth, D, of the late winter mixed layer. The other definitions are given in the text.

Table IV: Same as Table III for the run presented in Fig. 15.

Table V: Summary of total transports across the entire model domain for runs discussed in the text. Unless noted otherwise, the parameters used are those given by equation (54). Cubic forcing was used in the heating runs, and Gaussian forcing with an e-folding scale of $L/2$ was used in the convecting runs.

Table I

Definitions	Free Surface Terms		Main Thermocline Terms		Seasonal Layer Buoyancy Flux Terms	
	$B\rho_o g\delta\eta$	$\rho_o g\delta\eta^2/2$	$B\beta\Delta D g\delta H$	$g(-H+\Delta D/2)\beta\Delta D\delta H$	$Bg\bar{Q}_o$	$g(-h_D/2)\bar{Q}_o$
Barotropic	✓	-	✓	-	✓	-
Baroclinic	-	✓ (neglect)	-	✓	-	✓
Oceanographic	-	-	-	✓	-	✓
External	✓	✓	-	-	-	-
Internal	-	-	✓	✓	✓	✓

Table II

	Y/ΔY	TRBCW SV	TRBC SV	TRBTW SV	TRBT SV	TRT SV	TRL SV	VT cm^2/s	UGM cm/s	UGS cm/s	US cm/s	UB cm/s
	0	.0	.0	.0	.0	.0	.0	.0	.00	.00	.00	.00
	1	-.0	-.0	.0	.0	.0	.0	-.3	-.00	-.29	-.29	.00
	2	-.0	-.0	.0	.0	.0	.0	.6	-.00	-.78	-.78	.01
	3	-.0	-.1	.1	.1	.0	.1	1.8	-.00	-1.16	-1.14	.01
	4	-.1	-.1	.1	.2	.1	.1	3.1	.00	-1.40	-1.38	.02
L = 1000 km	5	-.1	-.2	.1	.3	.1	.2	4.1	.00	-1.53	-1.50	.03
	6	-.1	-.3	.2	.5	.2	.3	4.7	.00	-1.53	-1.49	.03
	7	-.1	-.3	.2	.6	.3	.4	4.7	.00	-1.40	-1.37	.03
	8	-.1	-.4	.1	.8	.4	.5	4.1	.00	-1.16	-1.12	.03
	9	-.0	-.5	.1	.9	.4	.6	2.8	.00	-.78	-.76	.02
	10	-.0	-.5	.0	.9	.4	.6	1.0	.00	-.29	-.28	.01
	0	.0	.0	.0	.0	.0	.0	.0	.00	.00	.00	.00
	1	-.0	-.0	-.1	-.1	-.1	-.1	-2.7	-.00	-.12	-.13	-.01
	2	-.0	-.0	-.0	-.1	-.1	-.1	-.6	-.00	-.31	-.32	-.00
	3	-.0	-.1	.1	.0	-.0	.0	2.7	-.00	-.46	-.45	.01
L =	4	-.1	-.1	.3	.3	.2	.2	6.1	.00	-.56	-.54	.02
2500 km	5	-.1	-.2	.4	.7	.6	.5	9.0	.00	-.61	-.58	.03
	6	-.1	-.3	.5	1.2	1.0	.9	10.8	.00	-.61	-.57	.04
	7	-.1	-.3	.5	1.8	1.4	1.2	11.2	.00	-.56	-.52	.04
	8	-.1	-.4	.5	2.2	1.8	1.6	9.9	.00	-.46	-.42	.04
	9	-.1	-.5	.3	2.6	2.1	1.8	7.0	.00	-.31	-.29	.03
	10	-.0	-.5	.1	2.7	2.2	1.9	2.6	.00	-.12	-.11	.01
	0	.0	.0	.0	.0	.0	.0	.0	.00	.00	.00	.00
	1	-.0	-.0	.0	.0	.0	.0	.0	-.02	-.58	-.59	.01
	2	-.0	-.0	.0	.0	.0	.0	.5	-.01	-1.57	-1.57	.01
	3	-.0	-.1	.0	.1	.0	.1	.9	-.00	-2.31	-2.30	.02
L =	4	-.1	-.1	.1	.1	.0	.1	1.3	.00	-2.81	-2.78	.02
500 km	5	-.1	-.2	.1	.2	.0	.2	1.6	.01	-3.06	03.01	.03
	6	-.1	-.3	.1	.3	.0	.2	1.6	.02	-3.06	-3.00	.03
	7	-.1	-.3	.1	.4	.1	.3	1.5	.02	-2.81	-2.75	.03
	8	-.1	-.4	.1	.5	.1	.3	1.1	.02	-2.31	-2.26	.02
	9	-.0	-.4	.0	.5	.1	.4	.7	.02	-1.57	-1.53	.02
	10	-.0	-.5	.0	.5	.1	.4	.2	.01	-.58	-.56	.01

Table III

	Y/ΔY	TRBCW SV	TRBC SV	TRBTW SV	TRBT SV	TRT SV	TRL SV	δD M	UGM cm/s	UGS cm/s	US cm/s	UB cm/s
	0	.0	.0	.0	.0	.0	.0	0	.00	.00	.00	.00
	1	.1	.1	-.1	-.1	-.0	-.1	.2	.71	1.14	1.60	-.24
	2	.1	.3	-.1	-.3	-.0	-.2	1.5	.08	3.08	2.89	-.27
	3	.1	.4	-.1	-.4	.0	-.3	3.4	-.52	4.54	3.77	-.25
L =	4	.1	.5	-.1	-.5	.0	-.3	5.7	-.99	5.51	4.32	-.21
100 km	5	.1	.6	-.1	-.6	.1	-.4	8.2	-1.34	6.00	4.52	-.15
	6	.1	.8	-.0	-.6	.2	-.4	11.0	-1.49	6.00	4.42	-.09
	7	.1	.9	-.0	-.6	.2	-.4	13.1	-1.50	5.51	3.98	-.04
	8	.1	.9	-.0	-.6	.3	-.4	15.3	-1.31	4.54	3.22	-.00
	9	.0	1.0	.0	-.6	.4	-.4	16.2	-.96	3.08	2.15	.02
	10	.0	1.0	.0	-.6	.4	-.4	17.1	-.35	1.14	.79	.01
	0	.0	.0	.0	.0	.0	.0	.0	.00	.00	.00	.00
	1	.0	.0	-.0	-.0	.0	-.0	.4	.01	.09	.09	-.01
	2	.1	.1	-.1	-.1	.0	-.1	1.0	.00	.16	.15	-.01
	3	.1	.2	-.1	-.2	.0	-.1	2.0	.00	.26	.24	-.02
L =	4	.2	.4	-.2	-.4	.0	-.3	3.4	.00	.40	.36	-.03
1000 km	5	.2	.6	-.2	-.6	.0	-.4	5.4	.00	.54	.49	-.05
	6	.3	.9	-.3	-.9	.0	-.6	7.7	-.01	.66	.59	-.06
	7	.3	1.3	-.3	-1.2	.0	-.9	10.0	-.01	.70	.63	-.07
	8	.3	1.5	-.3	-1.5	-.0	-1.1	12.1	-.01	.64	.56	-.06
	9	.2	1.7	-.2	-1.8	-.0	-1.2	14.0	-.01	.45	.40	-.04
	10	.1	1.8	-.1	-1.8	-.0	-1.3	14.1	-.00	.16	.14	-.02

Table IV

Y	TRBCW	TRBC	TRBTW	TRBT	TRT	TRL	δD	UGM	UGS	US	UB
km	SV	SV	SV	SV	SV	SV	M	cm/s	cm/s	cm/s	cm/s
0	.0	.0	.0	.0	.0	.0	0	.00	.00	.00	.00
5	.1	.1	-.1	-.1	-.0	-.0	.3	.43	1.72	1.93	-.23
10	.1	.1	-.1	-.1	-.0	-.1	1.0	-.15	3.15	2.78	-.22
15	.1	.2	-.0	-.2	.0	-.1	2.1	-1.01	5.25	4.06	-.18
20	.1	.2	-.0	-.2	.0	-.1	3.9	-2.20	7.93	5.67	-.07
25	.0	.3	.0	-.2	.1	-.1	6.4	-3.53	10.81	7.37	.08
30	.0	.3	.1	-.1	.2	-.1	9.5	-4.72	13.16	8.71	.26
35	.0	.3	.1	.0	.4	.0	13.2	-5.33	14.07	9.14	.40
40	.0	.4	.1	.1	.5	.1	16.3	-5.02	12.76	8.19	.45
45	.0	.4	.1	.2	.6	.2	18.1	-3.63	8.97	5.71	.36
50	.0	.4	.1	.3	.6	.2	18.2	-1.33	3.24	3.05	.14

Table V

Run #	TRBC	TRBT	TRT	TRL	DESCRIPTION
1	-.5	.9	.4	.8	L = 1000 km, B = 10,000 m, heating
2	-.5	.8	.3	.1	L = 1000 km, B = 1600 m, heating
3	-.5	.9	.4	.6	L = 1000 km, B = 5000 m, heating
4	-.5	2.7	2.2	1.9	L = 2500 km, B = 5000 m, heating
5	-.5	.5	.1	.4	L = 500 km, B = 5000 m, heating
6	1.0	-.6	.4	-.4	L = 100 km, B = 5000 m, convecting
7	1.8	-1.8	-.0	-1.3	L = 1000 km, B = 5000 m, convecting
8	.4	.3	.6	.2	L = 50 km, B = 5000 m, convecting

APPENDIX A - Dynamical Scale Analysis

The equations of motion in spherical coordinates, (ϕ,θ,r) being longitude eastward, latitude, and vertical upward, are:

$$\frac{D\rho}{Dt} + \rho\{\frac{\partial w}{\partial r} + \frac{2w}{r} + \frac{1}{r\cos\theta}\frac{\partial(v\cos\theta)}{\partial\theta} + \frac{1}{r\cos\theta}\frac{\partial u}{\partial\phi}\} = 0$$

$$\frac{Du}{Dt} + \frac{uw}{r} - \frac{uv\tan\theta}{r} - 2\Omega\sin\theta v + 2\Omega\cos\theta w = -\frac{1}{\rho r\cos\theta}\frac{\partial p}{\partial\phi}$$

$$\frac{Dv}{Dt} + \frac{vw}{r} + \frac{u^2\tan\theta}{r} + 2\Omega\sin\theta u = -\frac{1}{\rho r}\frac{\partial p}{\partial\theta}$$

$$\frac{Dw}{Dt} - \frac{(u^2+v^2)}{r} - 2\Omega\cos\theta u = -\frac{1}{\rho}\frac{\partial p}{\partial r} - g$$

Where (u,v,w) are eastward, northward, and upward velocities; ρ is in situ density; p is dynamic pressure corrected for the centripital acceleration in the earth's reference frame and atmospherically corrected ($p \equiv 0$ at sea surface); Ω is the angular velocity of the earth and g is the acceleration due to gravity (assumed constant); and

$$\frac{D(\ )}{Dt} \equiv \frac{\partial(\ )}{\partial t} + \frac{u}{r\cos\theta}\frac{\partial}{\partial\phi} + \frac{v}{r}\frac{\partial}{\partial\theta} + w\frac{\partial}{\partial r}$$

In anticipation of scales of motion less than the earth's radius, we go to a Cartesian coordinate system centered at a mid-latitude θ_o. We define our new coordinates relative to a reference radial distance r_o as:

$$x = r_o \cos\theta_o \phi \qquad \partial/\partial\phi = r_o \cos\theta_o \; \partial/\partial x$$

$$y = r_o(\theta - \theta_o) \qquad \partial/\partial\theta = r_o \; \partial/\partial y$$

$$z = r - r_o \qquad \partial/\partial r = \partial/\partial z$$

We next nondimensionalize our parameters, again anticipating the balances we expect to hold, and retaining the asymmetry inherent in a two dimensional limit:

$$x = L_x x^*$$

$$y = L_y y^*$$

$$z = D z^* \qquad * \text{ denotes nondimensional quantities}$$

$$u = U_x u^*$$

$$v = U_y v^*$$

$$t = \omega^{-1} t^*$$

Where we have used the seasonal frequency to nondimensionalize time. We proceed to scale the vertical velocity by an expected <u>two</u> term continuity balance for a 2-D limit:

$$w = Ww^* \equiv \left[\frac{DU_y}{L_y}\right] w^*$$

Because our scales will be large enough that horizontal density gradients of the mean field will be comparable to the mean vertical gradients, rather than partition the density about a mean vertical state we use a constant value ρ_o to write:

$$\rho = \rho_o + \tilde{\rho}$$

Using the expected hydrostatic balance to scale pressure, and retaining the presence of a free surface, yields:

$$p = \rho_o g(\eta - z) + \tilde{p}$$

We now scale the horizontally variable parts of the pressure geostrophically, again in consideration of a 2-D limit:

$$\tilde{p} = Pp^* \equiv (2\Omega \sin\theta_o U_x L_y \rho_o) p^*$$

$$\eta = \eta_o \eta^* \equiv (2\Omega \sin\theta_o U_x L_y / g) \eta^*$$

From the hydrostatic assumption this yields:

$$\tilde{\rho} = (2\Omega \sin\theta_o U_x L_y \rho_o / gD) \rho^*$$

We now define a set of nondimensional parameters which will subsequently appear and whose magnitudes are less than unity.

$$\ell \equiv L_y / L_x$$

$$\gamma \equiv U_y / U_x$$

$$\epsilon \equiv U_x / f_o L_y$$

$$\delta \equiv D / r_o$$

$$\Delta \equiv L_y/r_o$$

$$F \equiv f_o^2 L_y^2/gD \quad \text{where} \quad f_o \equiv 2\Omega\sin\theta_o$$

$$\omega_o \equiv U_y/\omega L_y$$

$$\sigma \equiv \omega/f_o$$

Plugging in the scales above, and multiplying the mass conservation equation by $L_y\omega_o/\rho_o U_y$ yields:

$$[\varepsilon F]\frac{\partial\rho^*}{\partial t^*} + [\varepsilon F\omega_o]\{[\frac{\ell}{\gamma}\cdot\frac{r_o}{r}\cdot\frac{\cos\theta_o}{\cos\theta}]u^*\frac{\partial\rho^*}{\partial x^*} + [\frac{r_o}{r}]\,v^*\frac{\partial\rho^*}{\partial y^*} + w^*\frac{\partial\rho^*}{\partial z^*}\}$$

$$+ [\omega_o](1 + [\varepsilon F]\rho^*)\{\frac{\partial w^*}{\partial z^*} + [\frac{2\delta r_o}{r}]w^* + [\frac{r_o}{r}]\frac{\partial v^*}{\partial y^*} + [\Delta\cdot(\frac{r_o}{r})\cdot\tan\theta]\,v^*$$

$$+ [\frac{\ell}{\gamma}\cdot\frac{r_o}{r}\cdot\frac{\cos\theta_o}{\cos\theta}]\,\frac{\partial u^*}{\partial x^*}\} = 0$$

Where terms in square brackets are the only nondimensional coefficients multiplying terms expected to be order one. Plugging in scales and dividing the horizontal momentum equations by $f_o U_x$ yields for x-momentum:

$$[\sigma]\frac{\partial u^*}{\partial t^*} + [\varepsilon\gamma]\{[(\frac{\ell}{\gamma})\cdot(\frac{r_o}{r})\cdot(\frac{\cos\theta_o}{\cos\theta})]u^*\frac{\partial u^*}{\partial x^*} + [\frac{r_o}{r}]\,v^*\frac{\partial u^*}{\partial y^*} + w^*\frac{\partial u^*}{\partial z^*}$$

$$+ [\delta\cdot(\frac{r_o}{r})]u^*w^* - [\Delta\cdot(\frac{r_o}{r})\cdot\tan\theta]u^*v^*\} - [\gamma\cdot\frac{\sin\theta}{\sin\theta_o}]v^* + [\gamma\cdot\frac{\delta}{\Delta}\cdot\frac{\cos\theta}{\sin\theta_o}]w^*$$

$$= -[(\frac{r_o}{r})\cdot(\frac{\cos\theta_o}{\cos\theta})\cdot\frac{1}{(1 + [\varepsilon F]\rho^*)}\cdot\ell](\frac{\partial p^*}{\partial x^*} + \frac{\partial\eta^*}{\partial x^*})$$

Similarly for y-momentum:

$$[\gamma]\{[\sigma]\frac{\partial v^*}{\partial t^*} + [\varepsilon\cdot\gamma]\{[(\frac{\ell}{\gamma}) \cdot (\frac{r_o}{r}) \cdot (\frac{\cos\theta_o}{\cos\theta})]u^* \frac{\partial v^*}{\partial y^*} + [\frac{r_o}{r}]v^* \frac{\partial v^*}{\partial y^*} + w^* \frac{\partial v^*}{\partial z^*}$$

$$+ [\delta \cdot (\frac{r_o}{r})]v^*w^*\}\} + [\varepsilon \cdot \Delta \cdot (\frac{r_o}{r}) \cdot \tan\theta]u^{*2} + [\frac{\sin\theta}{\sin\theta_o}]u^*$$

$$= - [(\frac{r_o}{r}) \cdot \frac{1}{(1+[\varepsilon F]\rho^*)}](\frac{\partial p^*}{\partial y^*} + \frac{\partial \eta^*}{\partial y^*})$$

and finally z-momentum, showing hydrostatic balance for the perturbations as well as the mean (which cancels out):

$$[(\delta/\Delta)^2 \cdot \gamma \cdot (1+[\varepsilon F]\rho^*)]\{[\sigma]\frac{\partial w^*}{\partial t^*} + [\varepsilon\cdot\gamma]\{[(\frac{\ell}{\gamma}) \cdot (\frac{r_o}{r}) \cdot (\frac{\cos\theta_o}{\cos\theta})]u^* \frac{\partial w^*}{\partial x^*}$$

$$+ [\frac{r_o}{r}]v^* \frac{\partial w^*}{\partial y^*} + [\gamma]w^* \frac{\partial w^*}{\partial z^*}\}\} - [\varepsilon \cdot \delta \cdot (\frac{r_o}{r}) \cdot (1+[\varepsilon F]\rho^*)]u^{*2}$$

$$- [\gamma^2 \cdot \varepsilon \cdot \delta \cdot (\frac{r_o}{r}) \cdot (1+[\varepsilon F]\rho^*)]v^{*2} - [(\delta/\Delta) \cdot (\frac{\cos\theta}{\sin\theta_o})\cdot(1+[\varepsilon F]\rho^*)]u^*$$

$$= - \frac{\partial p^*}{\partial z^*} - \rho^*$$

The scales we choose are those necessary to reach the 2-D limit equations we desire, the following shows just how 2-D the length scales must be. These scales work out to be:

$L_y \sim 10^3$ km

$L_x > 10^3 L_y > 10^6$ km

$U_x \sim 10$ cm/s

$U_y \sim 10^{-3} U_x \sim 10^{-2}$ cm/s

$$f_o \sim 10^{-4}\ s^{-1}$$

$$g \sim 10^{3}\ cm/s^{2}$$

$$\omega = 2 \times 10^{-7}\ s^{-1}$$

$$D \sim 5\ km$$

$$r_o \sim 7 \times 10^{3}\ km$$

With these scales, the largest nondimensional parameter is $\Delta \sim 10^{-1}$. In terms of this expansion parameter, the other parameters are ordered as:

$$F \sim \Delta$$

$$\delta, \sigma, \varepsilon, \gamma \sim \Delta^{3}$$

$$\omega_o, \ell \sim \Delta^{4}$$

The parameter Δ is also the natural expansion parameter for the trigonometric functions:

$$\cos\theta = \cos\theta_o - \Delta \sin\theta_o y^* - \Delta^2 \frac{y^{*2}}{2} \cos\theta_o \ldots$$

$$\sin\theta = \sin\theta_o + \Delta \cos\theta_o y^* - \Delta^2 \frac{y^{*2}}{2} \sin\theta_o \ldots$$

$$\tan\theta = \tan\theta_o + \Delta \sec^2\theta_o y^* + \Delta^2 \frac{y^{*2}}{2} \tan\theta_o \sec^2\theta_o$$

When we expand the trigonometric functions as above, and plug in the ordering of parameters, we get a series of perturbation equations in the

single parameter Δ. Expanding the independent variables in terms of Δ so that, for example, $u^* = u^*_{(o)} + \Delta u^*_{(1)} + \Delta^2 u^*_{(2)} \ldots$, gives the following balances in our scaled equations:

$$O(1): \frac{\partial \rho^*_{(o)}}{\partial t^*} + \frac{\partial w^*_{(o)}}{\partial z^*} + \frac{\partial v^*_{(o)}}{\partial y^*} = 0$$

$$\frac{\partial u^*_{(o)}}{\partial t^*} = v^*_{(o)}(1 + \Delta(\cot\theta_o)y^*)$$

$$(1 + \Delta(\cot\theta_o)y^*)u^*_{(o)} = -\frac{\partial p^*_{(o)}}{\partial y^*} - \frac{\partial \eta^*_{(o)}}{\partial y^*}$$

$$\frac{\partial p^*_{(o)}}{\partial z^*} = -\rho^*_{(o)}$$

in the above, the factor $(\Delta \cot\theta_o)$ is retained to show the neglect of β terms. If this term becomes order one by the choice of θ_o and L_y, it would be necessary to extend the model to a β-plane.

The order Δ balances show that if $\Delta \to 1$ it becomes necessary to retain certain metric terms, β-effects and zonal gradients, even with our large scale asymmetry:

$$O(\Delta): \frac{\partial \rho^*_{(1)}}{\partial t^*} + \frac{\partial w^*_{(1)}}{\partial z^*} + \frac{\partial v^*_{(1)}}{\partial y^*} + \tan\theta_o v^*_{(o)} + \frac{\partial u^*_{(o)}}{\partial x^*} = 0$$

$$\frac{\partial u^*_{(1)}}{\partial t} = v^*_{(1)}(1 + \Delta(\cot\theta_o)y^*) + v^*_{(o)}(\cot\theta_o)y^* - \frac{\partial p^*_{(o)}}{\partial x^*} - \frac{\partial \eta^*_{(o)}}{\partial x^*}$$

$$(\cot\theta_o)u^*_{(o)} + (1 + \Delta(\cot\theta_o))u^*_{(1)} = -\frac{\partial p^*_{(1)}}{\partial y^*} - \frac{\partial \eta^*_{(1)}}{\partial y^*}$$

$$\frac{\partial p^*_{(1)}}{\partial z^*} = -\rho^*_{(1)}$$

APPENDIX B - Double Integral Trapezoidal Approximation

The following derivation shows the trapezoidal estimate for a particular double integral which occurs in Chapter III, resulting from double integration of the stretching terms of the governing vorticity equations. This integral, with boundary conditions coming in through the integration limits is:

$$I_y\{\ \} = \int_{-L}^{Y} d\hat{y} \int_{-L}^{\hat{y}} \{\ \} d\hat{\hat{y}} - \frac{(y+L)}{2L} \int_{-L}^{L} d\hat{y} \int_{-L}^{\hat{y}} \{\ \}\, d\hat{\hat{y}}$$

which is applicable for a mirror-image doubled domain.

We first break the two integrals up by parts:

$$I_y\{\ \} = y \int_{-L}^{Y} \{\ \} d\hat{y} - \int_{-L}^{Y} \hat{y}\{\ \} d\hat{y} - \frac{(y+L)}{2L}(L \int_{-L}^{L} \{\ \} d\hat{y} - \int_{-L}^{L} \hat{y}\ \{\ \} d\hat{y})$$

In the trapezoidal approximation we say there are M discrete intervals in the single domain so that $\Delta y = L/M$ and $y_i = (i - 1 - M)\Delta y$ $(i = 1, 2M+L)$. The individual integrals are then approximated as:

$$\int_{-L}^{Y} \{\ \} d\hat{y} \simeq \Delta y \left[\frac{\{\ \}_1 + \{\ \}_i}{2} + \sum_{j=2}^{i-1} \{\ \}_j\right]$$

$$\int_{-L}^{Y} \hat{y}\{\ \} d\hat{y} \simeq \Delta y^2 \left[\frac{-M\{\ \}_1 + (i-1-M)\{\ \}_i}{2} + \sum_{j=2}^{i-1} (j-i-M)\{\ \}_j\right]$$

and similarly for the integrals from -L to L by replacing i by 2M + 1.

Using our finite element forms for the integrals and for y then yields:

$$\int_{-L}^{y} d\hat{y} \int_{-L}^{\hat{y}} \{\ \} d\hat{\hat{y}} \simeq \Delta y^2 \left[(i-1)\frac{\{\ \}_1}{2} + \sum_{j=2}^{i-1} \{\ \}_j (i-j)\right]$$

Similarly:

$$\int_{-L}^{L} d\hat{y} \int_{-L}^{\hat{y}} \{\ \} d\hat{\hat{y}} \simeq \Delta y^2 \left[M\frac{\{\ \}_1}{2} + \sum_{j=2}^{2M} (\ )_j\ (2M+1-j)\right]$$

Again using the expression for y_i gives the approximation for the total integral:

$$I_i\{\ \} \simeq \Delta y^2 \left[\sum_{j=2}^{i-1} \{\ \}_j (i-j) - \sum_{j=2}^{2M} \{\ \}_j \frac{(i-1)(2M+1-j)}{2M}\right]$$

The formula actually used is obtained by adding and subtracting $\sum_{j=2}^{2M} (\ )_j (i-j)$ which yields:

$$I_i\{\ \} \simeq \Delta y^2 \left[\sum_{j=i+1}^{2M+1} \{\ \}_j (j-i) + \sum_{j=2}^{2M+1} \{\ \}_j (j-1)\left(\frac{i-1-2M}{2M}\right)\right]$$

with the stipulation that the first sum is zero if $j > i$ or if $i = 2M+1$. This formulation then specifies a set of weights to each point y_j when the integral is evaluated at point y_i:

$$I_i\{\ \} \simeq \Delta y^2 \sum_{j=1}^{2M+1} a_{ij}\{\ \}_j$$

where

$$a_{ij} = (j-i) + (j-1)\left(\frac{i-1-2M}{2M}\right) \qquad j > i\ ;\ i < 2M+1$$

$$= 0 + (j-1)\left(\frac{i-1-2M}{2M}\right) \qquad j > i\ ;\ i = 2M+1$$

These weights have the property that for a given value of i the maximum weight is for j = i. The largest weight for all i is that at the center of the double domain, which corresponds to the northern boundary. This maximum weight is given by j = i = M+1 so that $a_{ij} = -M/2$. It is also easy to show that the effective single domain weights reach the maximum value at j = i and are then constant from there to the gyre center weight at j = M+1. These weights again reach larger maximums as i increases to M+1.

APPENDIX C - Glossary of Terms (in order of appearance by section)

II.B

ρ	density (implicitly potential density after reaching equation 4)
c_p	specific heat of sea water at constant pressure
θ	potential temperature
S	salinity
Q_H, Q_S, Q_ρ	vertical fluxes of heat, salt and density
$D( )/Dt$	substantial derivative following a fluid parcel
ρ_θ	potential density
ρ_o, θ_o, S_o	constant reference values of potential density, potential temperature, and salinity
α_*	thermal expansion coefficient
β_*	haline expansion coefficient
(x,y,z,t)	independent variables: east, north, up, and time
$\vec{u}=(u,v,w)$	eastward, northward, and vertical velocity
∇	gradient operator
B	depth of ocean bottom
H	depth of main thermocline bottom
D	depth of main thermocline top
β	main thermocline vertical density gradient
ω	seasonal frequency
f	inertial frequency
β_T	main thermocline vertical temperature gradient

h, h_D	depth of seasonal influence
$h_s; h_{Ls}$	depth of seasonal thermocline; maximum late summer seasonal thermocline depth
h_m	depth of mixed layer eroding into seasonal thermocline
η	height of free surface above z = 0
Q_o	surface density flux
γ	seasonal thermocline vertical density gradient
ρ_{LW}	density of late winter deep mixed layer
ρ_S	density at the surface
L_y	meridional length scale
$\Delta\rho$	seasonal amplitude of density changes
Δz	seasonal amplitude of vertical fluid parcel excursions
$p; p_B$	pressure; pressure at the ocean bottom
g	earth's gravitational acceleration
g'	reduced gravity across the main thermocline

II.D

$\vec{N}_x, \vec{N}_y$	integrals of momentum advection , e.g., $\int_{-B}^{\eta} uvdz$
U, V	volume transports/width eastward and northward
β	planetary vorticity gradient (section IID between equations 35 and 37 only)
f_o	constant value of inertial frequency
Π	potential energy of total water column
ρ_B	constant bottom layer density
ΔD	main thermocline thickness H-D
U_L	lower layer eastward transport/width

Π_L	lower layer potential energy
H_o	constant value for H
δH	perturbation of H about H_o
λ	external Rossby radius of deformation $\equiv f_o^2/gB$

III.B

L	length of model single domain
ϕ,θ	dummy variables in schematic double integral derivation
I{ }	double integral of stretching terms in vorticity equation
Δy	distance between discrete points in space in numerical model
M	Number of points in model single domain
a_{ij}	double integral weights in "I" depending on all points j when "I" evaluated at point i
δt	time step of model
δH	perturbation of main thermocline over δt
$\delta\eta$	perturbation of free surface over δt
$\overline{Q_o}$	time integral of density flux over δt

III.C

x_1	δH in analytic equations
x_2	$\delta\eta$ in analytic equations
Δ	H_o/B in analytic equations
Δ'	$(H_o - \Delta D/2)/B$ in analytic equations
δ	$h_D/2B$ in analytic equations
ϵ	$\beta\Delta D/\rho_o$ in analytic equations

Q	$\overline{Q_o}/\rho_o$ in analytic equations
p_i	decay scales of exponential solutions to analytic equations

IV.A

γ_T	seasonal thermocline temperature gradient
T_B	constant bottom temperature
$\Delta( )$	difference of a quantity in latitude
$\hat{x}_1$	$\varepsilon\delta H$ in analytic equations